A toolbox for the use of electromagnetic induction technology and quasi-3D inversion to determine the spatial heterogeneity of soil texture and moisture in forested catchments

A thesis

submitted in partial fulfilment

of the requirements for the degree

of

Master of Science in Earth Science (Research)

at

The University of Waikato

by

Priscilla Lad

THE UNIVERSITY OF
WAIKATO
Te Whare Wānanga o Waikato

2023

Abstract

Forest soils are critical to forest health and productivity, and by recognising their spatial heterogeneity, we can optimise productivity and preserve our natural resources in the face of a changing climate. Electromagnetic induction (EMI) technology provides a repeatable, non-destructive, and cost-effective approach to studying soil heterogeneity in managed forests. Electromagnetic induction technology has proven its versatility in agricultural settings to map soil texture, moisture and crop productivity and geological and archaeological exploration to identify underground natural and anthropogenic structures. Yet, the application in forests has been limited, and it is essential to understand the impact of soil and environmental factors on apparent electrical conductivity (EC_a) if attempting to use this EMI technology in a forested environment. The overarching aim of this thesis was to determine if EMI can be used in a forested environment, focusing on two contrasting *Pinus radiata* D. Don production forests to capture the spatial heterogeneity of soil properties. Furthermore, this thesis can serve as a 'toolbox' for measurement protocols and analysis for forest owners interested in low-cost, time-efficient methods of understanding microsite heterogeneity in their forest soils to guide management practices. The research addressed the three main questions: The impact of various environmental factors on apparent electrical conductivity (EC_a), the ability of EC_a to characterise soil texture and moisture across forested catchments, and the effectiveness of quasi-3D inversion software in capturing the spatial heterogeneity of forest soils in three dimensions.

To answer the first question, measurements were taken on forest litter thickness, gravimetric water content, density, soil temperature, ambient temperature, instrument temperature, and instrument voltage. The study found no significant linear relationship between EC_a and these environmental factors, indicating that a correction factor for drift in EC_a caused by temperature and voltage variations was not required. The insulating effect of forest soils, the forest canopy, and the instrument's housing played a role in maintaining stability. In addition, there was no significant effect of the presence or absence of forest litter on EC_a, which was most likely due to the structure and makeup of forest litter, indicating that EMI technology could predict soil properties without considering the effect of forest litter.

Questions two and three aimed to evaluate the effectiveness of using apparent electrical conductivity and modelled electrical conductivity (EC^m) as predictors for soil properties, including gravimetric water content (GWC), the electrical conductivity of a 1-part soil to 5-part water solution ($ECe^{1:5}$), and the percentages of clay (CLAY), fine sand (FSAND), and medium sand particles (MSAND). Firstly, generalised linear mixed-effects models (GLMERs) were employed to assess the measured variables' main effects and interaction effects on EC_a and EC^m and the within and between site variability as a random effect. The GLMERs demonstrated that incorporating multiple predictor variables reduced unexplained variability, with specific interactions, such as GWC and $ECe^{1:5}$, playing crucial roles in explaining EC^m variability at particular depths. However, multicollinearity issues were observed, primarily driven by the GWC-$ECe^{1:5}$ interaction. The study also discussed the findings of 3D inversion maps of EC^m, which provided detailed insights into spatial distribution patterns, particularly when overlaid with topographic and soil variable data. Secondly, one-dimension and three-dimensional maps were produced and overlaid onto base maps of each catchment to identify spatial patterns within each catchment related to soil texture and moisture using standard kriging in Arc GIS Pro software and custom EM4Soil software designed to interpolate one-dimensional EC_a measurements into three dimensions.

Finally, the research delved into the implications of these findings for forest owners and their management practices. It emphasised that while EC_a technology is a valuable tool in predicting forest soil heterogeneity, it should not be used in isolation, and soil sampling and validation remain essential. The study recommended using EMI as a time and cost-effective tool for understanding soil heterogeneity, offering repeatable and non-destructive measurements for informed land use decisions. Overlaying spatial maps with additional geospatial data was recommended to comprehensively understand soil variability within catchments.

Acknowledgements

Firstly, I would like to thank my supervisors, Dr. Michael Clearwater and Dr. Dean Meason, who have supported me throughout my research. I am eternally grateful for your patience and advice and for getting me across the finish line. I have learned a lot through the process, and the experience has been invaluable. So, thank you so much for your encouragement and kind words; they meant a lot.

Thank you to my current and past colleagues at Scion (including but not limited to) Serajis Salekin, Jen Owen, Richard Vili, Elijah Vili, Daniel Unteregger, Jairus Wano, Christine Dodunski, Russell McKinley and John Henry. You were there to help with field and lab work and provided endless emotional support and advice. Also, a big thank you to Scion for funding my research.

Thank you to the forest managers and organisations who granted me access to their properties and enabled me to use data and access sites around the Motu. I want to thank my friends and family for supporting me throughout my thesis. I could not have done this without your endless advice and support from start to finish. To those who assisted with research or provided moral support, it meant the world to me.

Finally, I would like to thank my husband, Damian, and Boonie, who provided endless love, support, snacks, snuggles and encouragement.

Table of Contents

List of Figures

List of Tables

Chapter 1 :
Introduction

Forest soils are essential components of forest ecosystems as they provide a critical foundation for the growth and development of trees and other vegetation while also providing some of the best freshwater sources in the world (Neary et al., 2009). These highly complex and diverse soils support various biological, chemical, and physical characteristics crucial for sustaining healthy forests and delivering high-quality water (Neary et al., 2009; Von Wilpert, 2022).

Some of the critical functions of forest soils include the cycling of nutrients such as nitrogen, phosphorus, and carbon, which are essential for forest productivity and growth while also providing habitats for a diverse range of soil organisms that also play an integral role in nutrient cycling (Neary et al., 2009). They act as carbon sinks for carbon sequestration – an essential factor in mitigating the impacts of climate change. Forest soils also play a crucial role in forest hydrology as they regulate water flow by capturing, storing, filtering, and releasing water into groundwater aquifers, streams and rivers. All are essential for maintaining healthy watersheds and supporting aquatic ecosystems (Williams, 2016).

Studies conducted in New Zealand planted forests typically identify soil properties using resources such as S-MAP and The New Zealand Fundamental Soil Layer (FSL), which uses data from the New Zealand Land Resources Inventory and the National Soils Database (Manaaki Whenua - Landcare Research, 2019, 2023). These tools delineate homogenous polygons of soils down to soil type (Landcare Research Ltd, 2000), and the polygons' scale varies depending on how intensive surveying and sampling have occurred in the region.

Many forests, particularly in New Zealand, are located in remote, rugged, steep, difficult-to-access terrain. This makes soil sampling and surveying challenging to accurately capture the heterogeneity of forest soils over the landscape and at depth. In addition, soil sampling is destructive, cannot be replicated, and individual samples may not represent the soil properties *in situ*.

While these tools help provide a general understanding of soil properties, they do not capture the microsite heterogeneity of soil at the forest or catchment scale.

1.1 How forest soils differ from agricultural soils

Forest soils differ from agricultural soils as a result of complex interactions between soil-forming factors such as parent material, time, landscape position, organisms and climate (Jenny, 1941; Neary et al., 2009) and chemical, physical and biological soil properties such as soil structure, nutrient availability and the accumulation of humus (Von Wilpert, 2022). These differences include canopy cover, litter, rooting depth, soil structure and biodiversity.

1.1.1 The role of the forest canopy and litter

The forest canopy reduces the impact of rainfall on the forest floor, reducing soil disturbance (Neary et al., 2009). Any precipitation that does reach the forest floor is absorbed first by the litter layer. This continuous supply of organic matter from fallen fresh and partially decomposed leaves, twigs and dead trees slowly breaks down to enrich the soil, which overlies a semi-decomposed humus layer (Intergovernmental Panel on Climate Change, 2000). The leaf litter dissipates raindrop energy on the soil surface while acting like a sponge, slowly releasing water to the underlying mineral soil (Williams, 2016). Consequently, forest soil overland flow (Hortanian Flow) rarely occurs in forested catchments during heavy precipitation (Brandon, 2014; Williams, 2016).

In contrast, pasture and cover crops in agriculture do not necessarily provide the same protection that the forest canopy and the litter layer provide in forested soils. In addition, crop rotations are far shorter than in production forestry, and therefore, in agriculture, soil will often remain bare until a crop has established itself. Agricultural soils are more likely to suffer from overland flow during high-intensity precipitation events.

1.1.2 Biodiversity

Forest soils typically have a higher biodiversity of soil organisms, including invertebrates, microbes, fungi, insects and larger animals. Bioturbation and burrowing by this macro and micro fauna help mix and move organic matter, humus, and A horizons to the lower soil profile. The bioturbation also forms macropores, which help transport precipitation infiltrating the soil. This biodiversity is essential for maintaining the ecosystem's health and supporting various ecosystem services. In contrast, a few crop species often dominate agricultural soils, limiting biodiversity and reducing ecosystem resilience.

1.1.3 Rooting depth

Root systems of trees in forested ecosystems are limited by available water, climate, topography, geology and soil physical and chemical properties (Balneaves & De La Mare, 1989) and tend to be more extensive than those in agricultural systems (Neary et al., 2009; Thorup-Kristensen et al., 2020). On average, the rooting depth of forested ecosystems can vary between 7.0 ± 1.2m. In comparison, agricultural lands and grasslands are shallower, with an average rooting depth of 2.6 ± 0.1m and 2.1 ± 0.2m, respectively (Neary et al., 2009; Thorup-Kristensen et al., 2020). Tree root systems develop with age. For example, young Pinus Radiata has a shallow rooting depth, confined to the top 1 m of soil (Marden et al., 2016) and can increase to an average of 2.6 m depth by age 25 (Watson & O'loughlin, 1990). *P. radiata* root networks have been found to extend horizontally from 4.7 to 10.4 meters from the tree's stump and vary between < 0.2 cm and 26cm in diameter (Marden et al., 2016; Watson & O'loughlin, 1990).

1.1.4 Soil properties and structure

The structure of forest soils differs from that of agricultural soils. Below the fresh and partially decomposed litter layer are the mineral soils comprising an A horizon and a B horizon, which overlie bedrock. The vertical soil horizon is often more clearly defined in forest soils than they are in agricultural soils due to the cultivation practices which continually mix any presence of A horizon, usually forming a ploughed layer referred to as an Ap horizon (Intergovernmental Panel on Climate Change, 2000; Von Wilpert, 2022). Ploughing and other land and crop management practices can affect macroporosity and soil physical properties.

Soil pores larger than the microscopic scale are called macropores (Allaire et al., 2009), while a connected chain of macropores is called 'soil pipes' (Uchida et al., 2001; Williams, 2016). In forest soils, macropores and soil pipes typically occur as a consequence of vertical and lateral live and decayed tree root systems, bioturbation, floral and faunal pedoturbation, and large cracks and fissures in both soil and bedrock (Allaire et al., 2009; Aubertin, 1971; Sparling et al., 2008; Uchida et al., 2001; Williams, 2016). The highly permeable nature of macropores and soil pipes makes them essential to the hydrological process, particularly in forested hillslopes, as they act as conduits for rapid water movement or preferential flow, contributing to subsurface flow processes (Allaire et al., 2009; Aubertin, 1971; Uchida et al., 2001). Macropores also allow forest soils to be well aerated, an important factor in plant growth and soil health (Landcare Research Ltd; McLaren & Cameron, 1996).

Low macroporosity and high bulk density are physical indicators of soil compaction, which affects soil structure, soil water storage and movement, and root penetration and has been shown to reduce nitrogen fixation and crop yield (Landcare Research Ltd; Sparling et al., 2008). In agricultural environments, soils typically have low macroporosity. They are at a higher risk of soil compaction by stock and vehicles (Landcare Research Ltd), where soils regularly tilled and ploughed will have fewer macropores as the soil structure is destroyed (He et al., 2009).

1.1.5 Landscape position

In New Zealand, the placement of production forestry is typically on steep, erosion-prone land less suitable for agricultural use, which is generally situated on fine textured silt or fine sandy loams that are well drained and on flat or undulating slopes (Lynn et al., 2009). Forests and their understory vegetation are well suited to steep, erosion-prone land as the tree roots help anchor and stabilise slopes, and the trees help reduce water stored on slopes through evapotranspiration (Brandon, 2014; Bren, 2016). The small pores holding water in slopes at high tensions and the interaction of the tree roots and soil ensure a reduction in response to precipitation during storm events. However, the exact interaction between small pores, tree roots and soils is largely unknown (Amatya et al., 2016).

1.1.6 The implication of the difference in agricultural and forest soils

As noted above, a complex interaction of soil-forming factors and biological, chemical, and physical characteristics makes forest soils different from agricultural soils. Therefore, models applied to forested catchments based on agricultural soils can become difficult to use (Bren, 2016) and may yield inaccurate results.

1.2 Spatial heterogeneity of forest soils

It is more difficult to predict the movement of solids, liquids and gases in forest soils than in agricultural soils because of their heterogeneity (Allaire et al., 2009). Therefore, the measurement of soil properties needs to consider this spatial heterogeneity, not just on a regional or forest scale but also on a microsite scale. Soil sampling and measurement regimes must account for this variability by capturing a range of topographic indices when selecting sample locations (Salekin et al., 2021a).

Topographic indices include but are not limited to slope and slope location (toe, mid, plane), aspect, elevation, curvature, wind exposure and wetness (Salekin et al., 2021a).

These indices alter soil forming and weathering factors, making forest soils highly variable horizontally and vertically. For example, soils at high elevations in a catchment may also be exposed to harsher climactic conditions such as direct sunlight and wind. These erosion agents may cause higher weathering rates, meaning shallower and poorly developed soil. However, in the same catchment, soils may be well-formed, water-logged, or have different parent material at lower elevations. With this in mind, soil sampling must be conducted to capture this spatial heterogeneity.

1.3 Understanding Forest soil microsite heterogeneity and climate change

Sustainable forest management can positively combat the effects of climate change, help maintain biodiversity and contribute to local, national and global efforts to mitigate the impacts of climate change (De Jong, 2016). Climate change has brought on more frequent and more extreme weather events. Minimising the impact of these weather events on communities will become increasingly vital from a humanitarian, economic and social perspective (Brandon, 2014). Planted forests have historically been used on erosion-prone land for stabilisation and flood mitigation (Brandon, 2014; Lynn et al., 2009). While overland flow may be prevented in forested catchments during low and medium-intensity and duration precipitation events, they are ineffective during storm events of larger magnitudes with high-intensity precipitation. At best, flood mitigation appears localised (Bathurst, 2014; De Jong, 2016). With this in mind, managing individual, small catchments within a larger forested catchment using localised attributes such as slope, aspect, soil, bedrock, and parent material may be a far more effective strategy for deciding what species should be planted, where to plant trees and if in fact, planting would be an effective flood and erosion mitigation strategy.

In periods of drought, planted forests experience water stress, particularly in areas where irrigation treatments are unavailable (De Jong, 2016). Understanding the spatial heterogeneity of soils in planted forests would enable landowners to understand which soils are more prone to drought and carry out targeted planting and treatment. However, understanding the microsite variability on a more localised scale is necessary.

Therefore, a more efficient, low-cost, non-destructive approach to mapping forest soil properties would be helpful for mapping and understanding forest productivity, management, climate change impacts, and forest hydrology.

1.4 Research aim and objectives

1.4.1 Overarching objective and research questions

The overarching aim of this thesis is to identify if electromagnetic induction technology can be used in a forested environment to capture the spatial heterogeneity of soil properties. If so, this thesis can serve as a 'toolbox' for measurement protocols and analysis for forest owners interested in low-cost, time-effective methods of understanding microsite heterogeneity in their forest soils to guide management practices. To achieve this, the three questions posed were:

1. What effect (if any) does forest litter and instrument drift have on apparent electrical conductivity, and what implications does this have for users of EMI technology in forested environments?
2. Can soil texture and moisture properties be characterised across forested catchments using apparent electrical conductivity measured by the DualEm-1?
3. Can model electrical conductivity using quasi-3D inversion software adequately capture the spatial heterogeneity of forest soils. If so, what does this mean for users of EMI technology in forested environments?

1.4.2 Thesis structure

This thesis consists of five chapters. Chapter One discusses the importance of forest soils, how they differ from agricultural soils and the need for low-cost, time-efficient, portable methods of mapping soil heterogeneity in forested catchments.

Chapter two focuses on previous research into using electromagnetic induction technology to identify spatial trends in soil physical and chemical properties and locate the extent of underground geomorphological and anthropogenic structures. This chapter also recognises key knowledge gaps and the importance of further research, particularly into using this technology in forested environments.

Chapter three provides site history, geology, and soil classifications. To reduce repetition in explaining methodology, general methods for study setup that are alluded to in subsequent chapters are outlined in this chapter.

Chapter four evaluates the effect of forest litter and instrument drift on apparent electrical conductivity and the implications of these factors when using electromagnetic induction technology in forested catchments.

Chapter five uses statistical analysis to understand the relationship between measured soil variables and apparent electrical and modelled electrical conductivity. Spatial analysis of the relationship between soil variables and apparent electrical conductivity and modelled electrical conductivity using ordinary kriging and 1D-laterally constrained inversion software to map apparent electrical conductivity as well as using quasi-3D inversion to modelled electrical conductivity. Finally, this section discusses the implications of this research for forest managers who want to understand the microsite variability of soil properties in their forests.

Chapter six synthesises the main conclusions from this thesis in a general discussion. The findings will attempt to address this thesis's overarching objective and recommend ideas for future research.

Chapter 2 :

Previous research and knowledge gaps

2.1 Introduction to geophysical sampling technology

Various non-destructive geophysical methods are increasingly being used to expedite the measurement of soil properties and soil monitoring. Almost without exception, studies using non-destructive geophysical methods for soil monitoring and soil property measurements champion this technology as the time and cost of sampling are significantly reduced compared to traditional soil sampling methods. Examples of non-destructive, geophysical sampling technology used include the use of ground penetrating radar (GPR), electrical resistivity meters (ERM), and electromagnetic induction (EMI) produced by companies such as Veris Technologies Inc, GEONICS Limited and DualEm Inc. This technology is often used in landscapes where measurement equipment can be drawn by a vehicle or carried by hand to achieve the spatial resolution necessary to capture spatial variability. The use of these technologies is often limited to flat, easily accessible land as the equipment can be bulky, heavy or require setup and dismantling before and after measurements are taken. In some cases, for example, the VERIS 2000XA ER type sensor, the instrument must directly contact moist soil during measurements to a depth of 2.5 to 5 cm (Veris Technologies Inc, 2010). The DualEm (DualEm Inc, 2010) can take non-destructive, repeatable samples that can capture the spatial variability of soils in a forested catchment while being portable and can be held by the operator and used in difficult-to-manoeuvre and access terrain.

2.2 Dualem, electromagnetic induction, and general operation

2.2.1 DualEm

The DualEm is an instrument that uses electromagnetic induction to measure the conductivity of the earth's surface. It can be applied to many types of shallow earth investigations (DualEm, 2014) including, but not limited to, archaeological exploration and resource exploration (DualEm, 2014; Tang et al., 2020), soil contamination and precision agriculture (Farooque et al., 2020; Saey et al., 2009), locating gravel deposits, mapping saline intrusions, detecting carbonate rock cavities and karst structures, mapping bedrock topography and locating pipes (McNeill, 1980).

Each DualEm holds one electromagnetic (EM) transmitter (Tx) and dual geometry pairs of EM receiver coils (Rx) with the windings oriented horizontal co-planer (HCP) and perpendicular co-planer (PRP) to the transmitter (DualEm, 2014). Tx and Rx sensors are encased in a non-conductive, fibre/resin composite tube (DualEm, 2014). DualEm Inc. produces a series of DualEm devices with increasing numbers of dual geometry Rx sensor pairs. The quantity of Rx pairs and array lengths (Tx – RX separation distance) are indicated in the product name. For example, the DualEm-1 (the sensor used in this study) has one pair of Rx sensors with an array length of 1 m for PRP and 1.1 m for HCP. The DualEm-2 has one pair of Rx sensors with a 2m array length. Some DualEm devices have multiple Rx pairs. For instance, the DualEm-421 has three pairs of Rx sensors with 4m, 2m and 1m array lengths. The array length is important as this affects the depth of exploration and effective depth, which will be discussed in **Section 2.2.3**.

Figure 2.1. *DualEm array with one transmitter (Tx) and receiver coils (Rx) pairs with windings oriented in horizontal co planer (HCP) and perpendicular co planer (PRP) (DualEm, 2014) (above). DualEm-1 in use at Scion's Kauri nursery in Rotorua, New Zealand (below).*

2.2.2 Electromagnetic induction and low induction numbers

The sensors operate under low induction numbers (LIN), allowing surfaces that are typically non-conductive or have low conductivity, such as soil and rock, to be measured using EMI (DualEm, 2014; McNeill, 1980). Electromagnetic induction works when an alternating current at a frequency of 9-kHz (DualEm, n.d.) is generated within the Tx coil, which creates a primary magnetic field (H_p) within the soil profile when placed on the earth (**Figure 2.2**) (McNeill, 1980; Tang et al., 2020; Wait, 1962). Since most soils can conduct or accumulate an electrical charge, a time-varying magnetic field arises from the alternating current in the transmitter coil. This induces very small eddy currents (secondary alternating currents) in the earth, which generate a secondary magnetic field (H_s)(**Figure 2.2**) (McNeill, 1980; Tang et al., 2020; Wait, 1962). The Rx coils detect H_s together with the primary magnetic field, and a ratio of H_p to H_s is used to calculate apparent electrical conductivity (EC_a, mS/m) (**Figure 2.2**) (McNeill, 1980; Tang et al., 2020).

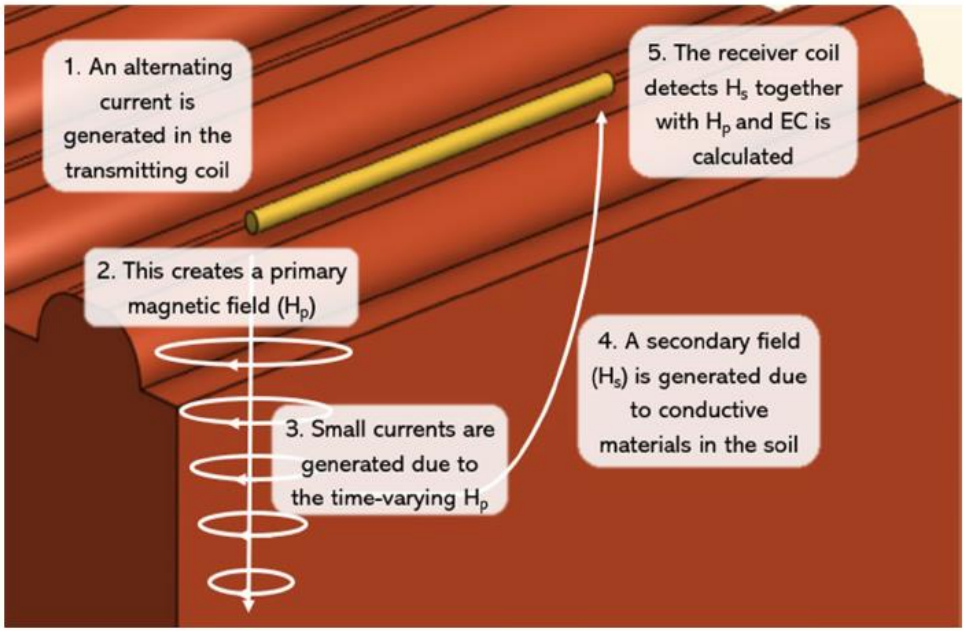

Figure 2.2. *Graphics showing the process of electromagnetic induction is generated through a soil medium using the DualEm (Tang et al., 2020).*

Equation 1. *Calculation of apparent electrical conductivity using the ratio of the primary and secondary magnetic field (McNeill, 1980).*

$$\frac{H_s}{H_p} \simeq \frac{i\omega\mu_o\sigma S^2}{4} \quad (1)$$

$$EC_a = \frac{4}{\omega\mu_o \sigma r^2}\left(\frac{H_s}{H_p}\right) \quad (2)$$

Where H_s = Secondary magnetic field at the receiver coil

H_p = Primary magnetic field at the receiver coil

ω = 2πf

f = Frequency (Hz)

μ_o = Permeability of free space

σ = Ground conductivity (mho/m)

S = Intercoil spacing (m)

i = $i = \sqrt{-1}$

2.2.3 Depth of exploration and effective depth

The DualEm-1 (the series of DualEm used in this study) comprises one Tx and one pair of dual geometry Rx sensors simultaneously measuring cumulative EC_a to two depths, 50cm and 160cm. The depths to which the Rx sensors reach depend on the depth of exploration and the effective depth (DualEm, 2014) (**Table 2.1**).

The effective depth (ED) of a DualEm is the depth to which a Tx – Rx configuration or array length accumulates half of its total sensitivity (DualEm, 2014). For the DualEm-1, the ED is 0.3 m for the PRP array and 0.9 m for the HCP array (**Table 2.1**) (DualEm, 2014).

The depth of exploration (DOE) is the depth to which an array length accumulates 70% of its total sensitivity (DualEm, 2014). The DualEm-1 has a DOE of 50cm for the PRP array and a DOE of 160cm for the HCP array (**Table 2.1**) (DualEm, 2014).

Table 2.1. Effective depth, depth of exploration and low induction number limits for the DualEm-1 (DualEm, 2014).

Receiver coil Orientation	Transmitter – Receiver separation (m)	Effective depth (m)	Depth of exploration (m)	Low induction number limit (mS/m)
PRP	1	0.3	0.5	2700
HCP	1.1	0.9	1.6	240

HCP and PRP sensitivity is also affected by array length (**Figure 2.3**). The PRP array accumulates more rapidly with depth and is, therefore, more sensitive as depth increases. Beyond a depth of 0.6, there is little to no sensitivity. In comparison, HCP accumulates sensitivity more gradually with depth (**Figure 2.3**)(DualEm, 2014). The cumulative sensitivity may be used as a guide for DOE as it indicates the depths where PRP and HCP are relatively insensitive to a response from the earth (DualEm, n.d.). The factors affecting cumulative sensitivity are outlined in **Sections 2.2.5** and **2. 3**.

The height of the Dualem above the earth's surface also affects the EC_a signal. It is assumed that ambient air has an EC_a of zero with an increase in the height of the DualEm above the earth's surface, there is a decrease in DOE(DualEm, n.d.; Serrano et al., 2014).

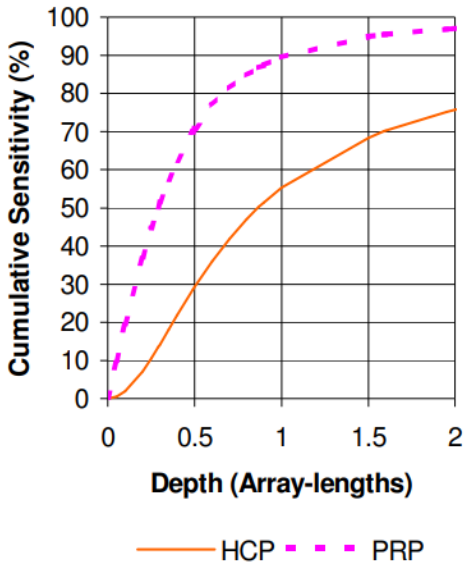

Figure 2.3. *Cumulative sensitivity of HCP and PRP receivers as Tx – Rx separation (Array-length) and, therefore, depth of exploration increases (DualEm, 2014).*

2.2.4 General operation

The DualEm can run in two modes: automatic and manual. Automatic mode allows a series of measurements to be taken at specified time intervals, whereas manual mode allows the user to prompt the device to take a measurement manually. Typically, DualEm devices with longer array lengths are set to automatic mode, attached to a cart or other protective structure and pulled by vehicle across relatively flat terrains, mainly in agricultural settings but also on archaeological sites (Dabas et al., 2016). Tests are conducted to ensure the vehicle itself, the noise from the engine, and the protective structure do not influence the signal (Dabas et al., 2016). Dabas et al. (2016) found that noise from the vehicle engine is more likely to affect the shallower PRP signal than the deeper HCP signal; however, the effect was insignificant, and they were unable to establish the exact cause.

2.2.5 Pitch and roll

The pitch and roll of all DualEm instruments are collected by DualEm's accelerometer simultaneously with each measurement (DualEm, 2014). While both are important, the orientation of the Tx and Rx to the earth's surface will affect how much ambient air, user interference (whether it be vehicles, humans, or other artefacts), non-target soil and other factors influence the signal. Therefore, the roll of the instrument provides the most significant change in EC_a. Since this variable can be measured, the instrument's recommended roll is no more than $10^{o}\pm$ (Dabas et al., 2016).

2.3 Applications of electromagnetic induction technology and factors affecting apparent electrical conductivity

2.3.1 Overview of the applications of electromagnetic induction sensors

Electromagnetic induction technology has been used in different environments because of the ease with which the technology can capture small and large-scale variability of soil properties across study sites. These include but are not limited to, agricultural and pastoral land with a variety of crop covers, orchards (Urdanoz & Aragüés, 2012), vineyards (Lardo et al., 2012), cacao plantations (Caires et al., 2014; Silva et al., 2021) and wetlands (Atwell et al., 2013). Only a handful of studies found used EMI technology in a forest environment. These include one study in native tropical forests and teak plots (Bréchet et al., 2012), another in marsh forest land in the humid tropics of Trinidad (Atwell & Wuddivira, 2019), a third in an

Eucalyptus plantation in western Australia affected by saltwater intrusion (Bennett & George, 1995) and two studies in New Zealand, the first in the central North Island in a P. radiata (D. Don) nursery (Lad et al., 2019) and the second in the Canterbury region of the South Island in a young P. radiata plantation with no canopy closure and on an ex pasture site (Gallart et al., 2019).

Each of these environments hosts a range of factors affecting the EMI signal and, therefore, EC_a, which will be discussed in more detail below. These environmental factors allow EMI technology to be used to explore soil and geological attributes in such a wide variety of environments.

2.3.2 Overview of factors affecting apparent electrical conductivity

The apparent electrical conductivity (EC_a) values calculated by electromagnetic induction (EMI) sensors are an "integrated value based on the depth-related sensitivities of the instrument and the depth dependant drivers of conductivity" (Hossain et al., 2010). Fluctuations in soil EC_a can vary significantly over space and a little over time and the causes of which include but are not limited to, soil physical properties (texture, porosity, permeability, bulk density, compaction, pans, stratification, temperature, soil-water repellence), chemical properties (pH, organic matter, mineralogy, salinity, cation exchange capacity), geology, hydrology and topographic features (depth to rock, rock type, age, geological structures, water table depth), water content (soil moisture content, the degree of saturation, rainfall), land management (tillage regimes, irrigation, drainage, land degradation, land use changes) (Atwell & Wuddivira, 2019) and anthropogenic artefacts (buried objects, soil disturbances, archaeological artefacts) (Callegary et al., 2007; Mari, 2020; McNeill, 1980; Palacky, 1988). Topographic features such as elevation, aspect and slope indirectly affect EMI, given these factors affect the development of the aforementioned factors.

2.3.3 Apparent electrical conductivity and soil texture

Soil textural properties impact electromagnetic induction (EMI) signals by increasing or reducing soil resistivity (**Figure 2.4**). Finer-grained soils (clays and silts) are more conductive and, therefore, have higher conductivity than coarser-grained soils (sands and gravel). Because of this, EMI technology is used to better understand the spatial variability of soil textural properties for varying purposes.

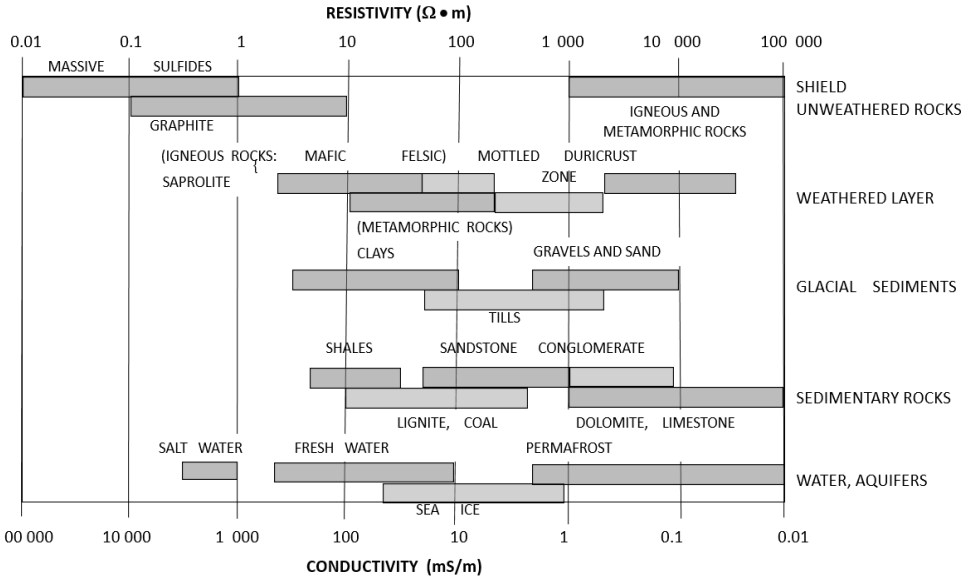

Figure 2.4. *Typical ranges of conductivities (mS/m) of earth materials (Palacky, 1988).*

The DualEm-2 (refer to **Section 2.2.1** details regarding DualEm versions) was used by De Smedt (2011) to model the depth to a sandy substrate to identify buried river systems (De Smedt et al., 2011). Triantafilis et al. (2011) used the DualEm-421 (refer to **Section 2.2.1** for details regarding DualEm versions) to identify the depth and spatial variation of a coarse-textured, highly permeable, aeolian sands to understand how a leachate plume of solid waste may travel to and enter groundwater in an ex-waste site from World War II in South East Sydney (Roe et al., 2010; Triantafilis et al., 2011). While Saey et al. (2009) used the DualEm-21s and the EM38DD to firstly compare the efficacy of both instruments and secondly to create a stratigraphic inventory to understand better the spatial variation of tertiary marine clay overlying aeolian loess in Heerstert, Belgium in the European Loess belt (Saey et al., 2009).

2.3.4 Apparent electrical conductivity and earthworm abundance

Soil texture and physical properties can also predict other ecological factors. Three studies looked at quantitatively predicting earthworm populations in a vineyard with varying cover crop and nutrient/pesticide regimes (Lardo et al., 2012), arable land rotating maise and cereal (Joschko et al., 2010), and in a tilled, arable field (Valckx et al., 2009). Earthworms influence soil structure by forming macropores and can decrease bulk density and available moisture content while increasing soil aggregate stability (Lardo et al., 2012). Valckx et al. (2009) refer to earthworms as ecosystem engineers who "determine the spatial patterns of important ecosystem processes at a field scale".

The three studies above found earthworm abundance and specific species of earthworm (anecic and endogeic) correlated with EC_a values. The instrument was ultimately helpful in identifying potential habitats for soil biota, which could predict the number of earthworms. However, one study also established that earthworms from the two ecological categories resided in habitats with specific soil characteristics, such as organic matter content, physical and chemical properties, soil volumetric water content and management practices (Valckx et al., 2009). These characteristics affected EC_a signals and were therefore determined as a proxy for understanding where earthworms reside. The more favourable the habitat, the more abundant earthworm presence was (Joschko et al., 2010; Lardo et al., 2012; Valckx et al., 2009).

Joschko et al. (2009) examined the change in soil textural properties on tillage and whether the texture difference affected earthworm spatial distributions. Joschko et al. (2009) found soil texture, particularly fine particle size, was an important factor in estimating earthworm parameters. Soil organic carbon (SOC) at 0 to 15 cm was the most important predictor of earthworm abundance that year. The study also found earthworm abundance increased in localised regions of finer textured soil under a reduced tillage regime, yet no uniform response to a reduced or conventional tillage regime (Joschko et al., 2009).

2.3.5 Apparent electrical conductivity and macroporosity

Earthworm engineering creates burrows which differ considerably between earthworm species in size, shape, depth, and orientation, and the structures can create nearly

impermeable and tortuous pathways that affect soil hydrology (Trojan & Linden, 1998). Despite earthworm engineering altering macroporosity and bulk density, the above studies did not test macroporosity as an influencing factor of EC_a. Trojan and Linden (1998) also identified a lack of research on soil's hydraulic properties related to macroporosity caused by earthworm activity (Trojan & Linden, 1998).

Macroporosity affects the infiltration rate and vertical and lateral water flow in forested catchments. Hewlett and Hibbert developed the variable source area (VSA) concept in the 1960s (McDonnell, 2009). Their theory was that areas near streams become saturated and very quickly contribute to overland runoff into streams. During heavy rainfall or drier periods, the VSA would expand or contract. However, large macropores, called soil pipes, channel water vertically and horizontally and store water, meaning forested catchments rarely experience runoff. These pipes form from various turbation processes, predominantly from the growth and decay of large roots. When rainfall occurs, the "old water" stored in macropores is pushed out into storm flow or groundwater and makes way for "new water" (Amatya et al., 2016; McDonnell, 2009). The storage of water in these macropores, or lack thereof, could alter the EC_a signal. Macropores that are dry or predominantly air-filled could reduce ECa, and macropores that are predominantly wet could increase EC_a. If this is the case, does this change depend upon the VSA of the catchment?

2.3.6 Apparent electrical conductivity and soil organic carbon

There is a relationship between soil organic carbon (SOC) and apparent electrical conductivity (EC_a), which has been used for spatial estimations of SOC. Martinez et al. (2009) found that EC_a could explain >25% of spatial variation in SOC (Martinez et al., 2009). Huggins and Uberuaga (2010) showed only a weak relationship between EC_a and SOC at shallow depths (0 – 30 cm) and no significant relationship at deeper depths (30 – 153 cm). However, both Huggins and Uberuaga (2010) and Terra et al. (2004) found EC_a, along with slope, elevation and other topographic indexes, could explain 50% - 57% of SOC variability.

2.3.7 Apparent electrical conductivity, vegetation cover and biological mats

In forest environments, a litter layer of varying degrees of thickness develops above the A horizon, while in agricultural settings, land cover is generally some form of crop, pasture or

bare soil. Serrano et al. (2014) investigated the effect of vegetation cover on EC_a measurements using two types of sensors: a resistivity sensor and the DualEm. In this scenario, vegetation cover was both ungrazed and grazed pasture measured in February 2012 and February 2013, respectively. The DualEm' s mean EC_a signal was more sensitive to changes in vegetation or crop cover as EC_a decreased (PRP = 66.1 mS/m & HCP = 76.3 mS/m for ungrazed and PRP = 20.0 mS/m & HCP 30.6 mS/m for grazed) after the site was grazed compared to the resistivity sensor which remained relatively consistent between treatments (4.0 mS/m for ungrazed and 6.8 mS/m for grazed at 0.30 m depth). The difference between sensors was most likely due to the resistivity sensor requiring soil contact during measurements at the same depth, whereas the DualEm does not need soil contact during measurements.

There were a few issues in the way the study collected data. Soil samples were collected at a depth of 0 to 30 cm with an assumption that this is representative of the full soil profile for organic matter, soil moisture, soil minerals and salt when, in reality, soil physical and chemical properties are heterogenous both horizontally and down a soil profile (McLaren & Cameron, 1996). The study notes that soil moisture content was lower during the 2012 ungrazed season and higher during the 2013 grazed season. Apparent electrical conductivity was measured on the same day in February 2012 and 2013, and the study did not go on to establish if soil moisture content was affected by grazing. However, it did investigate topographic factors which may have caused this difference. However, no control measurements were taken in either grazed or ungrazed treatments, and there is no mention of precipitation events during or before EMI measurements. If measurements were taken after grazing, could nutrients from urine patches or excrement, or soil compaction from stock have been a contributing factor to changes in EC_a and could it have been these changes that the DualEm is more sensitive towards when compared to the other instrument?

If vegetation or crop cover does affect EC_a, to what extent does it affect EC_a in a forest environment? The forest floor hosts an accumulation of litter from the understory and canopy, fine root and microbial activity (Ogée & Brunet, 2002). The litter layer and the upper few centimetres of mineral soil are like a biological mat covering the hillslope. It's most important aspect is high porosity and hydraulic conductivity (Amatya et al., 2016). "Litter tissue alone can account for more than 70% of above-ground litter fall in forests with the rest

composed of stems, small twigs and propagative structures" (Krishna & Mohan, 2017). The litter layer, in particular, is a source of water vapour, heat and CO_2 and is an exchange point between underlying soil and overlying air (Ogée & Brunet, 2002). The litter layer comprises rapidly draining, undecomposed leaves, twigs, and humified matter, all with water storage capacity. Studies using soil, vegetation, and atmosphere transfer models (used to predict water dynamics in agriculture and forestry) found these models to be sensitive to variables such as temperature and moisture present in the litter layer. Including this factor in their models meant they could better reproduce observed results at sites (Haverd & Cuntz, 2010; Ogée & Brunet, 2002).

Suppose this biological mat is highly porous and has a different moisture content or air temperature than the underlying soil. These factors may reduce or increase the EC_a signal, assuming the pores are filled with air or water. If this is the case, vertical sounding (discussed in **Section** 2.4.3) or a quasi-3D inversion of the EC_a can be conducted better to separate the biological mat from the mineral soil layers to understand the signal and underlying soil properties.

2.3.8 Apparent electrical conductivity and salinity

Apparent electrical conductivity increases with an increase in mineral salts as the electrolytes formed conduct electricity (Mari, 2020). The concentration of dissolved salts varies spatially and with depth depending on existing chemical elements found, soil texture and the ability of rainwater to penetrate the soil. As water dilutes salt concentrations in the upper soil horizons, this leaches at diluted concentrations to lower horizons (Mari, 2020). Electromagnetic Induction technology allows the distribution of saline soils in a soil profile across a landscape to be better understood to determine best management practices (Huang et al., 2017a). For example, shallow, saline water tables present in the drylands of Australia are used to produce crops that are both tolerant and intolerant to salt as well as pasture (Huang et al., 2017a).

The seasonal rise and fall of saline water tables remobilise salt concentrations in the soils, affecting crop and pasture growth (Huang et al., 2017a). Huang et al. (2017a) identified a positive correlation between changes in EC_a and soil salinity. They found soil salinity

increased with a decrease in elevation and used this understanding to predict secondary soil salinity (Huang et al., 2017a). The application of this modelling could be used as a management strategy to strategically plant tall native woodlands with deep roots in areas that would minimise recharge during rainfall events to lower-lying areas, which could decrease secondary soil salinity (Huang et al., 2017a).

2.3.9 Apparent electrical conductivity and volumetric water content

Volumetric water content (VWC) and the spatial variability of VWC is the most critical factor influencing the spatial variability of apparent electrical conductivity (EC_a) and has been correlated with the spatial variability of VWC even more so than its relationship of EC_a to soil salinity (Brevik et al., 2006; Hossain et al., 2010; McNeill, 1980). For example, Hanson and Kaita (1997) looked at the relationship between EC_a, soil moisture content and soil salinity using three different salinity treatments with decreasing soil moisture over time. The study found a strong, negative, linear relationship between EC_a and decreasing VWC over time, with the EC_a being more sensitive to changes with lower VWC and less sensitive with higher VWC. Conversely, EC_a was more sensitive to changes in soil salinity at high soil water contents and less sensitive to smaller water contents.

The study by Hanson and Kaita (1997) poses a few issues. This includes the proximity to the time domain reflectometry (TDR) sensor used to measure VWC when the EC_a measurements were taken and the effects of changes in soil moisture with no treatment (i.e., no control treatment with zero soil salinity). Furthermore, no consideration was given to the variable sensitivity of TDR sensors to low and high levels of salts in the soils. The salts cause a dampening effect on electrical conductivity to the TDR signal (Hook et al., 2005; McIsaac, 2010; Meter Group, n.d.) Because high EC_a affects the wave propagation, leading to errors estimating the dielectric permittivity of soil (Zemni et al., 2019).

TDR sensors and gravimetric measurements of soil water in the laboratory (as described below) are the most common in studies measuring VWC to identify a relationship between EC_a and VWC. Applications of this relationship predominantly reside in precision agriculture, where crop yield is directly related to soil moisture content and, therefore, EC_a (Tang et al., 2020; Triantafilis & Santos, 2013).

One limitation of TDR sensors is that they must be inserted into the ground and physically contact the soil. Destructive soil sampling and the use of TDR provide local information only about VWC and GWC and are invasive and time-consuming (Farooque et al., 2019). Because the sampling process is destructive, replication over time is not possible. Additionally, once sampling has taken place, EC_a measurements cannot be repeated in the exact location from the disturbance caused; therefore, studies such as Tang et al. (2020), who made multiple EC_a and TDR measurements throughout the year, were required to do so at different locations.

All studies that compare EC_a and VWC appear to use technology that measures VWC at singular points in time, whether by TDR or in a lab, to establish if VWC is a factor affecting EC_a. Continuous VWC data tends not to be used as only the relationship during the EMI measurements campaign is required. However, the spatial variability of VWC is essential to capture.

Volumetric water content is spatially variable; therefore, VWC sensor placement and sampling regimes must account for this variability by capturing a range of topographic indices (as discussed in Chapter 1) when selecting sample locations (Salekin et al., 2021a). The spatial variability of VWC has been studied extensively (Vereecken et al., 2015) in various settings, including forestry (Blume et al., 2009; Wiekenkamp et al., 2016). There are limitations and challenges to establishing a large-scale sensor network that captures VWC data to explain the spatial variation in VWC reliably to extrapolate localised data on a large scale. Therefore, using repeatable and non-destructive EMI sensing would be advantageous where time-series VWC data could be used as calibration and validation datasets. Thus, relationships between EC_a and VWC peaks, wetting and drying periods before and after precipitation could be studied. However, a question remains over what VWC data should be used: an average of VWC over time, only VWC outside of precipitation events and if extremely wet or dry periods should be included or excluded.

However, as VWC is dynamic, several variables could be considered to quantify this relationship. For example, EC_a could be used to predict peaks in VWC. Additionally, VWC is only more suitable for measuring changes in soil moisture, not available water to plants. So,

soil water potential could be a more appropriate parameter to establish a relationship (if any) with EC_a.

2.3.10 Apparent electrical conductivity and crop yield and plant growth

As with earthworm abundance (**Section 2.3.4**), apparent electrical conductivity (EC_a) has been used to predict crop yield and plant growth by using the relationship between EC_a and factors affecting EC_a. For example, the relationship between volumetric water content (VWC) and EC_a was used to predict tuber potato growth (Tang et al., 2020). The relationship between soil texture and EC_a was used to predict nitrogen fertiliser response and tree growth in a young P. radiata stand (Gallart et al., 2019) and again by Bottega et al. (2022) to predict soybean yield. The relationship between salt concentration and EC_a was used to predict the growth of Eucalyptus globulus to be harvested for timber and pulp (Bennett & George, 1995). Other researchers looked at the relationship between EC_a and the factors affecting EC_a to create management zones for, for example, irrigation regimes (El-Naggar et al., 2021b) and alter crop management regimes based on varying soil fertility indicators (Caires et al., 2014; Silva et al., 2021).

Gallart et al. (2019) investigated the genotype performance (growth) of P. radiata in response to different nitrogen fertiliser applications, and this study demonstrated why the heterogeneity of soil properties is an important factor in predicting plant growth (Gallart et al., 2019). Firstly, the use of EMI technology before establishing this trial would have enabled the study to consider the heterogeneity of soil properties when designing the experiment. The study found that the growth volume was higher in control plots than those chosen for various nitrogen treatments. It was later discovered that EC_a was higher in control plots than in treatment plots, which was attributed to differences in soil texture (Gallart et al., 2019). Soil heterogeneity was not captured by the block design of the experiment when EC_a was a covariant. It was hypothesised that soil EC_a represented courser soil and, therefore, had lower water holding capacity, which affected tree growth during periods of drought. Thus, water availability (as opposed to nitrogen availability) was the limiting factor in tree growth. Decreases with greater soil texture influence water holding capacity, and during periods of drought, courser textured soil was not favourable for N uptake in the treatment plots, which may have caused the unexpected, higher volume of growth in the untreated stands (Gallart et al., 2019) as the texture had a confounding effect

on the results. Had EMI been used before the experiment was established, the experimental design could have factored this spatial heterogeneity into the layout of the plots.

Secondly, the higher growth was due to a combination of three variables: spatial heterogeneity of soil properties, understory vegetation spatial distribution and nitrogen source. The study found that the interactive effect of these variables made some individual trees and genotypes more susceptible to drought conditions. Gallart et al. (2019) concluded the need for tree establishment criteria for breeding and planting programs that consider the strategies used by different P. radiata genotypes to adapt to efficient N use, which includes how microsite variability affects N use and tree growth. EMI technology offers an efficient and cost-effective method for such a detailed investigation.

2.3.11 Electromagnetic induction, geology and groundwater

Electromagnetic induction (EMI) technology has been used to identify subaerial structures without requiring intensive and destructive excavation. Farooque et al. (2020) used the DualEm-2 to investigate water table depth (WTD) and seasonal fluctuations of WTD as an indicator to determine irrigation schemes to increase crop yield (Farooque et al., 2020). They suggest using the findings to inform crop rotation to maximise yield (Farooque et al., 2020). Karst structures were examined in Ouldja, Algeria, where a deep sinkhole opened on farmland. The EM31 (GEONICS, Mississauga, ON, Canada) EMI sensor and the Syscal Junior ER sensor (IRIS, Orléans, France) were used to identify different subsurface and shallow geological features, respectively (Fatma et al., 2020). Using the combined dataset, the study was able to locate superficial limestone formations below the overlying alluvium deposits and the existence of growing karstic cavities. Both discoveries pose a significant hazard to those tending the land for agricultural purposes and future land uses (Fatma et al., 2020). Therefore, understanding the underlying geological hazard can help current and future landowners mitigate risk in the future.

2.3.12 Electromagnetic induction and artefacts

Electromagnetic induction (EMI) instruments that measure LIN simultaneously measure soil EC_a and apparent in-phase magnetic susceptibility (χ_a), measured in parts per thousand (ppt). Apparent in-phase magnetic susceptibility allows the instrument to be used when analysing

archaeological sites (DualEm, 2014; Thiesson et al., 2017). A soil's magnetic susceptibility is greater than zero, and the in-phase DualEm measurement illuminates near-surface magnetic features. Because of this, the DualEm can detect buried metal and non-metal objects as they present either regions of low or high magnetic susceptibility compared to their surrounding area (Huang et al., 2003). For example, the technology has been used to locate underground pipelines and metal drums (DualEm, 2014) and M19 anti-tank mines with very little metal content (Huang et al., 2003).

2.3.13 Apparent electrical conductivity, land use and land cover

Atwell and Wuddivira (2019) found the spatial variation of apparent electrical conductivity (EC_a) differed under different land uses, and more specifically, the dominant factor affecting EC_a differed. Volumetric water content (VWC) and silt content had a significant, positive relationship with EC_a under marsh forest. In contrast, the EC_a of an adjacent block of agricultural land had a strong negative relationship with VWC and pH. In addition, grassland in the same region had high EC_a due to a clay pan formed from regular ploughing, which had the most significant influence over the EC_a signal (Atwell & Wuddivira, 2019).

2.3.14 Apparent electrical conductivity and temporal changes

Over time, changes in EC_a depend on the study area's temporal dynamics. For example, coastal tidal flats are where storms, waves, tides, currents, and precipitation are dynamic, and moisture and salinity change simultaneously with these processes (Weymer et al., 2016). Seasonal measurement campaigns using electromagnetic induction (EMI) technology in Laguna Madre wind-tidal flats presented high variability of EC_a between seasons. Specifically, surveys were conducted during dry periods where the underlying geology could be characterised, whereas those features were masked during wet conditions. However, the study also found that EC_a was negatively correlated with topography (Weymer et al., 2016). Similarly, fluctuations in water tables can be measured over time, and EMI technology, specifically the DualEm-2, has been used to predict the seasonal oscillations and spatial distribution of WTD (Farooque et al., 2020).

Farooque et al. (2020) also acknowledged that crop moisture, evapotranspiration, variable meteorological data, and soil conditions were sources of error in predicting the

spatiotemporal variability of WTD using EC_a at the study site. However, a study conducted at a P. radiata nursery in the central north island of New Zealand found no significant changes in EC_a over time despite significant rain events occurring between measurement campaigns (Lad et al., 2019). Temporal changes in EC_a can also be caused by signal drift. More information on the causes of signal drift is outlined in **Section 2.5.6**.

2.4 Measurement protocol and interpolation of apparent electrical conductivity

2.4.1 Measurement frequency

Most studies using electromagnetic induction (EMI) technology, specifically the DualEm series instruments, were conducted in agricultural settings, on flat land, and accessible by vehicles (Serrano et al., 2014; Simpson et al., 2009). Consequently, most sampling was automated, and the instruments were typically towed by a vehicle with a sampling frequency ranging from 0.20 m to 1 m per second (Dabas et al., 2016; De Smedt et al., 2011; Saey et al., 2009). The devices were typically secured in and pulled by a sledge, resulting in a standard elevation of 0.16 m (Saey et al., 2009; Serrano et al., 2014; Simpson et al., 2009). Tang et al. (2020) manually placed the DualEm-2 sensor at each sampling location to measure EC_a at the height of 0cm, while Triantafilis et al. (2011), Triantafilis and Santos (2013) and Zare et al. (2018) manually carried the DualEm sensors of varying coil separation between 0.10 and 0.30 m above the ground.

2.4.2 Measurement protocols

Transects were the most common method of sample configuration (De Smedt et al., 2011; Saey et al., 2009; Simpson et al., 2009), followed by a grid-like formation where separation of transects within the grid often (Saey et al., 2009) but not always (Serrano et al., 2014; Simpson et al., 2009) related to the Tx and Rx separation of the sensor to ensure the entire study site was mapped. De Smedt et al. (2011) used the DualEm-2 to capture paleochannel morphology and used a 0.2 metres per second sampling frequency using transects two meters apart, which allowed 1 ha per hour coverage (De Smedt et al., 2011). Stockmann et al. (2017) capture a range of EC_a along topographic sequences using aerial maps to decide placement.

Other studies did not detail the exact measurement configuration; however, from produced maps, the sensors were either driven around study sites in the most effective/efficient manner or randomly selected locations were sampled (Urdanoz & Aragüés, 2012).

2.4.3 Vertical electrical sounding

To better understand changes in EC_a down the soil profile, vertical electrical sounding (VES) techniques were developed. Tang et al. (2020) created a plastic, non-conductive elevator to elevate the DualEm to a selected and repeatable height to conduct VES, a process by which apparent electrical conductivity (EC_a) readings are taken at the same location at varying heights (Tang et al., 2020) (**Figure 2.5**). As the height of the EMI instrument increases, its sensitivity to the earth and, therefore, EC_a decreases (**Figure 2.6**) (DualEm, n.d). Vertical electrical sounding works using the theory that "material below the array consists of a given depth of air with zero conductivity, over an earth with a greater conductivity. The apparent conductivity will be the sum of the sensitivity to the air times the conductivity of the air, plus the sensitivity to the earth times the conductivity of the earth" (DualEm, n.d). This study showed that this technique can be used for building stratigraphic correlations and profile analysis.

Figure 2.5. *DualEm-2 Elevator for vertical electrical sounding (VES) (Tang et al., 2020).*

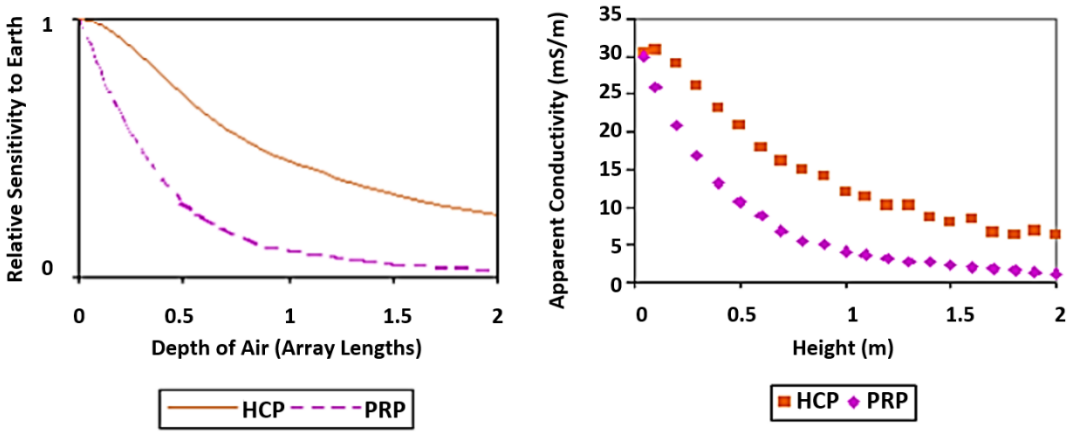

Figure 2.6. *Decreasing sensitivity (left) and apparent electrical conductivity (right) of the DualEM-1 to earth's conductivity as the depth of air (left) or the height of the DualEm-1 (right) increases.*

2.4.4 Apparent electrical conductivity interpolation

One common technique for preliminary spatial analysis of apparent electrical conductivity (EC_a) data is creating an EC_a map using ordinary point kriging (Bats et al., 2009; Simpson et al., 2009; Zare et al., 2018). Unsupervised classification methods are then used to homogenise sections of study areas, which are then sampled (Zare et al., 2018) or confined to a grid with a cell size relative to EC_a sampling frequency. The data is then smoothed with a radius mean filter (Simpson et al., 2009) if sampling was not taken in a grid or transect formation.

2.5 Soil sampling and other field and lab measurements for validating EMI data

2.5.1 Establishing a relationship between apparent electrical conductivity and factors affecting apparent electrical conductivity

Establishing a linear regression (LR) equation is the most common approach to determine the relationship between apparent electrical conductivity (EC_a) and the factors influencing EC_a (Triantafilis et al., 2011; Triantafilis & Santos, 2013), and therefore, soil sampling is still required though at a far less intensive rate, to realise EC_a in the context of the study site fully.

Soil samples are commonly used for calibration and validation of apparent electrical conductivity (EC_a) models (De Smedt et al., 2011; Simpson et al., 2009; Zare et al., 2018), and detailed characterisation of soil properties such as texture, structure, grain size, pH, groundwater level and general stratigraphic correlation (Zare et al., 2018).

2.5.2 Capturing the spatial variability of the study site

Capturing the spatial variability of the study site, sample depth, soil collection procedures (soil sampling and field-testing using instrumentation) and analysis vary depending on the needs of the study. Subsequent analysis of these samples relates directly to the purpose of the study, so both soil physical and chemical properties can be measured and used to validate measured EC_a.

Methods include taking a sample every nth distance along a transect (Stockmann et al., 2017), collecting EC_a data and categorising results into low, medium and high or maximum and minimum EC_a, then gathering samples from locations representative of each category (Huang et al., 2017a) or taking auger samples that cover "a range of EC_a" using kriged EC_a maps detailed in **Section 2.2.4** (De Smedt et al., 2011).

Auger samples were typically collected either by Dutch auger, gouge auger or mechanical auger to varying depths and repetitions over space and time. Samples are typically (but not always) taken post electromagnetic induction (EMI) measurement campaign. This way, soil sample locations can be strategically placed to minimise the number of samples required and allow EC_a measurements to occur in the exact location as the sample locations with no soil disturbance. Some studies pooled their samples (Simpson et al., 2009), while most retained individual samples for analysis. Other studies preferred to rely on previously collected samples. For example, Saey et al. (2009) used previously determined clay and silt fractions of quaternary loess material that overlaid a tertiary clay substrate. Formulas were then used to fit the theoretical relationship of EC_a and the clay and silt fractions to reconstruct the clay's depth below the loess material's surface (Saey et al., 2009). The study assumes homogeneity of the clay and silt fraction in the quaternary loess over the study area, so field validation of this model could be of use.

2.5.3 Sample depth

Apparent electrical conductivity is the cumulative response to the soil substrate; therefore, the depth of samples must also be considered, and the approach used depends on the survey conducted. Samples are typically collected either at one depth (e.g. 0 to 0.30 m) (Serrano et al., 2014), multiple samples at varying depths (e.g. 0 to 0.10 m, 0.10 to 0.30 m) (Huang et al., 2017a) or in increments (e.g. every 0.30 m up to 2 m) (Triantafilis & Santos,

2013; Urdanoz & Aragüés, 2012). Depths were selected based on the purpose of the study, for example, studies looking at the root zone of crops sampled to depths of those specific crops (Serrano et al., 2014). Other studies use classical soil sampling practised in their country (Zare et al., 2018). The use of mechanical augers and gouge augers, which accumulate samples, allow sampling to occur to (as opposed to at) a depth and, therefore, across a profile and were typically used in stratigraphic correlation and mapping studies(Bats et al., 2009; Simpson et al., 2009).

Where stratigraphic correlations were an integral part of the study, soil profiles were recorded using samples collected from gouge augers (Simpson et al., 2009), mechanical coring (Bats et al., 2009) and trenches(Bats et al., 2009). Profile locations were selected as described above. Soil profile records and stratigraphic correlation are helpful when using software allowing one, two and three-dimensional modelling of EC_a data.

2.5.4 Soil sample analysis

Once samples were collected, most studies weighed, air dried, and reweighed samples for gravimetric water content (Urdanoz & Aragüés, 2012), then ground and passed through a <2 mm sieve. The sample is then either turned into a saturated soil paste to extract the electrical conductivity (EC_e) (Huang et al., 2017a; Stockmann et al., 2017; Triantafilis & Santos, 2013; Urdanoz & Aragüés, 2012) or cation exchange capacity (CEC) (Triantafilis & Santos, 2013). Volumetric water content was calculated using bulk density (Hossain et al., 2010; Triantafilis & Santos, 2013), while particle size fraction (PSF) of clay, silt and sand was calculated using the Hydrometer method (Atwell & Wuddivira, 2019; Stockmann et al., 2017; Triantafilis & Santos, 2013) or a sedimentographer (Serrano et al., 2014) to inferred soil textural properties Soil carbon content (Serrano et al., 2014; Stockmann et al., 2017), pH (Serrano et al., 2014; Stockmann et al., 2017) and other macronutrients such as nitrogen, potassium and phosphorus (Serrano et al., 2014) were measured in a lab.

2.5.5 Soil temperature

Factors affecting soil temperature include slope, aspect, elevation, soil texture, soil moisture, organic matter, soil tillage and vegetation cover. These factors alter differences in maximum and minimum temperatures and diurnal and seasonal fluxes in temperature. During wet

periods, heat fluxes in forest soils are five to six times smaller in forests than in pasture (Alvalá et al., 2002). Pasture soils have higher average soil temperatures and greater fluxes because the temperature is driven by solar radiation rather than conduction (Beltrami & Kellman, 2003).

Soil temperature can influence EC_a, particularly on frozen soils or when soils reach extreme temperatures (Abdu et al., 2007). Often, soil temperature is collected as a reference dataset to standardise EC_a measurements, and the effect of temperature showed varying results. Several studies showed little change in soil temperature over a measurement campaign (Saey et al., 2009; Simpson et al., 2009; Urdanoz & Aragüés, 2012). However, these studies only used one study site, and soil temperature did not change or change very little over the measurement campaign as measurements were conducted over a day (Saey et al., 2009; Simpson et al., 2009; Urdanoz & Aragüés, 2012).

Abdu et al. (2007) used six thermocouples both in the air around a DualEm-1 and on the bare ground to continuously measure changes in ambient temperature and the ground while setting a DualEm-1 to auto-sample over eight hours. They did so at two sites with both high and low EC_a. Abdu et al. (2007) found signal drift as a function of soil and ambient air temperatures. Hysteresis (refer to **Section** 2.5.6) was more significant in sites with low EC_a than with sites with high EC_a, which was ascribed to a change in soil temperature, which increased soil conductivity and the instability of the sensor mechanics to change in temperature. However, the study did not distinguish between the effect of changes in soil temperature and air temperature hysteresis (Stockmann et al., 2017), so further research may be required to make this distinction, if any.

2.5.6 Air temperature hysteresis and diurnal effects

Over time, the electromagnetic signal (EMI) can drift both in the short term (several minutes) and long term (several hours) (Dabas et al., 2016; DualEm, 2014). Short-term drift (in terms of minutes) can create artefacts in maps if sub-surface features present short wavelengths, which can occur during archaeological exploration (Dabas et al., 2016). Long-term drift (in terms of hours) is less noticeable and most often presents when measurement frequency is set to automatic in metres per second. The drift can be "corrected by standard image

filtering procedures" (Dabas et al., 2016; Delefortrie et al., 2014). Signal drift can be caused by changes in internal temperature, battery voltage, direct sunlight and both sudden and gradual changes in ambient temperature and soil temperature (DualEm, 2014). For consistency, many studies attempt to complete EMI measurement campaigns on the same day where possible (Simpson et al., 2009) or at least choose sampling days within a short space of time and with similar ambient conditions.

DualEm (2014) attempted to minimise drift in their EMI instruments, including housing the sensors in a fibre/resin composite tube, which has the stability to minimise drift and noise while still allowing the instrument to be light and portable (DualEm, 2014). They also calibrate their devices before shipping to ensure drift is less than 1 mS/m and that data should not deteriorate with the recommended use of the instrument (DualEm, 2014). Even still, DualEm recommend allowing the instrument to reach ambient temperature before measurements begin a set of measurements in one singular location for upwards of 10-minute intervals to monitor drift and to leave the instrument on between surveys, in particular in cold conditions to minimise drift (DualEm, 2014)

At least three studies using the EMI instruments consider temperature hysteresis and EC_a signals, with results varying from no short-term effect on the perpendicular and horizontal coplanar arrays (PRP and HCP) (Dabas et al., 2016) to diurnal changes in temperature having a significant impact on signal, particularly PRP (Abdu et al., 2007; Huang et al., 2017c) to the point where it is recommended the sensor is insulated or shaded throughout the measurement campaign (Huang et al., 2017c).

2.6 Summary and knowledge gaps

Geophysical modelling, specifically using electromagnetic induction (EMI) technology such as the DualEm series of sensors, allows for repeatable, cost-effective, non-destructive sampling on a large scale and over a relatively short period of time. The signal is affected by many factors, enabling EMI to be used for various sub-surface investigations.

Most international studies using EMI technology have been in agricultural and archaeological settings. However, very few were in forested environments (Atwell & Wuddivira, 2019; Bennett & George, 1995; Bréchet et al., 2012). In New Zealand, EMI technology, specifically the DualEm, was used in three studies. The first study investigated the relationship between soil volumetric water content and apparent electrical conductivity (EC_a) in a field covered with pasture (El-Naggar et al., 2017; El-Naggar et al., 2021b). The second study was based on a P. plantation (Gallart et al., 2019), and the third was in a P. radiata nursery (Lad et al., 2019). Neither of the studies that used EMI technology in a forest environment considered the effect of the litter layer or "biological mat" on EC_a signal. Therefore, understanding the impact of this variable will either provide a framework to help those seeking to use EMI technology in a forest environment, how to account for this layer when taking and interpreting EC_a data or provide validation that there is no effect on the signal.

Considering the observations made by Gallart et al. (2019), the methodology established in this study could be used as a toolbox for EMI use in the forestry sector. The toolbox's output includes one-dimensional and 3-dimensional maps and datasets to understand better subsurface heterogeneity and microsite variability of factors affecting growth, such as soil moisture, texture and salinity. This is instead of or in addition to using tools such as SMAP and Fundamental Soil Layers – New Zealand Classification, which are too coarse to define heterogeneity on a local or microsite scale. The outputs could be used as part of the criteria for selectively and effectively breeding and planting different P. radiata genotypes.

Chapter 3 :

Study sites and background

This chapter details the selected study sites, including location, climate, soil, geology and land use information. In addition, details of previous field campaigns will also be provided as the data was used in this research and will be referred to in subsequent chapters

3.1 Study Sites

Two *P. radiata* production forests in the North Island of New Zealand were selected as study sites (**Table 3.1**, **Table 3.2** & **Figure 3.1**). Mahurangi forest (site 3) is located in the upper North Island of New Zealand, approximately 15 km north-west of Warkworth (-36.36 latitude,174.56 longitude, WGS84) and Te Hiku forest (site 4) is located in the far north of the North Island of New Zealand, on the southern end of the Aupouri peninsula (-34.91,17 latitude, 173.13 longitude, WGS84) (**Figure 3.1** & **Table 3.2**). The sites were selected as part of a wider study called Forest Flows – Creating Water Resilient Landscapes, funded by the Ministry of Business, Innovation and Employment (contract number: C04X1905), focusing on forest hydrology (Meason, 2023). Sites were selected based on their contrasting soil properties and topography (**Table 3.2**). Catchments within each site were selected and broken down into plots for intensive measurements (**Table 3.1**).

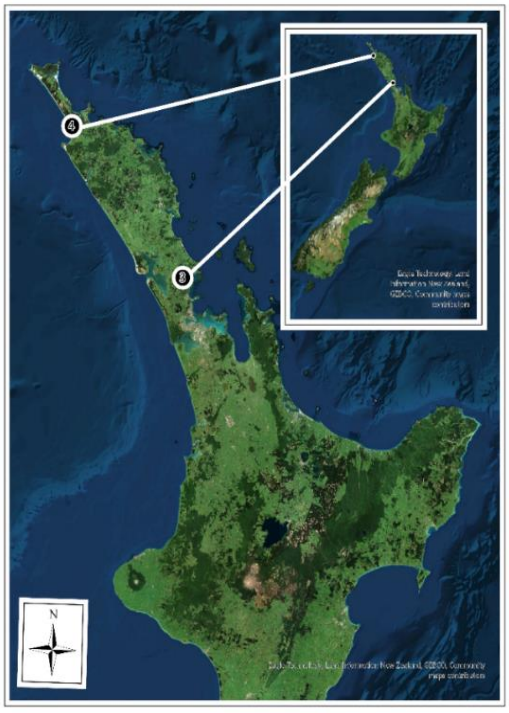

Figure 3.1. *Study sites located in the North Island of New Zealand.*

Table 3.1. *Study site terminology*

Term	Description
Site	A P. radiata production forest was planted in New Zealand, where meteorological, stream, tree, soil, and subsurface measurements occurred.
Catchment	One drainage basin was located within a forest site where sensor networks were deployed, and a range of point measurements took place.
Plot	A 20 x 20-metre square area is typically set up within a catchment, selected to represent the catchment's topographic, wind and moisture variability. Intensive tree and soil measurements were taken within this area.

Table 3.2. *Study site location, climate, land use, soil and geology summary.*

	Mahurangi Forest	**Te Hiku Forest**
Site code	3	4
Location (WGS84)	-36.36 (lat),174.56 (long)	-34.91,17 (lat), 173.13 (long)
Location	15 km west of Warkworth, upper North Island	Aupouri Peninsula, Far North Island
Catchment size (hectares)	36.85	1846.28
No. of plots	25	24
Current land use	2nd rotation, exotic forestry (P. radiata)	2nd rotation, exotic forestry (P. radiata)[2]
Pre-European land use	Native hardwood & podocarp forests[1]	Kauri Forest[2]
Climate[1]	Temperate[3]	Sub tropical[4]
Median Annual Temperature (°C)	14 – 16[3]	16 – 18[4]
Median Annual Rainfall (mm)	1250 – 1500[3]	1000 – 12504[2]
Topography	Undulating, with steep Slopes and valleys	Low-relief sand dunes
Mean Slope	38.51	9.97
Mean Aspect	192.2	203.1
Mean Elevation	199.13	199.13
New Zealand Soil Classification (NZSC)[3]	Yellow Ultic (YU)[5]	Sandy recent (RS) & Sandy raw (WS)[5]
Soil parent Material	Strongly altered quartz-rich rock[5]	Unweathered, lower quartzitic sands, coastal dune sands 60% quartz and <33% feldspare[2]

[1] (Groenendijk et al., 2002; Henderson & McMahon, 2001)
[2] (Rigby, 1985; Thode, 1983; Wilson, 2015)
[3] (Chappell, 2013a)
[4] (Chappell, 2013b)
[5] (Manaaki Whenua - Landcare Research, 2023)
[6] (Schofield, 1970)

3.1.1 Past and current land use of Mahurangi forest and Te Hiku forest

Both Mahurangi and Te Hiku were cleared of native forests in the early 20th century after the early arrival of European settlers (Henderson & McMahon, 2001; Wilson, 2015) (**Table 3.2**). Te Hiku forest, located on the Aupouri Peninsula, was first planted in marram grass as part of several dune stabilisation programs during the early 1920s and 1930s by the Land & Survey Department and the Public Works Department and later in the 1970s (Rigby, 1985; Thode, 1983). In the 1940s and more extensively in the early 1960s, the peninsula adjacent to 90-Mile Beach was planted in *P. radiata* to stabilise dune complexes and act as a buffer against coastal winds to reduce the encroachment of aeolian sand on inland settlements and remains today (Rigby, 1985; Thode, 1983). The wider Mahurangi Forest was contained in the "Hoteo Block" of land settlements to European settlers (Rigby, 1998) and was subsequently cleared of native forest, some of which was converted to pasture (Groenendijk et al., 2002). Current land use for both Mahurangi and Te Hiku forests is exotic forestry, predominantly planted in P. radiata and both in their second rotation (**Table 3.2),** which is important to note as local land management practices, in this case, forest silviculture, harvesting and biological processes influence soil forming factors (Groenendijk et al., 2002; Martindale, 2018; Rigby, 1985).

3.1.2 Climate of Mahurangi forest and Te Hiku forest

Mahurangi Forest is in a temperate region in the upper North Island, while Te Hiku Forest lies in a subtropical region in the Far North Island of New Zealand (**Table 3.2**) (Chappell, 2013a; Chappell, 2013b). Te Hiku forest has slightly higher median rainfall and temperature than Mahurangi Forest (**Table 3.2**), which is due to anticyclone weather systems that track down the north island, carrying with it air warmed by the surface waters north of New Zealand (Chappell, 2013b).

3.1.3 Geology, soils and topography of Mahurangi forest

Mahurangi Forest is dominated by sedimentary deposits from the Waitemata group, which includes the Pakiri and Waitakere facies that were laid during the upper Oligocene to the Lower Miocene age and overly a greywacke basement (Ballance, 1976; Hayward & Smale, 1992). The Waitemata group consists of uplifted sandstone, siltstone and mudstone flysch sequences, suggesting they developed on the continental side of a mountain-forming regime (Ballance, 1976). This accounts for the current hilly, undulating topography, eroded and cut by tributaries forming steep Slopes and valleys (**Table 3.2**).

Soils are predominantly Yellow Ultic soils under the New Zealand Soil Classification (**Table 3.2**). These soils are typically low in calcium, acidic, strongly leached, and strongly weathered. They can be characterised by a well-structured clay subsoil and an E horizon, relatively deficient of clay and predominantly derived from strongly altered, quartz-rich parent material (Manaaki Whenua - Landcare Research, 2023). These soils are prone to slips, particularly those overlying the Waitemata Group of sedimentary rock (Hewitt et al., 2021).

3.1.4 Geology, soil and topography of Te Hiku Forest

The Aupouri Peninsula is a tombolo on the west coast of the Far North Island (Wilson, 2015). The tombolo was formed by longshore drift and predominantly consists of Pleistocene and Holocene dune sands (Wilson, 2015). Quaternary sand and silt sequences overlay a limestone basement rock (Wilson, 2015). The presence of peat and clay lenses, which form in low-energy environments, suggests the region underwent a period of marine stability (Wilson, 2015). A consequence of marine regression was the ample supply of overlying sand, resulting in progradation along the west coast (Wilson, 2015). The boundary between marine and terrestrial sand deposits can be defined by a change in colour due to increased oxygen, making the sands yellow or brown (Wilson, 2015). These soils dominate the topography, forming low-relief, low-elevation, aeolian dunes (**Table 3.2**). The soils are classified under the New Zealand Soil Classification as sandy recent soil, sandy raw and sandy brown, the latter forming eastward (**Table 3.2**). Raw soils are poorly developed, often resemble the original parent material, lack a B horizon, and have topsoil <5cm thick (Hewitt et al., 2021). Raw soils often occur in active erosion and depositional environments, including active sand dunes (Hewitt et al., 2021). Recent soils differ from raw soils due to topsoil > 5cm thick (Hewitt et al., 2021).

3.2 Site selection, access and setup

Fieldwork was undertaken over two periods: Initial trial establishment and measurements occurred from October 2020 to March 2021, and subsequent validation measurements and sample collection occurred between October and November 2022. Methods for the former are outlined below, and methods for the latter will be outlined in subsequent chapters.

3.2.1 Site selection

Sites were selected to cover a range of soil and topographic regimes in exotic P. radiata plantations. Mahurangi forest is dominated by steep, hilly slopes, valleys, and ridges with well-weathered, sandy,

silty and clay soils (**Table 3.2**). Dune complexes dominate Te HIku Forest with a relatively low-lying relief consisting of raw and recent sandy soils (**Table 3.2**). Different stakeholders own and manage the sites; therefore, contact with forest managers and owners was sought to gain permission to establish and regularly access a trial in their forests and gain regular access to them throughout the study. Each site was divided into catchments and plots for intensive measurement (**Table 3.2**).

3.2.2 Catchment selection

Each site was broken down into catchments and plots to allow extensive measurements within concentrated areas of interest to understand the microsite variation within each site better. Catchment selection criteria predominantly depended on health and safety, ease of access and no planned harvesting operations throughout the study. In addition, selecting a catchment representative of the forest was also considered where practical. For the wider Forest Flows study, each catchment required one main outlet to measure stream flow. Considering these criteria, the Mahurangi and Te Hiku catchments were selected with differing catchment sizes ().

3.2.3 Cluster analysis and plot selection

A cluster analysis was conducted to capture a representative spread of topographic, wind and soil features at randomly selected locations within each catchment, allowing the site to be stratified by the respective features. This follows the methodology that Salekin et al. (2021a) used and developed.

Firstly, 300 random points were created using the random points function from the Arc GIS Pro toolbox (Esri Inc., 2023) with three criteria: All points were to fall no closer than 15m from the catchment boundary, points were to be a minimum of 15m distance from any anthropogenic structures such as roads, skid sites and tracks, and a minimum of 20m distance between each point. Using the random points, secondary geo-morphometric and hydrologic features reported in Salekin et al. (2021a); Salekin et al. (2019); Salekin et al. (2021b) were produced using available digital elevation models (DEMs) with a resolution of 1m and a standalone geospatial analysis software SAGA (V 7.6.3) (Conrad et al., 2015). These secondary features included slope, aspect, elevation, wetness, wind exposure, soil moisture, curvature and georeferenced coordinates extracted for each random point.

The complete dataset was used in R statistical environment (R Development Core Team, 2018) to run a clustering routine by using the "res.hcpc" function from the "factormineR" package (Lê et al., 2010). This procedure is summarised in (**Figure 3.2**). Generally, this function produces an optimised number of clusters, enforced by setting a pre-determined cluster quantity. In this case, the pre-determined quantity was 25 sites chosen within each study catchment to represent the micro topology and morphology of the respective catchments. This allowed the site to be stratified to generate selected plot locations without bias.

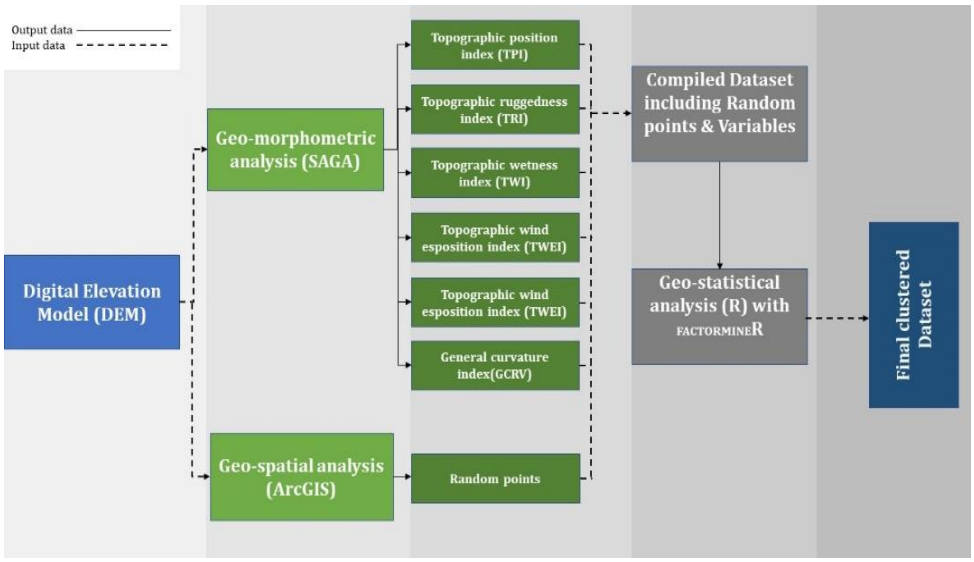

Figure 3.2. *Cluster analysis procedure produced by Salekin (2021).*

3.2.4 Plot establishment

Out of the random points, 25 points representing a range of topographic features were selected to establish 20 m x 20 m plots within each catchment to intensively measure above and below-ground attributes. Plots were established at or near the point chosen by the cluster analysis, with adjustments made for animal and anthropogenic disturbances.

Plots were established at each site using criteria from the Permanent Sample Plots Field guide for sample plots in New Zealand forests (Ellis & Hayes, 1997). Corners and the centre of each plot were marked with pegs, and geospatial information was recorded using a high-grade Trimble GPS (Lemmon & Wetherbee, 2005). Plot level apparent electrical conductivity (EC_a) measurements were also taken before the soil moisture sensor network establishment to ensure that little interference from the sensors occurred on the EC_a measurements. In total, 25 plots were established at Mahurangi Forest, and 24 plots were established at Te Hiku Forest.

3.2.5 Volumetric water content and soil temperature sensors

The TEROS 11 sensor measures soil volumetric water content and soil temperature simultaneously (Meter Group, n.d.). These sensors were deployed in the centre of each plot at a depth of 30cm where practical (**Figure 3.3**). Sensors were deployed at the most practical depth possible and were set to take soil temperature measurements at five-minute intervals. Soil removed from the hole was put onto a tarp, then returned to the hole after sensor deployment to match original field conditions and cordoned off to prevent through traffic (**Figure 3.3**)

A. Mud auger to dig hole.
B. Contents of hole set aside in the same order it was removed so it can be returned to the hole to replicate previous field conditions post sensor deployment.
C. & D. – Inserting TEROS 11 sensor into the ground.
E. – Area surrounding sensor cordoned off.

Figure 3.3. *Installation of TEROS11 combined soil volumetric water content and soil temperature sensors at Mahurangi Forest.*

Chapter 4 :

Factors influencing apparent electrical conductivity when using electromagnetic induction technology to measure soil properties

---

4.1 Introduction

Six factors may need to be accounted for when using electromagnetic induction technology to measure the apparent electrical conductivity of forest soils: forest litter thickness and moisture, ambient temperature and soil temperature, and instrument voltage and temperature.

4.1.1 Forest Litter

Forest Litter has a common presence on the forest floor, and it's moisture content is a crucial component of the forest ecosystem's hydrological cycle by facilitating the exchange of water and energy between the canopy, sub-canopy atmosphere, and the soil (Acharya et al., 2017; Sato et al., 2004) as well as water cycling via processes such as soil evaporation, water infiltration, and surface runoff (or lack of) (Liu et al., 2022).

Forest litter comprises fragmented organic materials that fall on the forest floor, including, but not limited to, twigs, leaves, stems, and bark (Liu et al., 2022; Sato et al., 2004). Forest litter comprises three distinct organic horizons, which present three decomposition levels (McLaren & Cameron, 1996; Sato et al., 2004). The top layer (L horizon) consists of undecomposed material, which still resembles its original form. The middle, fragmented F horizon contains partially decomposed organic material that still resembles its original form. The bottom humic or H horizon consists of decomposed organic matter no longer resembles any original plant structure (McLaren & Cameron, 1996; Sato et al., 2004). For this reason, forest litter will be referred to as LFH.

The presence of the LFH layer ensures any precipitation not intercepted by the canopy via throughfall and stem flow redistributes across the forest floor and consequently reduces soil moisture evaporation, protects the underlying soil from compaction and erosion by absorbing impact energy from precipitation and reduces or in some cases, eliminates surface runoff by keeping infiltration rates high (Li et al., 2014; Liu et al., 2022; Sato et al., 2004). The forest LFH layer also helps insulate the underlying soil against

significant temperature changes (Sato et al., 2004). The moisture content of LFH is mainly affected by climactic factors such as temperature, precipitation quantity, duration and intensity, relative humidity, evaporation, wind speed (Liu et al., 2022), tree canopy cover and understory cover, planting density, forest management practices, present and past land use, LFH layer depth, composition, mass, type, shape and density (Acharya et al., 2017; André et al., 2015; Ewell, 2006; Li et al., 2014; Sato et al., 2004).

Given the LFH layer plays an integral role in forest hydrology and ecosystems, it is essential to include variables that describe the LFH layer, such as thickness and moisture content, in analysis and modelling to truly understand the effect these variables may have (if any) on the hydrological cycle in a forest environment. Understanding the effect forest LFH may have on apparent electrical conductivity measurements (EC_a) is no exception. The limited studies found that use electromagnetic induction to explore the spatial variability of forest soils (Altdorff et al., 2017; Atwell & Wuddivira, 2019; Bennett & George, 1995; Bréchet et al., 2012; Feikema & Baker, 2011; Gallart et al., 2019; Kinal et al., 2006; Lad et al., 2019; Ryland et al., 2020), none directly studied the effect the LFH layer had on EC_a results. Altdorff et al. (2017) acknowledged the presence of forest LFH in a study using electromagnetic induction technology to predict soil water content. However, the LFH layer was described as part of the A horizon of the soil, and the LFH's effect on EC_a alone was not investigated (Altdorff et al., 2017).

Forest LFH was the focus of another study using ground penetrating radar (GPR) to determine if the noise created by backscattering from beech forest LFH distorted the characterisation of forest LFH moisture content and thickness in a central Belgium beech forest (André et al., 2015). The study created three different forest floor configurations from beech LFH of varying thicknesses using just the L horizon (OL) or the F horizon (OF) and the L horizon overlying the F horizon (OL-OF). The study found the GPR could estimate the thickness of both the OL, OF and OL-OF layers to a 1cm accuracy with higher errors for OF and OL-OF LFH configurations (11%) compared with 6% for OL. The study identified that signal attenuation increased with increasing water content, explaining why the OF layer could be distinguished from the OL layer as the OF layer had a higher moisture content and density. The study also measured the EC_a of the beech LFH, which resulted in values of $32mSm^{-1}$ and $80mSm^{-1}$ using a measurement frequency of 4.0 GHz. Ground penetrating radar works under higher frequencies (Ghz and Mhz) compared to EMI technology, which runs at lower frequencies. For example, the DualEm uses a frequency of 9khz (Dal Bo et al., 2021; DualEm, 2014). There is a trade-off between resolution and depth whereby higher frequencies measure the sub-surface at higher resolution at the expense of depth (Dal Bo et al., 2021). In this study, different frequencies were not experimented with; therefore, it is unclear if

the EC_a measured by the GPR were accurate. Despite this, the study did show that it was possible to measure the thickness of forest LFH due to its moisture content, but whether the same result would apply to electromagnetic induction technology is unclear (André et al., 2015).

4.1.2 Ambient temperature, soil temperature and temperature hysteresis, instrument temperature and voltage

Factors causing drift in apparent electrical conductivity (EC_a) over time include sudden and gradual changes in ambient temperature, soil temperature and instrument temperature, ambient temperature and direct sunlight (Dabas et al., 2016; DualEm, 2014). This short-term (several minutes) and long-term (several hours) drift can create undesirable artefacts in data and maps, which need to be corrected during data processing (Dabas et al., 2016; Delefortrie et al., 2014). For consistency, many studies attempt to complete EMI measurement campaigns on the same day where possible or at least choose sampling days within a short space of time and with similar ambient conditions (Simpson et al., 2009).

Previous studies have reported drift in apparent electrical conductivity by running EMI instruments such as the DualEm and EM-38 in controlled and uncontrolled environments over time. The results varied from minor drift in EC_a over time (Mat Su & Adamchuk, 2023; Saey et al., 2009; Simpson et al., 2009; Urdanoz & Aragüés, 2012) to moderate and extreme drift over time (Abdu et al., 2007; Mester et al., 2014; Robinson et al., 2004) caused by external (ambient and soil temperature) and internal (instrument voltage and temperature) factors. Of those studies where changes in EC_a drift were pronounced, differences were ascribed to soil temperature hysteresis, where increased temperature resulted in increased soil conductivity. Increases and decreases in ambient and internal instrument temperatures also showed a near-linear relationship due to the sensitivity of the copper wires used to generate magnetic fields within the EMI instruments (Robinson et al., 2004). While the sensitivity of the copper wires is ideal for generating electrical currents, their susceptibility to heterogeneous internal and external temperatures may mean a correction factor is necessary to compensate for drift (Mester et al., 2014; Robinson et al., 2004; Stockmann et al., 2017).

DualEm (2014) attempted to minimise drift in their EMI instruments, including housing the sensors in a fibre/resin composite tube, which has the stability to minimise drift and noise while still allowing the instrument to be light and portable (DualEm, 2014). They also calibrate their devices before shipping to ensure drift is less than 1 mS/m and that data should not deteriorate with the recommended use of the

instrument (DualEm, 2014). Even still, DualEm recommend allowing the instrument to reach ambient temperature before measurements begin a set of measurements in one singular location for upwards of 10-minute intervals to monitor drift and to leave the instrument on between surveys, in particular in cold conditions to minimise drift (DualEm, 2014)

At least three studies using the EMI instruments consider temperature hysteresis and EC_a signals, with results varying from no short-term effect on the perpendicular and horizontal coplanar arrays (PRP and HCP) (Dabas et al., 2016) to diurnal changes in temperature having a significant impact on signal, particularly PRP (Abdu et al., 2007; Huang et al., 2017c) to the point where it is recommended the sensor is insulated or shaded throughout the measurement campaign (Huang et al., 2017c).

4.1.3 Chapter objectives

Chapter has three primary purposes. The first is to identify if a correction factor is required to compensate for drift caused by instrument voltage and temperature, ambient temperature, and soil temperature. The second and third purpose is to identify if apparent electrical conductivity (EC_a) in a forest environment is affected by the presence or absence of forest litter (LFH) and the thickness and moisture content of LFH. If forest LFH does influence EC_a, what impact will this have on users of EMI technology in forested catchments?

4.2 Methodology

Section 4.2 details the methodology used to collect field samples and conduct subsequent analysis in the lab. This section also outlines the statistical analysis used to establish if the effect of soil, ambient and instrument temperature and voltage causes drift in apparent electrical conductivity over time and if forest litter causes statistically significant changes in apparent electrical conductivity. Antecedent methods and actions are detailed in Chapter 3.

4.2.1 Sample location

Soil samples were limited to one per plot instead of repeating multiple sample points within a plot. This aligns with the study's overarching purpose: to capture spatial heterogeneity on a catchment level using soil samples as a reference or validation point. In addition, there is an assumption that the endophatic

and topographic cluster analysis ensured microsite topography was captured when selecting plot locations.

This allowed the capture of data from various topographic features (slope, aspect, elevation) and a variety of soil moisture and physical properties within the forested catchment. Sample locations within a plot were selected based on proximity to the TEROS 11 sensors. Samples were taken at Mahurangi Forest between November 22nd and 24th of November, 2022 and Te Hiku Forest between October 18th and 20th of October 2022.

Sample locations within each plot were to be taken where there was no overlap between the zone of influence of the electromagnetic induction (EMI) instrument and the TEROS 11 soil volumetric water content (VWC) and temperature sensors. In addition, the sample location was selected to not interfere with the flow of soil water, which would affect VWC sensor readings. Therefore, the criteria for choosing a sample point was for all EMI and destructive soil sampling using a core auger to be taken at least two meters away from, downhill or adjacent to the TEROS 11 sensor (**Figure 4.1**).

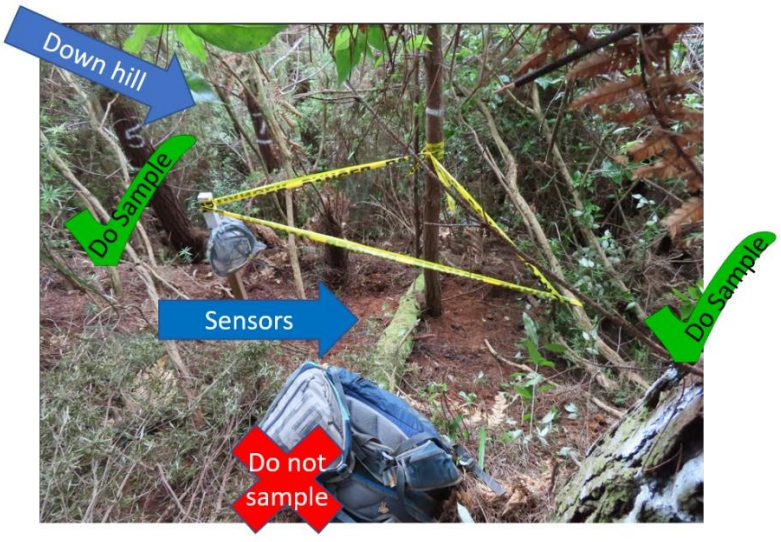

Figure 4.1: *Appropriate sample locations within a plot for both electromagnetic induction and destructive soil sampling.*

4.2.2 Measurement of apparent electrical conductivity and ambient temperature

Apparent electrical conductivity (EC_a) was measured using the DualEm-1 at two cumulative depths simultaneously (0.5cm and 1.6cm). Measurements were repeated 48 times in the presence of forest litter ($LFH^{Present}$) and 48 times in the absence of LFH (LFH^{Absent}) with the DualEm-1 transmitter facing north and the roll of the tube set to zero (±3). The removal process of the LFH is outlined in **Section 4.2.3**.

Apparent electrical conductivity of $LFH^{Present}$ was measured by placing the DualEm-1 directly on top of undisturbed LFH at a height of 10cm and remained stationary during the 48 repetitions. The location of this measurement was near the centre of the plot and at least 2 meters away from the volumetric water content sensors. The apparent electrical conductivity of LFH^{Absent} was measured in the exact same position, using the same measurement protocol as for $LFH^{Present}$. The only difference was that the LFH was removed, and the DualEm-1 was placed directly on the A horizon of the soil.

The EMI data was cleaned and sorted in the office. The DualEm-1 simultaneously measured the instrument temperature, ensuring every EC_a measurement had a related ambient temperature measurement. Criteria for data removal were strict and only occurred if the field notes stated a measurement was taken in error. For example, the user tripped, or another instrument was too close to the DualEm-1. Consequently, no data from either Mahurangi or Te Hiku EMI datasets is missing.

4.2.3 Forest litter sampling and instrument temperature

The methods used to sample forest litter were adapted from Ewell (2006), which sampled forest litter in conifer forests to assess how forest litter acted as fuel for forest fires. After apparent electrical conductivity (EC_a) was measured in the presence of undisturbed forest litter (LFH), the DualEm-1 was gently placed to the side, and the thickness of the forest LFH was measured where the centre of the DualEm once lay (**Figure 4.2**). Next, a 0.20 m^2 x 0.20 m^2 slice of forest LFH was placed in a plastic ziplock bag. The samples were placed into the bag like a serving of lasagna, so all forest LFH remained relatively intact. Samples were transported in a chilly bin, and on return to the lab, the samples were weighed and oven-dried at 80°C for 48 hours – the time it took for the weight to stabilise.

Figure 4.2. *Measuring litter thickness at the centre of the DualEm-1 tube using a rigid measuring tape. Site (Mahurangi), Plot (12) and thickness were recorde.*

4.2.4 Litter gravimetric water content and litter density

Once samples were oven-dried, they were quickly reweighed to ensure they did not reabsorb moisture. Using the litter fresh weight (LFH^{Fresh}) and dry weight (LFH^{Dry}), litter gravimetric water content (LFH^{GWC}) was calculated using (**Equation 2**) and litter density using **Equation 3**.

Equation 2. *Percentage of the gravimetric water content.*

$$LFH^{GWC} = \left(\frac{LFH^{Fresh} - LFH^{Dry}}{LFH^{Dry}}\right) * 100$$

Where:

LFH^{Fresh} = weight of fresh litter (g)

LFH^{Dry} = weight of dry litter (g)

LFH^{GWC} = gravimetric water content of forest litter (%)

Equation 3*. Litter density.*

$$LFH^{Density} = \frac{LFH^{Dry}}{LFH^{Thickness}}$$

Where:

LFH^{Fresh} = weight of fresh litter (g)

$LFH^{Thickness}$ = weight of dry litter (g)

$LFH^{Density}$ = litter density (g/cm^3)

4.2.5 Statistical analysis

All statistical analysis was conducted in R studio version 4.3.0 (R Development Core Team, 2018), including summary statistics and graphs to analyse the effect of forest litter on apparent electrical conductivity. Before analysing forest litter variables, there was a need to establish if a correction factor was required to adjust apparent electrical conductivity due to ambient temperature (**Section 4.2.5.1**). **Section 4.2.5.2** looks at the overall effect of the presence and absence of forest litter on apparent electrical conductivity was investigated. Next, the main effects and interactions of measured litter variables were evaluated to test any significant effect on apparent electrical conductivity (**Section 4.2.5.3**).

4.2.5.1 Drift caused by instrument, soil and ambient temperature and voltage

This section uses methods developed by Allaire et al. (2009), Delefortrie et al. (2014) and Mat Su and Adamchuk (2023) to determine if correction is needed for apparent electrical conductivity (EC_a) drift in electromagnetic induction instruments. Pearson correlation coefficient was used to measure the degree of linear association between electrical conductivity at 50cm (EC_a^{50}) and 160cm (EC_a^{160}) cumulative depths and internal instrument temperature, instrument voltage, ambient temperature and soil temperature. Furthermore, a generalised linear model was used to ensure no interaction effects between these predictor variables. The generalised linear model ('glm' function) (R Development Core Team, 2018) used a gamma distribution with a log-link function as the response variables EC_a^{50} and EC_a^{160} were continuous, right skewed and zero bounded, which helped meet the assumptions of normality and heteroscedasticity (Schabenberger & Pierce, 2001).

4.2.5.2 Statistical analysis of the presence and absence of forest litter

For this analysis, a generalised linear model was created for the response variable apparent electrical conductivity (EC_a) using the 'glm' function in R studio (R Development Core Team, 2018). To better meet the assumptions of normality and homoscedasticity, a gamma distribution with a log-link was used because EC_a was continuous, right-skewed, and zero-bounded (Schabenberger & Pierce, 2001). Site, cumulative depth and LFH presence and absence were all used as two-level factors (**Equation 4**).

Equation 4. *A generalised linear model was used to assess the effect of litter presence and absence on apparent electrical conductivity.*

$$\left(Ec_a^{\square} \sim LFH * Site * Depth, distribution = gamma, link = log\right)$$

Where:
EC_a = Apparent electrical conductivity to both 50cm and 160cm cumulative depths
Predictor variables
LFH = Litter presence or absence as a two-level factor
Depth = Cumulative depth to 50cm and 160cm as a two-level factor
Site = Mahurangi and Te Hiku as a two-level factor

A likelihood ratio test compared GLMs with and without the two-level factor, presence and absence of LFH, using the 'lmtest' function, part of R studio's 'lmtest' package (Zeileis & Hothorn, 2022). Likelihood ratio Chi-square tests allow nested models to be compared to identify if the presence or absence of model parameters significantly affects model fit by comparing a global or full model with a restricted or

simplified model (Westfall & Henning, 2013). Variable inflation factors were also assessed using the 'vif' function in R studio's 'car' package (Fox & Weisberg, 2019).

4.2.5.3 Statistical analysis to assess the effect of litter variables on apparent electrical conductivity

For this analysis, two generalised linear models were created for response variables apparent electrical conductivity to 50cm (EC_a^{50}) and apparent electrical conductivity to 160cm (EC_a^{160}) using the 'glm' function in R studio (R Development Core Team, 2018). To better meet the assumptions of normality and homoscedasticity, both GLMs used a gamma distribution with a log-link function as the response variables EC_a^{50} and EC_a^{160} were continuous, right-skewed, and zero-bounded (Schabenberger & Pierce, 2001), which helped to meet the normality assumptions. The final GLM used to determine if litter variables can explain the variability in EC_a^{50} and EC_a^{160} is outlined in **Equation 5**.

A likelihood ratio test compared the global GLM outlined in **Equation 5** to a simplified GLM using only weakly significant predictor variables. This was done using the 'lmtest' function, part of R studio's 'lm test' package (Zeileis & Hothorn, 2022). Likelihood ratio Chi-square tests allow nested models to be compared to identify if the presence or absence of model parameters significantly affects model fit by comparing a global or full model with a restricted or simplified model (Westfall & Henning, 2013). Variable inflation factors were also assessed using the 'vif' function in R studio's 'car' package (Fox & Weisberg, 2019).

Equation 5. *Generalised linear model used to assess the effect of litter presence and properties on apparent electrical conductivity to two cumulative depths.*

$$(EC_a \sim Site * LFH^{Thick} * LFH^{GWC} * LFH^{Density}, distribution = gamma, link = log)$$

Where:
EC_a = Apparent electrical conductivity to either 50cm or 160cm
Predictor variables
LFH = Forest Litter layer
Thick = Thickness (cm)
GWC = Gravimetric water content (%)
Density = GWC / Thickness

4.3 Results

This section comprises three parts. **Section 4.3.1** determines if a correction factor is required to compensate for temperature and instrument drift in apparent electrical conductivity data. **Section 4.3.2** assesses the effect of the presence and absence of forest litter on apparent electrical conductivity. Finally, **Section 4.3.3** determines if the variables making up forest litter have a significant effect on apparent electrical conductivity.

4.3.1 Drift caused by instrument, soil and ambient temperature and voltage

4.3.1.1 Summary statistics

Table 4.1 provides summary statistics of factors that may cause drift in apparent electrical conductivity over the duration of measurement campaigns, including ambient temperature, instrument temperature, soil temperature and instrument voltage at both Mahurangi Forest and Te Hiku. Box plots also show medians, interquartile, upper and lower ranges and any outliers at both sites (**Figure 4.3**). All three temperature variables and voltage fluctuations vary little between sites with similar means and medians and standard errors and interquartile ranges overlapping between sites (**Table** 4.1**, Figure 4.3**). Ambient temperature had the most significant temperature fluctuations both within and between sites, with similar minimum temperatures of around 11˚C and maximum temperatures between 18 and 22˚C (**Table** 4.1). Instrument and soil temperature had minimal fluctuation over the measurement campaigns, with low standard errors between 0.03 and 0.08 and temperature differences between 0.65 ˚C and 1.70˚C (**Table** 4.1). Median and mean voltage were similar for both sites, and minimum and maximum voltage were within adequate operational range for the instrument (DualEm, 2014).

Table 4.1. *Summary statistics of variables that may cause drift in apparent electrical conductivity at Mahurangi Forest (3) and Te Hiku Forest (4).*

	Mean		S.E.M		LQ		Median		UQ		IQR		Min		Max		Range	
Site	**Mahu**	**TeHi**	**Mahu**	**TeHi**	**Mahu**	**TeHi**	**Mahu**	**TeHi**	**Mahu**	**TeHi**	**Mahu**	**TeHi**	**Mahu**	**TeHi**	**Mahu**	**TeHi**	**Mahu**	**TeHi**
Ambient Temperature (°C)	16.18	16.03	0.39	0.55	15.36	14.24	16.42	16.24	17.70	18.20	2.34	3.95	11.72	11.67	18.92	21.62	7.20	9.95
Instrument Temperature (°C)	29.02	29.09	0.03	0.07	28.97	28.73	29.05	29.18	29.10	29.37	0.13	0.63	28.63	28.47	29.29	29.60	0.65	1.14
Soil Temperature (°C)	15.68	15.43	0.08	0.07	15.40	15.28	15.70	15.40	15.90	15.60	0.50	0.33	15.10	14.80	16.80	16.20	1.70	1.40
Voltage (V)	10.53	10.25	0.14	0.15	9.99	9.52	10.60	10.28	11.00	10.62	1.01	1.10	9.38	9.15	11.71	11.96	2.34	2.81

S.E.M = Standard error of mean, UQ = Upper quartile, LQ = Lower quartile, IQR = Interquartile range, Min = Minimum, Max = Maximum
Mahu = Mahurangi Forest, TeHi = Te Hiku Forest

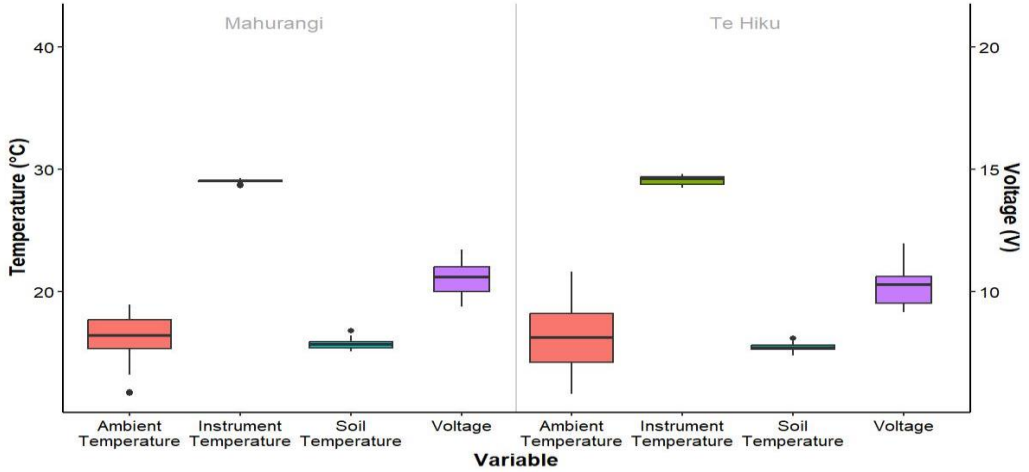

Figure 4.3. *Box plot of measured variables which may cause drift in apparent electrical conductivity.*

4.3.1.2 Analysis using Pearson correlation and generalised linear models

Figure 4.4 shows apparent electrical conductivity (ECa) changes over the measurement campaign at Mahurangi and Te Hiku. The measurements are in sequential order of when they were measured, starting from the first measured plot to the last measured plot at each site.

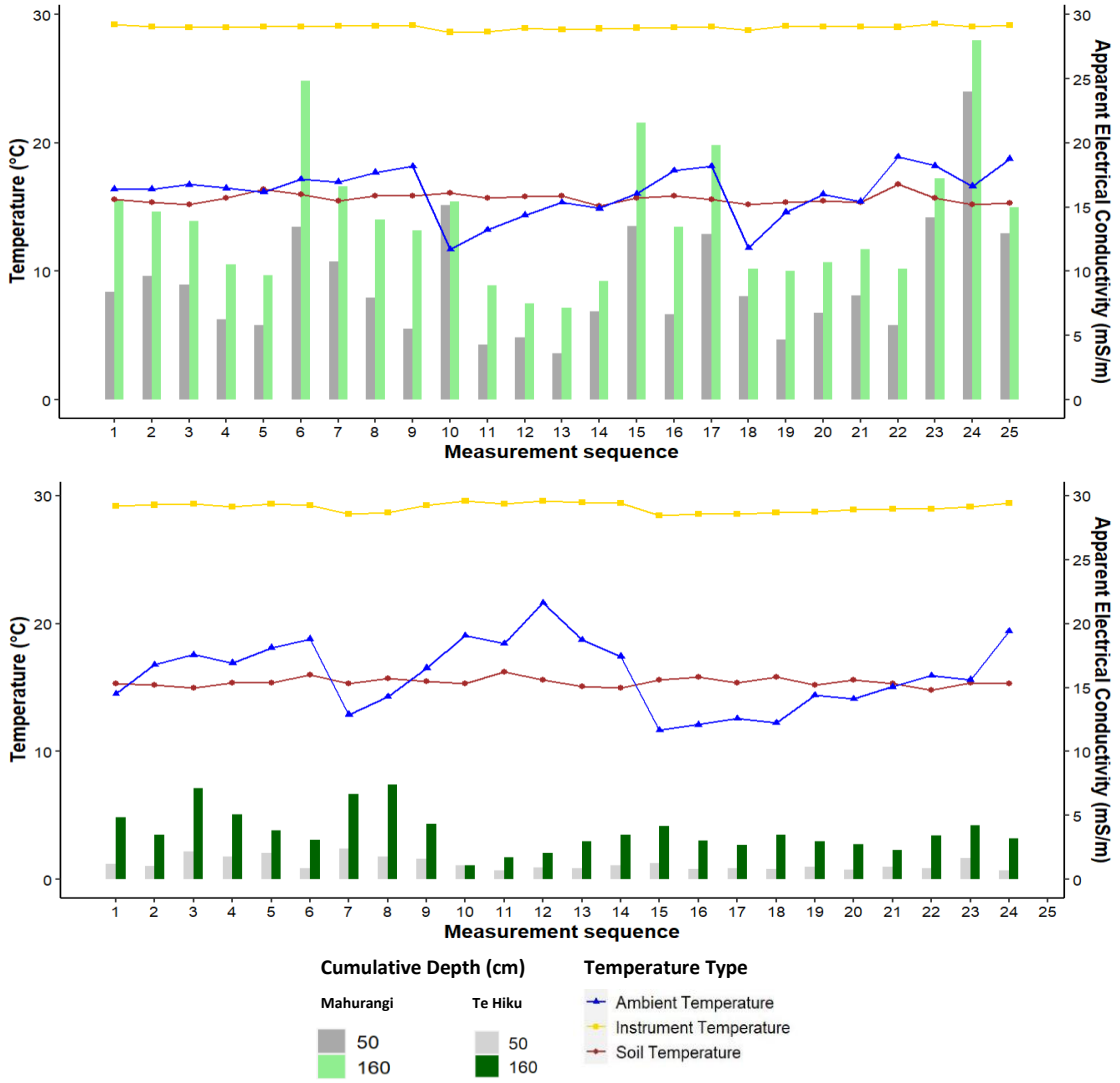

Figure 4.4. *Bar chart of apparent electrical conductivity at 50cm (grey) and 160cm (green) cumulative depths measured in each plot (secondary y-axis) and ambient (blue triangle), instrument (yellow square) and soil temperature (red circle) (primary y-axis) at time of measurement at Mahurangi Forest (top) and Te Hiku forest (bottom). Plots were not measured in numerical order. Therefore the measurement sequence on the x-axis shows the order in which measurements were taken to create a time series.*

Overlaying the EC_a data at 50cm and 160cm cumulative depths are temperature measurements for ambient air, soil, and the instrument. While Mahurangi does not show any obvious patterns between apparent electrical conductivity and fluctuations in temperature, Te Hiku Forest may show a weak, inverse relationship between apparent electrical conductivity and ambient temperature, whereby a decrease in ambient temperature results in an increase in EC_a and vice versa.

A Pearson product-moment correlation was conducted (**Table 4.2**) to investigate this artefact further, and any other potential effects the ambient, soil, and instrument temperatures and voltage may have on EC_a throughout the field campaigns.

Table 4.2. *Pearson Correlation Coefficient and p-value (in brackets0 for variables affecting apparent electrical conductivity at Mahurangi and Te Hiku Forests at cumulative depths 50cm and 160cm.*

Site	Cumulative depth (cm)	**Ambient Temperature (°C)**	**Instrument Temperature (°C)**	**Soil Temperature (°C)**	**Voltage (V)**
Mahurangi	**50**	0.15 (0.48)	0.16 (0.44)	-0.25 (0.23)	-0.06 (0.79)
	160	0.34 (0.10)	0.31 (0.13)	-0.14 (0.49)	-0.11 (0.61)
Te Hiku	**50**	-0.08 (0.72)	-0.06 (0.78)	-0.23 (0.28)	-0.17 (0.44)
	160	-0.29 (0.16)	-0.29 (0.17)	-0.19 (0.38)	-0.01 (0.95)

Pearson's correlation did not show a correlation between EC_a and either ambient, soil or instrument temperature or voltage at either Mahurangi or Te Hiku at both cumulative depths. While some weak correlations were observed, they were not statistically significant, suggesting these relationships could be due to chance rather than having any meaningful associations. For example, for ambient temperature and instrument temperature, there is a negative linear correlation with EC_a to a depth of 160cm at Te Hiku Forest, which may have been observed in **Figure 4.4**. However, the weak *p-value*s of 0.16 and 0.17, respectively, suggest either this relationship is more likely due to chance or a different test may be required to check this association, which was why generalised linear models were used to test if both the main effects and the interactions of these variables could explain changes in apparent electrical conductivity.

For both GLM^{50} and GLM^{160}, neither the main effects nor their interactions were statistically significant (*p-value*s > 0.3) for $GGLM^{50}$ and (*p-value*s < 5) for $GGLM^{160}$. Therefore, at the 0.05 significance level, both GLMs show insufficient evidence to reject the null hypothesis that neither ambient, soil or, instrument temperature or voltage and their interactions can explain the variability in EC_a at both depths beyond random chance. The lack of a significant relationship is further visualised in **Figure 4.5**, which shows the temperature and voltage variables graphed against apparent electrical conductivity at 50cm and 160cm at both sites.

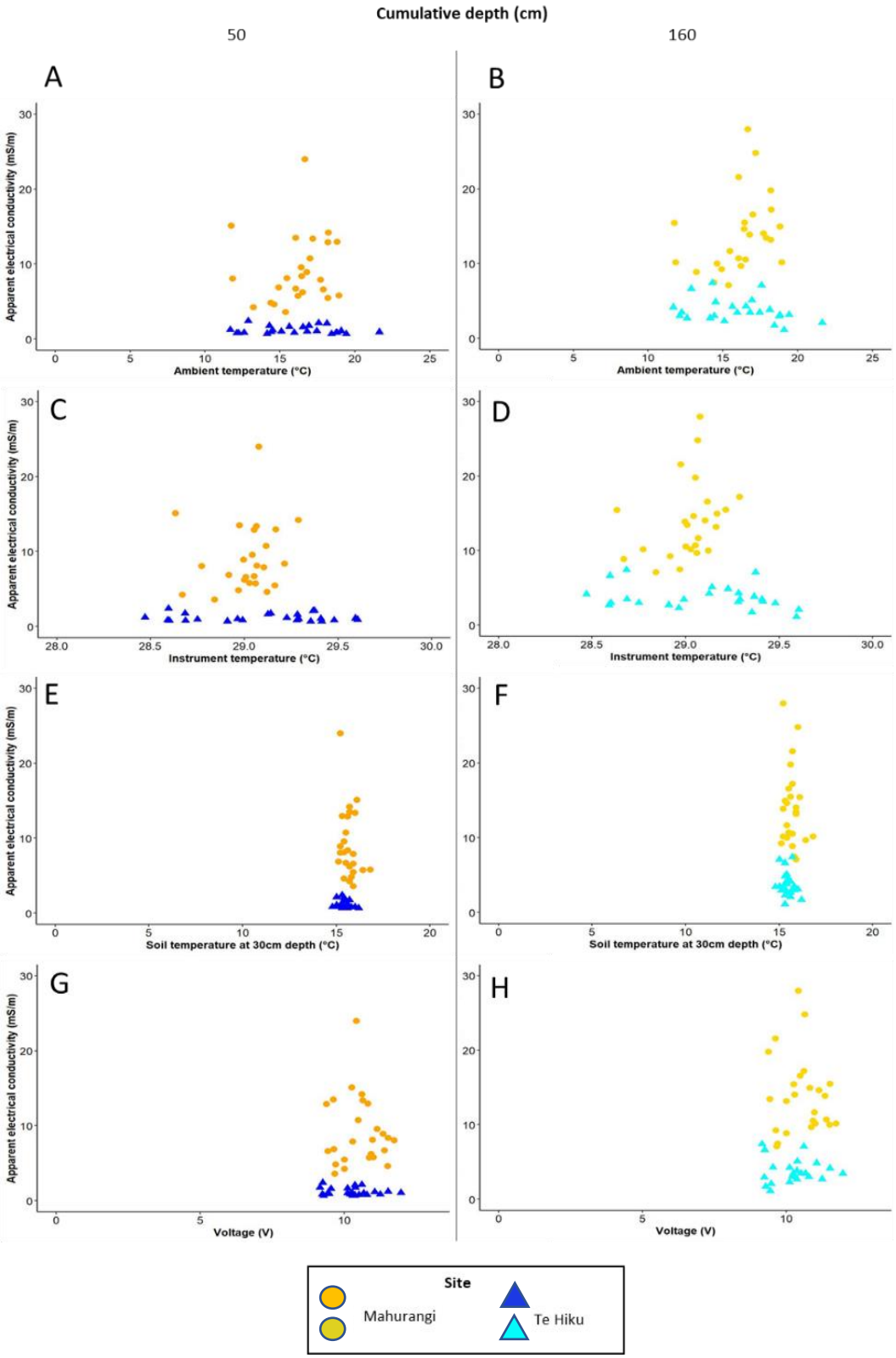

Figure 4.5. *Scatter plots of Mahurangi (circle) and Te Hiku forest (triangle) apparent electrical conductivity (y-axis) at cumulative depths 50cm (left) and 160cm (right) for ambient temperature (A & B), soil temperature (C & D), instrument temperature (E & F) and voltage (G and H).*

4.3.2 The effect of the presence and absence of forest litter on apparent electrical conductivity

4.3.2.1 Summary statistics

Summary statistics (**Table 4.3**) and box plots (Figure 4.6) show that overall, apparent electrical conductivity (EC_a) for Mahurangi was higher than for Te Hiku. Mean EC_a at both sites to a cumulative depth of 160cm (EC_a^{160}) was also higher than to a cumulative depth of 50cm (EC_a^{50}) (**Table 4.3**). The median EC_a for Mahurangi and Te Hiku were similar in the presence ($LFH^{Present}$) and absence (LFH^{Absent}) of forest litter to both EC_a^{50} and EC_a^{160} with little difference in standard errors for $LFH^{Present}$ and LFH^{Absent} at each site at each depth. Apparent electrical conductivity at Mahurangi was more variable for both depths than Te Hiku, regardless of $LFH^{Present}$ or $LFH^{Absence}$ (Figure 4.6), with a larger range of EC_a at Mahurangi than at Te Hiku to both depths (**Table 4.3**). The range differed between sites however, at both cumulative depths, minimum, maximum, upper and lower quartiles remained very similar in $LFH^{Present}$ and LFH^{Absent}.

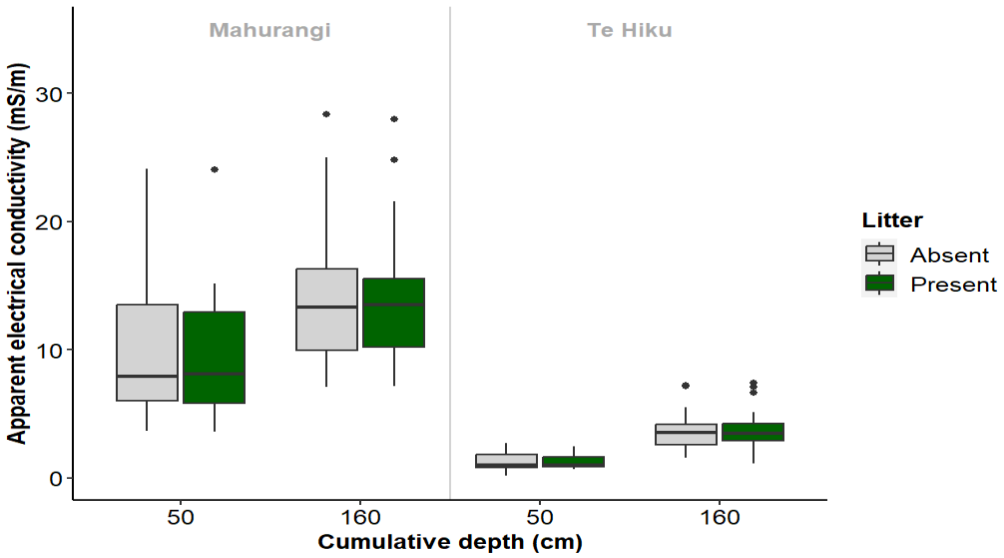

Figure 4.6. *Box plot of apparent electrical conductivity in the presence and absence of forest litter at cumulative depths to 50cm and 160cm showing median line.*

Table 4.3. *Summary statistics of apparent electrical conductivity (mS/m) in the presence and absence of forest litter (LFH) at two cumulative depths at Mahurangi and Te Hiku.*

Independent variables		Site	Mean	S.E.M	LQ	Median	UQ	IQR	Min	Max	Range
Cumulative depth (cm)											
50		Mahurangi	9.22	0.64	5.81	8	13.08	7.27	3.59	24.09	20.5
160			13.96	0.73	10.01	13.3	16.33	6.32	7.11	28.34	21.23
50		TeHiku	1.24	0.08	0.82	1.01	1.76	0.94	0.18	2.7	2.52
160			3.76	0.23	2.67	3.44	4.29	1.62	1.11	7.41	6.3
LFH presence											
Absent		Mahurangi	11.61	0.77	7.67	10.2	14.12	6.45	3.66	28.34	24.68
Present			11.57	0.77	7.41	10.38	14.31	6.91	3.59	27.99	24.4
Absent		TeHiku	2.54	0.26	0.96	2.11	3.58	2.61	0.18	7.22	7.04
Present			2.47	0.25	1	2.07	3.45	2.45	0.68	7.41	6.73
Overall site apparent electrical conductivity											
		Mahurangi	11.57	0.44	7.5	10.38	14.2	6.7	3.59	27.99	24.4
		TeHiku	2.47	0.14	1	2.07	3.45	2.45	0.68	7.41	6.73
Cumulative depth (cm)	**Litter**										
50	Absent	Mahurangi	9.27	0.92	5.89	7.91	13.5	7.61	3.66	24.09	20.44
	Present		9.16	0.92	5.8	8.08	12.94	7.13	3.59	24.02	20.43
160	Absent		13.95	1.05	9.75	13.29	16.4	6.65	7.11	28.34	21.23
	Present		13.97	1.05	10.11	13.47	16.08	5.96	7.14	27.99	20.86
50	Absent	Te Hiku	1.27	0.13	0.81	0.98	1.81	1	0.18	2.7	2.52
	Present		1.21	0.1	0.84	1.01	1.64	0.8	0.68	2.42	1.74
160	Absent		3.80	0.33	2.56	3.51	4.27	1.71	1.56	7.22	5.66
	Present		3.72	0.32	2.77	3.44	4.29	1.52	1.11	7.41	6.3

S.E.M = Standard error of mean, UQ = Upper quartile, LQ = Lower quartile, IQR = Interquartile range, Min = Minimum, Max = Maximum

4.3.1.2 Generalised linear model and likelihood ratio test

A generalised linear model was fitted to establish if the presence or absence of forest litter (LFH) explained variability in apparent electrical conductivity (EC_a) using (LFH) presence and absence, site and cumulative depth, as well as their interactions (**Table 4.4**). The high *p-value*s for LFH show no statistically significant difference in mean EC_a between LFH presence or absence and that any differences are likely due to chance (**Table 4.4**). However, the low *p-value*s of cumulative depth and site suggest these variables are highly significant and that there is a significant difference between EC_a at individual sites and EC_a at each cumulative depth. The same can be said for the interaction between site and cumulative depth (*p-value* <0.001) (**Table 4.4).** The interaction effect of LFH and cumulative depth and site on EC_a were also tested in (**Table 4.4)** which further showed no evidence to suggest that the combined effect of LFH, cumulative depth and site significantly influenced EC_a given such high p values.

Next, a likelihood ratio test was performed to establish if including LFH in the GLM enhanced model fit. A *p-value* (0.99) of the Chi-squared (0.22) indicated that including LFH did not improve model fit, substantiating the null hypothesis that the presence or absence of LFH has no effect on apparent electrical conductivity.

Table 4.4. *Results of analysis of variance (ANOVA) of the effect of litter (LFH) presence using log-transformed apparent electrical conductivity*

	Estimate	Std. Error	*t-value*	*p-value*	Sig.
LFH	2.23	0.09	24.95	0.00	
Cumulative depth	-0.01	0.13	-0.09	0.93	**
Site	0.41	0.13	3.24	0.00	***
LFH:Cumulative depth	-1.98	0.13	-15.56	0.00	
LFH:Site	0.01	0.18	0.07	0.94	
Cumulative depth: Site	-0.04	0.18	-0.22	0.82	***
LFH:Cumulative depth: Site	0.68	0.18	3.79	0.00	

Signif. codes: 0 '***' 0.001 '**' 0.01 '*' 0.05 '.' 0.1 ' ' 1

4.3.2 The effect of litter gravimetric water content, thickness and density on apparent electrical conductivity

4.3.2.1 Summary statistics

Summary statistics and box plots of forest litter variables between the Mahurangi Forest and Te Hiku Forest were calculated for ambient temperature, litter thickness (LFH^{Thick}), litter fresh weight (LFH^{Fresh}), litter dry weight (LFH^{Dry}), litter moisture mass (LFH^{MM}), litter gravimetric water content (LFH^{GWC}) and litter density ($LFH^{Density}$) (**Table 4.5**).

Mean and median ambient temperatures for both sites were similar, with low standard errors within 0.2 of each other (**Table 4.5** & **Figure 4.7)** and very small and overlapping upper, lower and interquartile ranges (**Table 4.5 & Figure 4.7**). However, Te Hiku had a slightly higher capacity than Mahurangi. Likewise, the mean and median (**Table 4.5** & **Figure 4.7**) LFH^{Thick} at both sites were similar, with overlapping ranges and low standard errors. However, Te Hiku had a slightly smaller range in LFH^{Thick} (**Table 4.5 & Figure 4.7**). At Mahurangi, LFH^{Fresh}, LFH^{Dry} and LFH^{MM} all had higher mean and median weights than at Te Hiku (**Table 4.5** & **Figure 4.7**), with little to no overlap between interquartile ranges between the two sites (**Table 4.5** & **Figure 4.7**). Mahurangi had greater LFH^{MM} than the LFH at Te Hiku (**Table 4.5** & **Figure 4.7**); however, LFH^{GWC} was far greater for LFH at Te Hiku than it was at Mahurangi (**Table 4.5** & **Figure 4.7**). Forest litter had a higher mean and median grams per centimetre density at Mahurangi than was found at Te Hiku, with a greater standard error and much more extensive range with minimum and maximum values that did not overlap with those at Te Hiku (**Table 4.5** & **Figure 4.7**).

Table 4.5. *Summary statistics for litter variables at Mahurangi (3) and Te Hiku (4).*

	Site		Mean		S.E.M		LQ		Median		UQ		IQR		Min		Max	
Site -> Litter variable ↓	**Mahu**	**TeHi**	**Mahu**	**TeHi**	**Mahu**	**TeHi**	**Mahu**	**TeHi**	**Mahu**	**TeHi**	**Mahu**	**TeHi**	**Mahu**	**TeHi**	**Mahu**	**TeHi**	**Mahu**	**TeHi**
Ambient temperature (°C)	29.16	29.25	0.04	0.06	29.08	28.97	29.20	29.31	29.29	29.52	0.22	0.56	28.76	28.61	29.49	29.75	0.73	1.14
Thickness (cm)	4.40	4.06	0.41	0.32	3.00	2.50	4.00	4.00	6.25	5.00	3.25	2.50	1.00	1.50	8.00	7.00	7.00	5.50
Fresh weight (g)	245.95	97.81	21.75	12.90	177.05	51.48	202.45	88.09	352.38	123.27	175.33	71.79	103.52	25.85	464.38	304.12	360.86	278.27
Dry weight (g)	100.47	9.65	8.83	1.38	71.66	4.69	87.54	7.60	133.09	12.66	61.43	7.97	45.55	1.78	211.80	29.91	166.25	28.12
Mass of moistures (g)	145.48	88.16	13.22	11.66	98.81	45.95	117.62	82.02	211.64	110.70	112.82	64.76	57.97	24.07	263.09	274.21	205.12	250.15
Dry weight (%)	41.17	9.97	0.67	0.55	38.11	6.92	40.66	9.85	43.71	12.18	5.60	5.26	34.88	6.55	47.10	14.75	12.22	8.20
GWC (%)	58.83	90.03	0.67	0.55	56.29	87.82	59.34	90.15	61.89	93.08	5.60	5.26	52.90	85.25	65.12	93.45	12.22	8.20
Density (g/cm)	26.48	2.34	2.91	0.28	18.11	1.59	23.55	1.95	27.82	2.54	9.71	0.95	9.72	1.19	76.00	7.48	66.28	6.29

S.E.M = Standard error of mean, UQ = Upper quartile, LQ = Lower quartile, IQR = Interquartile range, Min = Minimum, Max = Maximum
Mahu = Mahurangi Forest, TeHi = Te Hiku Forest

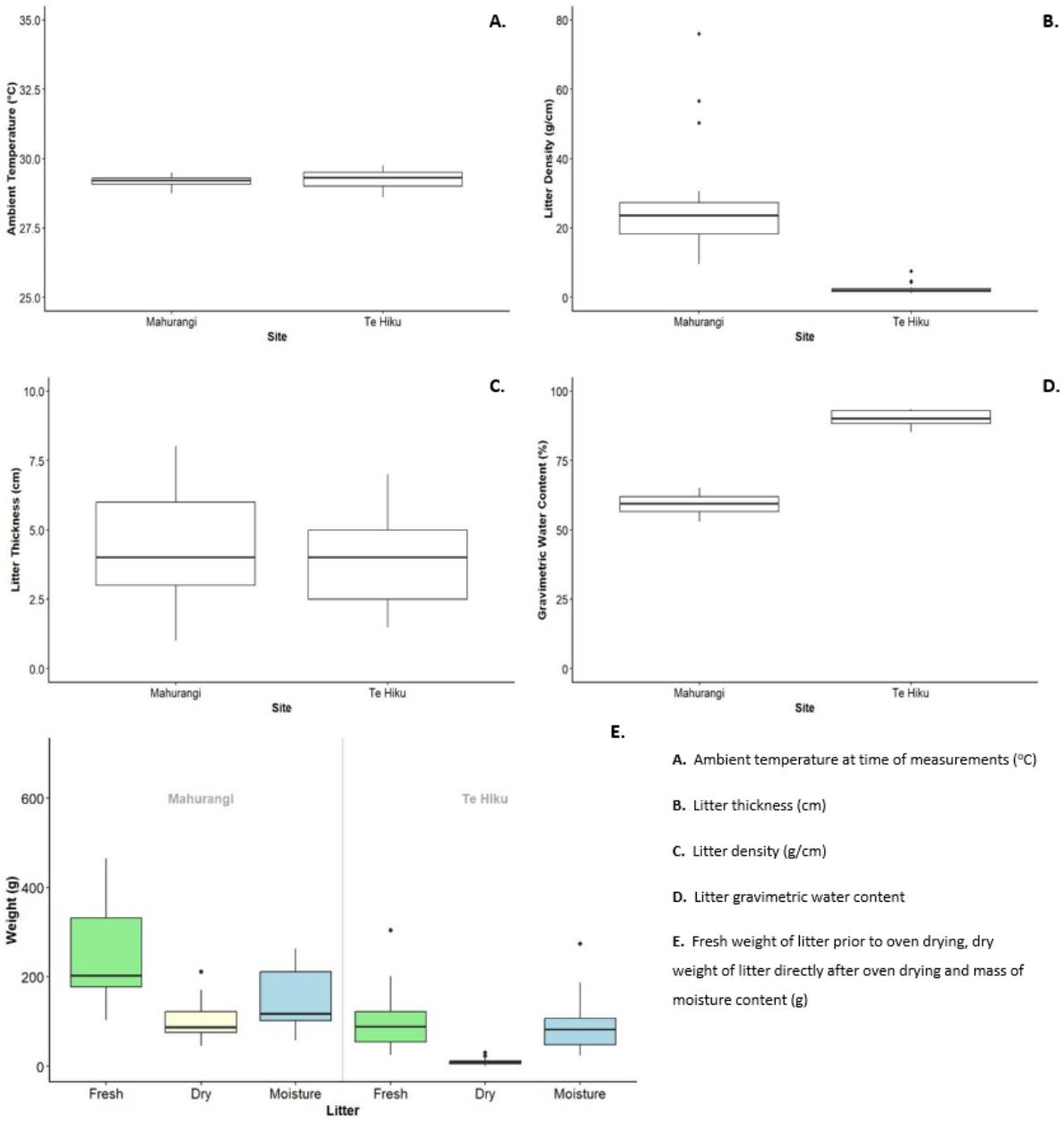

Figure 4.7. *Box plots of forest litter variables collected from Mahurangi and Te Hiku Forest with line showing the median.*

4.3.2.2 Analysis using generalised linear model

A generalised linear model was created using predictor variables litter (LFH) thickness ($LFH^{Thickness}$), litter gravimetric water content (LFH^{GWC}), litter density ($LFH^{Density}$) and site as main effects as well as their interactions **(Table 4.6 & Table 5.8**).

Both generalised linear models (GLM) showed they could explain 91% and 82% of the variability in EC_a^{50} and EC_a^{160} (**Table 4.6**). Of all the main effects and their interactions in both GLMs, only one interaction showed a weak correlation with EC_a^{160}. The interaction between $LFH^{Thickness}$ and $LFH^{Density}$ had a weak, negative correlation with EC_a^{160}. No other litter variables showed significance with *p-value*s above the 0.05 significance level (**Table 4.6**).

A likelihood ratio test compared the GLM with all litter variables and their interactions and the simpler GLM with only $LFH^{Thickness}$ and $LFH^{Density}$ as main effects and their interactions with EC_a^{160} as a response variable. The test showed no significant benefit in adding or removing the predictor variables. The simple model could only explain 62% of the variability in EC_a^{160} with weakly significant to non-significant *p-value*s (0.02 – 0.40). Variable inflation factors (VIF) of the variables in the simple GLM had scores <4, indicating multicollinearity was not an issue. Still, the VIFs for the global model had outrageously large VIFs > 1700 for all main effects and their interactions. Based on these results, litter variables cannot explain variability in EC_a.

Table 4.6. *Summary of the generalised linear model using the main and interaction effect of all litter variables as predictors of apparent electrical conductivity to 50cm and 160cm cumulative depths.*

	Cumulative depth to 50cm				Cumulative depth to 160cm			
Coefficients:	Estimate	Std. Error	*t-value*	*p-value*	Estimate	Std. Error	*t-value*	*p-value*
(Intercept)	-4.16	9.20	-0.45	0.65	-5.95	7.88	-0.75	0.46
Site	16.71	30.88	0.54	0.59	-17.43	26.46	-0.66	0.51
$LFH^{Thickness}$	3.36	2.05	1.64	0.11	3.18	1.75	1.82	0.08
LFH^{GWC}	0.10	0.16	0.62	0.54	0.14	0.13	1.01	0.32
$LFH^{Density}$	0.24	0.22	1.11	0.27	0.29	0.19	1.56	0.13
Site: $LFH^{Thickness}$	-9.39	6.87	-1.37	0.18	-1.29	5.89	-0.22	0.83
Site: LFH^{GWC}	-0.25	0.36	-0.69	0.50	0.12	0.31	0.39	0.70
$LFH^{Thickness}$: LFH^{GWC}	-0.05	0.03	-1.55	0.13	-0.05	0.03	-1.74	0.09
Site: $LFH^{Density}$	-9.77	14.28	-0.68	0.50	4.44	12.23	0.36	0.72
$LFH^{Thickness}$: $LFH^{Density}$	-0.15	0.08	-1.97	0.06	-0.14	0.07	-2.05	0.05
LFH^{GWC}: $LFH^{Density}$	0.00	0.00	-1.07	0.29	0.00	0.00	-1.51	0.14
Site: $LFH^{Thickness}$: LFH^{GWC}	0.12	0.08	1.54	0.13	0.03	0.07	0.50	0.62
Site: $LFH^{Thickness}$: $LFH^{Density}$	3.47	3.14	1.10	0.28	0.19	2.69	0.07	0.94
Site: LFH^{GWC}: $LFH^{Density}$	0.11	0.16	0.73	0.47	-0.04	0.14	-0.30	0.76
$LFH^{Thickness}$: LFH^{GWC}: $LFH^{Density}$	0.00	0.00	1.91	0.06	0.00	0.00	2.01	0.05
Site: $LFH^{Thickness}$: LFH^{GWC}: $LFH^{Density}$	-0.04	0.03	-1.16	0.26	0.00	0.03	-0.14	0.89
Dispersion parameter	0.17				0.12			
Null deviance (degrees of freedom)	51.87 (48df)				27.063 (48df)			
Residual deviance (degrees of freedom)	5.52 (33df)				4.22 (33df)			
AIC	197.72				241.37			
R^2	0.91				0.82			

LFH = Litter, Thickness = Thickness (cm), GWC = Gravimetric water content (%), Density = litter g/cm

4.4 Discussion

The results of this section show that the variability in apparent electrical conductivity at both cumulative depths 50cm and 160cm cannot be explained by temperature or instrument drift (**Table 4.2**), the presence or the absence of forest litter (**Table 4.4**) and forest litter variables such as litter gravimetric water content, litter thickness or litter density (**Table 4.6**).

4.4.1 Drift caused by instrument temperature, soil temperature, ambient temperature and voltage

The analysis of apparent electrical conductivity (EC_a) data collected during the measurement campaign at Mahurangi and Te Hiku Forests reveals no substantial correlation between EC_a and variations in temperature, whether it be ambient temperature, soil temperature, or instrument temperatures, as well as voltage levels (**Table 4.2**), to both cumulative depths of 50cm (EC_a^{50}) and 160cm (EC_a^{160}). While some weak correlations were observed, they were not statistically significant, indicating that any apparent relationships could be attributed to chance rather than meaningful associations.

The most likely reason for the lack of relationship is, firstly, during measurement campaigns, the battery pack on the instrument was changed regularly to ensure the instrument was not affected by decreases in voltage. This caution appears to have worked well. Next, the lack of relationship between ambient temperature, air temperature, soil temperature and apparent electrical conductivity could be ascribed to the environmental conditions in forested catchments. The temperature data collected for this study, particularly the ambient and soil temperature for both catchments, were relatively stagnant both within and between sites (**Table** 4.1). The DualEm-1's sensors are well insulated, which was an intentional act of the manufacturers to protect the sensors against extreme temperature changes (DualEm, 2014). In addition, at the time of measurement, both forests had achieved full canopy cover, providing shade and reducing direct sunlight exposure to the forest floor. With limited, direct solar radiation accessing the forest floor, the result was more stable and moderate temperatures under the forest canopy (McLaren & Cameron, 1996). Finally, forest litter acts as an insulator for the upper horizons of the forest floor, meaning temperature variability is far less extreme than in more exposed soils (Bren, 2016; Park et al., 1998).

Based on these findings, there is no requirement in this study to conduct an error correction to compensate for drift caused by instrument voltage, temperature, and ambient and soil temperature. These results apply to the findings in this study only. If measurements of this kind are conducted in the future, it would be wise to check for relationships between EC_a, temperature and voltage, as it cannot be assumed the unique set of conditions in this study would be the same for all forested catchments.

4.4.2 The effect of the presence and absence of forest litter and the litter water content, thickness and density

The lack of significant difference in apparent electrical conductivity (EC_a) in the presence and absence of forest litter and the lack of significant relationships between EC_a and litter gravimetric water content, litter thickness and density could be attributed to several factors.

Forest floor litter is a loose assortment of organic matter in varying stages of decay (Liu et al., 2022; Santos et al., 2010). Because forest litter is not densely packed, there is a lot of pore space between solids filled with air. Air is not conductive and is assumed to have a neutral effect on the electromagnetic induction signal (DualEm, n.d). Therefore, if forest floor litter has large air spaces, the effect would be the same as holding the DualEm at the height of litter thickness. Soil salinity (Huang et al., 2017b; Stockmann et al., 2017), water content (Gallart et al., 2019; Martinez et al., 2018) and texture (Caires et al., 2014; Gallart et al., 2019) are considered the most influential factors in the variability of EC_a along with soil depth and soil organic matter (Atwell & Wuddivira, 2019). These soil variables can have high attenuation rates. If they did occur in the litter layer, then it would be difficult for the EMI signal to penetrate past these attributes, which is likely why the presence or absence of forest litter could not be used to explain the variability of EC_a.

In summary, when using electromagnetic induction technology such as the DualEm- 1 in forest catchments, an adjustment factor is not required to compensate for the presence of forest litter on EC_a, nor is there a need to remove forest litter before conducting electromagnetic induction surveys. However, if forest litter is considerably thick, saturated or has other qualities not discussed here, it would be best to test for changes in EC_a in the presence and absence of forest litter.

Chapter 5

Using electromagnetic induction technology and software to predict soil texture and moisture properties in forested catchments

---

5.1 Introduction

Soil texture and moisture are crucial in understanding hydrological processes and ecosystem dynamics within forested catchments. The characterisation of these soil properties is essential for land management, water resource management and ecological studies (Allaire et al., 2009; Bren, 2016)

Capturing microsite heterogeneity of forest soils is crucial because it allows a more accurate understanding of hydrological processes and ecosystem dynamics within forested catchments (Amatya et al., 2016). The variability of soil texture and moisture across different microsites can significantly impact water availability, nutrient cycling, and plant growth, ultimately affecting forest ecosystems' health and productivity (Bren, 2016). Forest owners can make more informed decisions regarding land use and water resources by characterising the soil properties at a microsite level (Atwell et al., 2013; Atwell & Wuddivira, 2019). Therefore, they can better predict and mitigate the impacts of climate change on water availability and even provide insights into the relationships between soil properties and biodiversity, which can inform conservation efforts and help maintain healthy and resilient forest ecosystems (De Jong, 2016).

Traditional methods for soil characterisation, such as soil sampling and laboratory analysis, are often labour-intensive, time-consuming, and costly and may not be feasible for large-scale assessments or frequent monitoring of remote, steep, and rugged landscapes. Thus, the natural microsite heterogeneity of forest soils is less likely to be captured (Lardo et al., 2012; McBratney et al., 2005; Serrano et al., 2014; Triantafilis & Monteiro Santos, 2013). Therefore, an alternative, cost-effective method of capturing forest soil heterogeneity over both small and large scales is required, and this comes in the form of geophysical sensing using electromagnetic induction (EMI) technology (Lardo et al., 2012; McBratney et al., 2005; Serrano et al., 2014; Triantafilis & Monteiro Santos, 2013).

5.1.1 Geophysical sensing using electromagnetic induction

Geophysical sensing using electromagnetic induction (EMI) technology has successfully been used to infer soil properties, including soil texture and moisture content in various environments, particularly in agriculture and archaeological and geotechnical exploration (Atwell et al., 2013; Caires et al., 2014; Lardo et al., 2012; Serrano et al., 2013; Silva et al., 2021; Uchida et al., 2001; Urdanoz & Aragüés, 2012). Such technology measures apparent electrical conductivity (EC_a), which is primarily affected by soil texture and moisture and thus can discern soil heterogeneity without destructive sampling, both repeatable and on a large scale. Although EMI technology is used extensively to determine the impacts of soil physical and chemical properties in agriculture as a tool for land management and crop productivity, the same cannot be said for forest soils, with only a handful of studies found using the technology in forest environments (Altdorff et al., 2017; Atwell & Wuddivira, 2019; Bennett & George, 1995; Bréchet et al., 2012; Feikema & Baker, 2011; Gallart et al., 2019; Kinal et al., 2006; Lad et al., 2019; Ryland et al., 2020) and two studies found using the technology in a P. radiata production forests in New Zealand. (Gallart et al., 2019; Lad et al., 2019).

5.1.2 Forest soils and how they differ from agricultural soils

Forest soils have a vast biodiversity of flora and fauna and tend to have high porosity and low bulk density (Amatya et al., 2016; Bren, 2016; Clinton & Owens, 2023; De Jong, 2016). The soil is regularly worked as a direct result of bioturbation and pedoturbation caused by micro and macro-organisms in and on the forest floor (Amatya et al., 2016). Forest soils rarely experience overland flow due to the thick, sponge-like forest litter which overlies the forest soil (Li et al., 2014; Neary et al., 2009; Uchida et al., 2001). In addition, decaying tree roots create soil pipes that help divert and redistribute precipitation, which reaches the forest soil through lateral flow (Uchida et al., 2001). Because forests have long harvesting rotations or may not be harvested at all, their roots can penetrate beyond 40cm depth, range in size from <2mm to <5cm and grow radially (**Figure 5.1**) from the trunk beyond a 2-metre distance (Phillips et al., 2023).

Figure 5.1. *Root excavation of a 25 year old P. radiata (Phillips et al., 2023).*

The soil moisture is redistributed during the wetter months via lateral flow and stored in micro and macro pores, which are slowly released and less likely to suffer from drought in drier summer months (Uchida et al., 2001). In contrast, agricultural soils typically have lower porosity and higher bulk density with lower diversity and presence of micro and macro flora and fauna as the soils are regularly exposed to an anthropogenic modification such as tilling, compaction by machinery and stock (Sparling & Schipper, 2004) and are left exposed while crops are re-establishing after harvest which allows compaction and erosion during precipitation events, loss of soil moisture via evaporation and erosion, and loss of soil during wind events which all promote poor soil physical properties (Colazo & Buschiazzo, 2015; Fryrear, 1985; Lyles, 1975).

5.1.3 Electromagnetic induction and forest soils

Measuring apparent electrical conductivity (EC_a) using electromagnetic induction technology (EMI), such as the DualEm-1, is a way of assessing soil properties in a non-destructive and repeatable manner. Its original primary use was to determine soil salinity in areas prone to saltwater intrusion, as there is a strong positive relationship between EC_a and saline content in the soil (McNeill, 1980). Apparent electrical conductivity was also found to correlate with changes in soil moisture, texture (Gallart et al., 2019; Martinez et al., 2018), bulk density, porosity, carbon content (Atwell & Wuddivira, 2019), and clay content (Neeraj & Chandra, 2021; Triantafilis & Lesch, 2005), in addition

to other chemical and physical properties, which makes EC_a measurements using EMI a valuable tool for understanding soil properties.

Other benefits of the EMI technology and, more specifically, the DualEm-1 include portability, allowing surveys on rugged and difficult-to-access locations, and non-destructive measurements, where the instrument is placed on the ground in an upright position (DualEm, 2014). Apparent electrical conductivity at multiple depths are simultaneously recorded with the press of a button (DualEm, 2014). Therefore, measurement surveys can be repeated, and measurement density can be as course or fine as end users of the data require at both a small and large scale due to the cost-effective, efficient, and straightforward nature of measurement collection. These features of EMI technology make them an excellent candidate for predicting soil properties in challenging forested environments.

As long as geospatial data is collected at each measurement point (often this occurs simultaneously with in-built GPS), the data can then be mapped in one dimension using ordinary Gaussian kriging to create a map of EC_a across the study site. Soil sampling is still required to establish relationships between EC_a and the soil property in question; however, sampling is far less intensive and more strategic. For example, choosing sample locations defined by specific topographic features (e.g. aspect, Slope, elevation). Or, because geolocation data is simultaneously collected, summary statistics, including minimum, maximum, mean and outlier EC_a values, can be assessed and remeasured before soil sampling in these unique locations. Electromagnetic induction technology such as the DualEm-1 measures EC_a at two cumulative depths, allowing inversion software such as EM4Soil to disseminate the EC_a down the soil profile. If EC_a is collected in transects, two-dimensional maps can be created to visualise the changes across a study site along those transects. In addition, software such as EM4Soil (EMTOMO LDA, 2018) can use geospatial data such as latitude/longitude and elevation to visualise EC_a in three dimensions using quasi-three-dimensional inversion.

5.1.4 Quasi-3D inversion of apparent electrical conductivity

Quasi-three-dimensional inversion refers to a geophysical technique used to interpret subsurface data, such as apparent electrical conductivity (EC_a) using electromagnetic induction (EMI), to create a three-dimensional (3D) model of the earth's subsurface (EMTOMO LDA, 2018). Inversion refers to inferring subsurface properties based on measured geophysical data such as EC_a. The term "quasi" is

used because EMI surveys collect data in one dimension and are used along with geospatial data to create a more comprehensive but approximate 3D representation (Davies et al., 2015; El-Naggar et al., 2021b; McNeill, 1980; Triantafilis et al., 2011; Triantafilis & Santos, 2011). Quasi-three-dimensional inversion involves solving complex mathematical equations and optimisation algorithms considering measured EC_a, geological constraints (such as elevation), and regularisation techniques to create a model that best fits the observed data (Kang et al., 2015; Triantafilis & Monteiro Santos, 2013). Therefore, quasi-3D inversion bridges the gap between two-dimensional and 3D representations of geophysical data such as EC_a. It is important to note that quasi-3D inversion is not the same as true 3D inversion, which considers the full spatial variability of the subsurface and is, therefore, more complex and accurate, with the caveat of it being more computationally intensive. Quasi-3D inversion is a practical compromise between 2D and full 3D inversion, balancing computational efficiency and improved subsurface characterisation (Triantafilis & Santos, 2013).

5.1.5 Chapter objectives

Chapter 5's objectives are to establish if apparent electrical conductivity and modelled electrical conductivity adequately capture the spatial heterogeneity of soil physical properties (texture), chemical properties (electrical conductivity) and soil moisture in forested catchments using a mixture of statistical analysis and one-dimensional and 3D maps and comparison between ordinary kriging and quasi-3D inversion.

5.2 Methods

5.2.1 Soil sampling and lab analysis

The following sampling protocol and analysis were developed, in part, using the methods outlined by Triantafilis and Santos (2013), El-Naggar et al. (2021a), Davies et al. (2015); Huang et al. (2017b) who used EM4Soil EC_a inversion modelling software to predict the spatial variability of soil properties such as electrical conductivity (EC), clay and content using EC_a measurements taken using DualEm-421. Field samples were collected, and these properties were measured in a lab at various depths to validate DualEm apparent electrical conductivity data (Triantafilis & Santos, 2013).

5.2.1.1 Soil Sample Collection

Forest litter and DualEm EC_a measurement protocol are outlined in **Sections 3.2.2** – **3.2.4**. The methods outlined below occurred directly after those summarised in Chapter 3 and were developed using Manderson et al. (2007). Soil samples were taken in each plot from the centre of the EC_a measurement site using a stainless-steel Hoffer sampler with a diameter of 2.3 cm and sampling lengths of 30cm, 60cm and 90cm (**Figure 5.2, Table 5.1 & Table 5.2**). The cores were taken from the same hole using the three different hoffers to obtain samples down the soil profile at the three depths (**Figure 5.2, Table 5.1 & Table 5.2)**.

Due to instrument availability and time constraints, the field team could not retain intact soil cores to analyse in the lab. Therefore, to obtain a record of the soil profile, all three cores were laid on a laminated sheet adjacent to a measuring tape and photographed (**Table 5.1 & Table 5.2**). Samples were then put in a clean, airtight bag, labelled with site, plot, depth and sample date and kept cool and dry in a chilly bin until they were returned to the office, where they were immediately put in a 4°C fridge before processing for lab analysis (**Figure 5.2**).

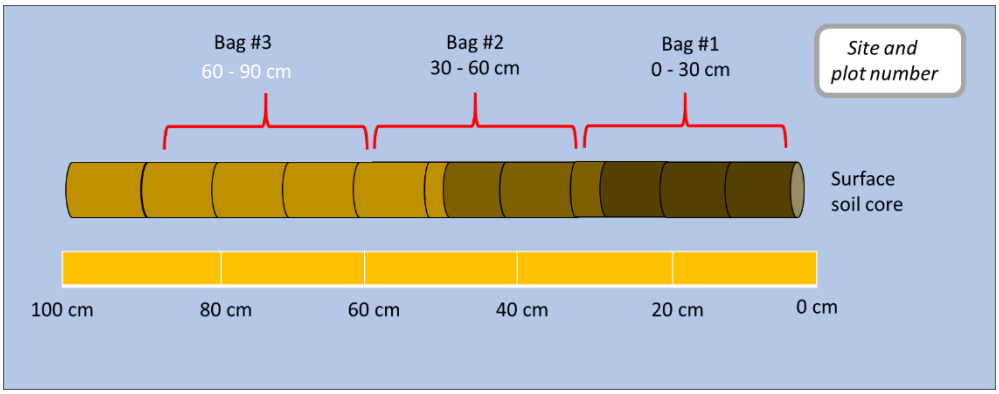

Figure 5.2: *Soil cores were taken in 30cm lots regardless of soil profile/texture boundaries. Photo courtesy of Jen Owens (2022).*

Table 5.1. *Soil auger samples from the centre of each of the 25 plots at Mahurangi Forest for depths 0 - 30 (left), 30 - 60cm (centre) and 60-90cm (right) in order of highest to lowest apparent electrical conductivity to a depth of 160cm.*

03A18 **03A07** **03A24** **03A14** **03A01** **03A19** **03A06**

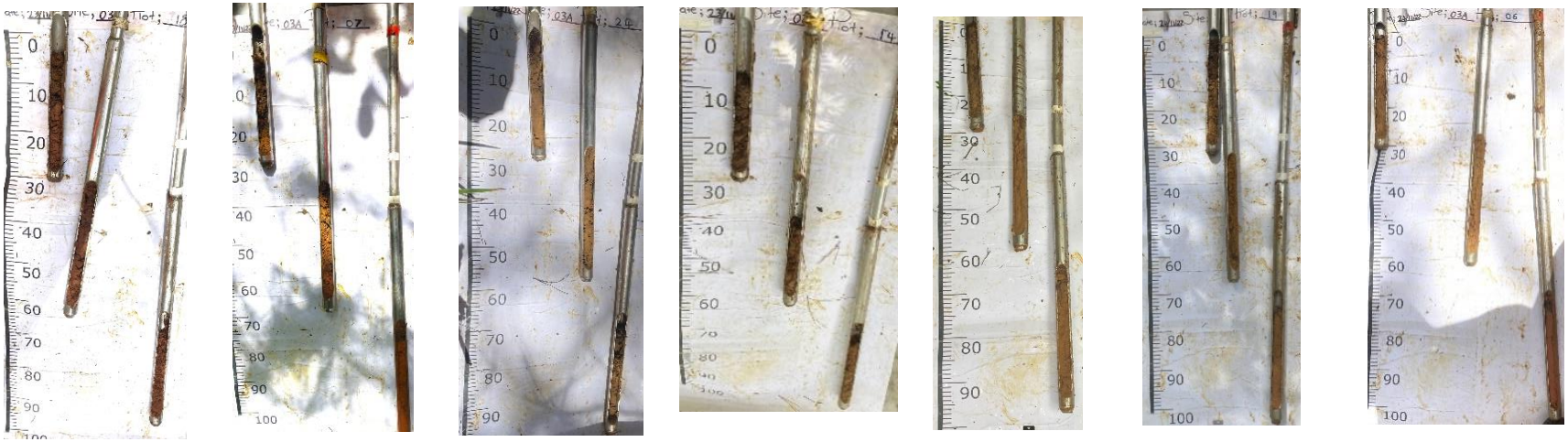

03A09 **03A20** **03A16** **03A15** **03A21** **03A02** **03A12**

03A03

03A04

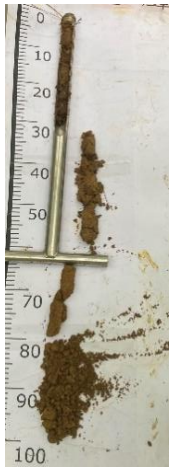

03A08

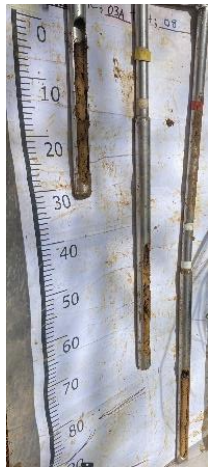

03A05

03A17

03A23

03A25

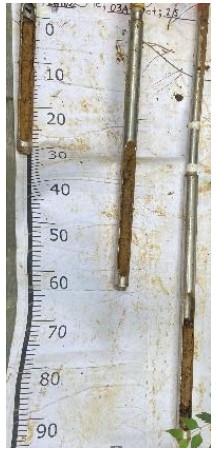

03A13

03A11

03A10

03A22

Table 5.2. *Soil auger samples from the centre of each of the 25 plots at Te Hiku Forest for depths 0 - 30 (left), 30 - 60cm (centre) and 60-90cm (right) in order of highest to lowest apparent electrical conductivity to a depth of 160cm.*

04A17

04A06

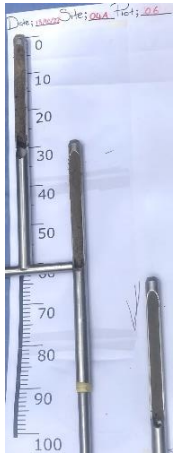

04A15

04A25

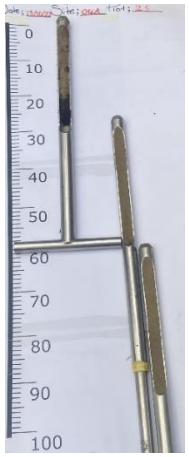

04A20

04A04

04A05

04A03

04A14

04A07

04A18

04A24

04A12

04A11

04A01

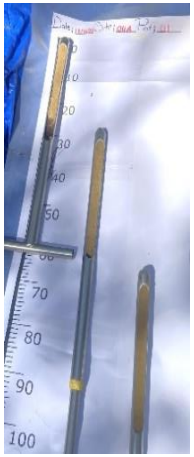

04A09

04A13

04A08

04A21

04A10

04A02

04A16

04A22

04A23

Standard operating procedures were provided to the field team to ensure the samples were not compacted during sampling and that equipment was cleaned between sampling to reduce cross-contamination. Where health and safety were concerned, or bedrock was shallower than 1 metre, sampling was limited to a sampling depth practical for the sample collection team. Additionally, geo-referencing data of the core site was collected using a Garmin GPS.

5.2.1.2 Gravimetric water content and sample preparation

Samples were weighed, oven-dried at 105^{o}C for 48 hours and then reweighed. Gravimetric water content was calculated using **Equation 2**, replacing litter values with wet and dry soil weights. Samples were then passed through a 2mm sieve to remove leaf litter and debris. Each sample was subsampled by placing 30g of soil into a clean, plastic sample container for further analysis. It was noted that particles of different sizes and shapes naturally sort themselves when shaken, with fine-grained particles settling to the bottom and coarse-grained particles at the top. Therefore, to ensure a representative sub-sample was obtained, the dried sample was well mixed in a tray, and sub-samples were taken by dragging a spatula down the middle of the dried sample to get particles from the top and the bottom of the sample. The subsample was analysed using a particle fraction analyser. Then, the same sample was measured for electrical conductivity by creating a solution of one part soil to five-part water (Triantafilis & Santos, 2013).

5.2.1.3 Particle fraction analysis and soil texture classification

Using the 30mg sub-samples, percentage volume and percentage number of particles of clay (<0.002mm), silt (0.002 – 0.06mm), fine sand (0.06 – 0.2mm), medium sand (0.2 – 2mm) and course sand (>2mm) (Milne et al., 1995) was calculated using a particle fraction analyser called CAMSIZER® X2 (CX2) (Microtrac, 2020). The CAMSIZER® can characterise the grain size of particulate materials ranging from 0.0008mm to 8mm, which is made possible because the combined zoom camera and primary camera allow optimum image resolution (Microtrac, 2020). This particle fraction analyser consists of a sample feeder, a particle dispersal module, and an imaging module controlled by proprietary CX2 software (**Figure 5.3**). "Particles are dispersed past the field of view of two high-resolution digital cameras to image the moving particles that an LED backlights" (Buckland et al., 2021). The software processes the images created in real-time and generates shape and grain size distributions and statistics (**Figure 5.3**).

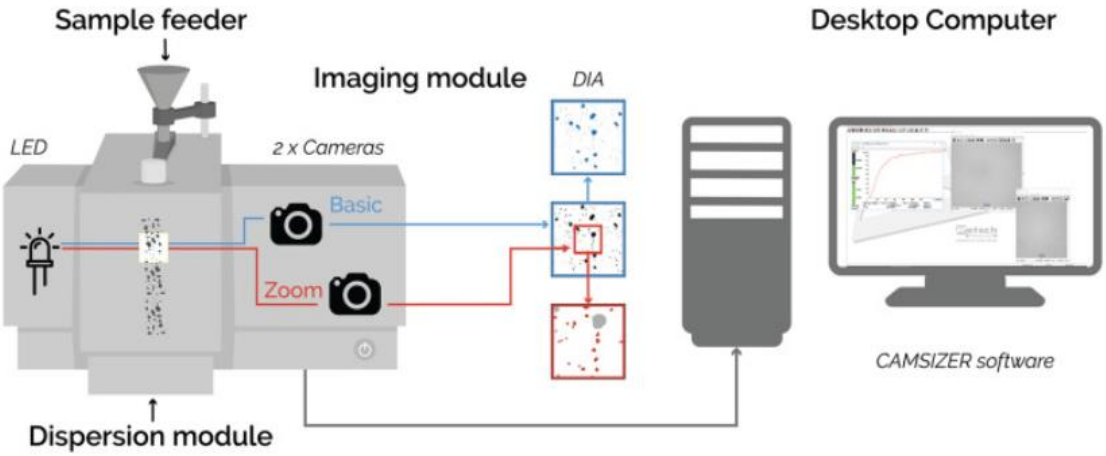

Figure 5.3. *Components of the particle fraction analyser CAMSIZER ®(Microtrac, 2020).*

Particle fraction analysis was used for statistical analysis purposes, specifically the percentage number of particles per sample by size class because the volume of clay in each sample was <0.0001%. When rounded, this would incorrectly imply no clay-sized particles were in each sample. Texture descriptions were assigned using the ribbon method to determine stickiness, plasticity, and friability/deformability. In addition, soil colour was given a number and name description using the Munsell colour chart, and overall texture classification was determined using data from the particle fraction analysis and the soil texture triangle (Milne et al., 1995; Webb & Lilburne, 2011). Assignment of texture descriptions, colour and texture classification was done based on samples from the three sample depths (0 – 30cm, 30 – 6cm and 60 – 90cm), as sampling could not preserve the soil horizon profiles.

5.2.1.4 Electrical conductivity of 1-part sample to 5-part water

The electrical conductivity of soil is traditionally measured using a saturated paste extract to estimate salt contents (Sonmez et al., 2008). However, 30mg sub-samples were used to measure electrical conductivity using a Thermo Scientific TDS 6+ TDS meter. The sample was mixed with deionised water to create a one-part soil to five-part water solution, which was shaken for 30 minutes and then allowed to settle for 24 hours before being measured for electrical conductivity (Blakemore et al., 1981; Manaaki Whenua - Landcare Research, n.d). The electrical conductivity meter was temperature compensated (meaning post-measurement temperature calibration was not required). The probe was also checked against a pre-prepared KCL solution with a measured electrical conductivity of 1.413 dS/m at 25 °C.

5.2.2 Statistical analysis

All statistical analysis was conducted in R studio version 4.3.0 (R Development Core Team, 2018), including summary statistics and graphs to determine if apparent electrical conductivity can predict soil texture and soil moisture properties. For all subsequent analyses, cumulative electrical conductivity to 50cm and 160cm were treated as separate response variables with the same predictor variables to see if one sensor was more sensitive to soil properties than the other.

5.2.2.1 Exploratory analysis and assumption testing

Summary statistics were obtained for each measured variable by site and depth, including the mean, quartiles, minimum, maximum and standard error of mean. To test the data for normality, heteroscedasticity and skew, a Kolmogorov-Smirnov (K-S) test using the R package "fitdistrplus" (Delignette-Muller & Dutang, 2015) was conducted on response variables along with visual inspections of Q-Q plots and histograms. While the K-S test on apparent electrical conductivity EC_a at 160cm (EC_a^{160}) had a better fit with a normal distribution than EC_a at 50cm (EC_a^{50}), the histograms showed EC_a^{50} and EC_a^{160} were right-skewed, likely due to all variables being zero bounded. Q-Q plots showed a good fit at the centre of the data but did not fit well at the bottom and top tail.

Multicollinearity was tested using variable Inflation Factors (VIF), which was checked for each independent variable using the "car" package in R studio (Fox & Weisberg, 2011). A variable inflation factor value <4 generally shows a lack of multicollinearity between variables, although some variables were greater than this (<10). It has been cautioned to avoid using variables with high VIFs, as suggested by O'Brien (2007).

To manage the high VIFs caused by soil texture, Salomão et al. (2022) used methods to determine which soil texture percentage should be used in subsequent generalised linear mixed effect models. Pearson Correlation Coefficient was calculated for soil texture to determine which variable should remain for future analysis to reduce the instances of high VIFs (Fox & Weisberg, 2019) (**Table 5.3)**. The percentage number of silt particles had a strong, negative correlation with clay (R^2 = -0.79) and sand (R^2 = 0.90) and was therefore not used in subsequent analysis. Clay and sand percentages were weakly correlated (R^2 = 0.45) with even weaker correlations when sand was split into medium and fine categories and were, therefore, used to represent soil texture in further analysis, in line with the treatment of sand, silt and clay variables by Salomão et al. (2022).

Table 5.3. *Pearson's product-moment correlation coefficient to determine which variables should remain in subsequent analysis to reduce multicollinearity*

	CLAY	SILT	FSAND	MSAND	SAND	Sphericity	GWC
SILT	-0.79						
FSAND	0.43	-0.89					
MSAND	0.34	-0.52	0.42				
SAND	0.45	-0.90	0.99	0.52			
Sphericity	0.08	0.06	-0.24	0.68	-0.14		
GWC	-0.07	-0.03	0.19	-0.67	0.10	-0.93	
ECe	-0.04	-0.02	0.15	-0.64	0.06	-0.86	0.85

In addition, extremely high VIFs (>2000) were caused when interactions between predictor terms were included in generalised linear mixed effects models. All predictor terms were treated as main effects, and no interactions were used except for gravimetric water content and electrical conductivity of a one-part soil to five-part water solution. More appropriate statistical models that can deal with high inflation factors, multicollinearities and variable removal, such as ridge or lasso regression, principal components analysis or non-linear statistical models, could be used for future analysis.

5.2.2.2 Calculating weighted means of measured soil variables

Using similar methods to those used by (Sudduth et al., 2001), (McNeill, 1980) and (Hedley et al., 2004), apparent electrical conductivity to cumulative depths 50cm (EC_a^{50}) and 160cm (EC_a^{160}) were correlated with weighted mean values for gravimetric water content (GWC (%)), the electrical conductivity of a one part soil to five-part water solution ($EC^{1:5}$ (mS/m)), clay, fine sand and medium sand particle percentage per sample (CLAY, FSAND, MSAND). Weighted means were calculated using the following equation:

Equation 6. *Calculation of weighted mean of soil variables*

$$\mu = (\Sigma(\text{weight} * \text{value})) / \Sigma\text{weight}$$

Where:
μ = the weighted mean of soil variable
Σ = sum over all relevant data points
Weight = weight associated with depth (either 60 or 90)
Value = actual value of each soil variable

The weighted means were calculated twice, once with a weight of 0 - 60cm and again for 0 - 90cm to account for the influences on shallow soil characteristics as well as the characteristics of the full profile (Hedley et al., 2004; McNeill, 1980; Sudduth et al., 2001) and were then input as predictor variables in generalised linear mixed effects models for subsequent analysis.

5.2.2.3 Statistical analysis to assess if variables affect apparent electrical conductivity

As the dataset had a hierarchical structure, a generalised linear mixed effects model (GLMER) was applied by assigning the weighted mean values of measured soil variables as (gravimetric water content (GWC), electrical conductivity of a soil solution ($ECe^{1:5}$) and clay, fine sand and medium sand particle percentage) as fixed effects and site as a random effect (Lee & Nelder, 2001). The package used in R studio was 'lme4' using the 'glmer' function(Bates et al., 2014). Given that EC_a was continuous, positively skewed, non-negative, and 0 – 100 bounded, a gamma distribution family with a log link function (**Equation 7**) was used to accommodate these attributes Schabenberger and Pierce (2001).

Equation 7. *Global generalised, linear mixed effects model.*

$$GLMER\big(EC_a \sim (1|Site) + Clay_{WM} + FSAND_{WM} + MSAND_{WM} + GWC_{WM} * ECe^{1:5}_{WM}\ distribution = Gamma\ (\ link = (log)\big)$$

Where:
EC_a = Either apparent electrical conductivity to 50cm or 160cm
$(1|Site)$ = Site as a random effect
CLAY = Weighted mean of clay sized particles (%)
FSAND = Weighted mean of fine sand sized particles (%)
MSAND = Weighted mean of fine sand sized particles (%)
WM = Depth range of weighted mean, either 60cm or 90cm

All four global GLMER derived from **Equation 7** were simplified using the 'dredge' function, accessed via the 'MuMIn' package in R studio (Barton, 2023), which allows the parameters of the global model to automatically subset all possible simplified model combinations (Barton, 2023). The global and simplified models were ranked based on Akaike information criterion (AIC) selected for small sample sizes (AICc) (**Equation 8**). Akaike information criterion is a commonly used model selection tool to assess the parsimony of model structures (Akaike, 1974; Bonakdari & Zeynoddin, 2022). Akaike information criterion is "minus two times the log-likelihood plus two times the number of model parameters"(Akaike, 1974) and measures both model fit whilst penalizing for overfit (Bonakdari & Zeynoddin, 2022).

***Equation 8**. Akaike's Information Criterion equation corrected for small sample size (Bonakdari & Zeynoddin, 2022).*

$$AICc = AIC + \frac{2k(k+1)}{n-k-1}$$

Where:
n = number of resiuals
k = Sum of model parameters
AIC = $AIC = -2ln(\sigma_\varepsilon^2 2) + 2k$
Where :
σ_ε^2 = maximum likelihood of is the residuals' variance

The "-2" in **Equation 8** ensures models with the best fit have a lower AIC score (Akaike, 1974; Bonakdari & Zeynoddin, 2022). A higher penalty term is introduced when the sample size is small, allowing AIC to be corrected and making the selection process more reliable (**Equation 8**) (Bonakdari & Zeynoddin, 2022). The top-ranking models were considered to be those within 3 points of the lowest AICc score, along with their R^2 values and log-likelihood. The dredge function assigned a delta value to identify how far each model sat from the lowest AICc score (delta = 0 is the lowest AICc scoring GLMER).

The drawback of using this form of the selection process is that AICc does not have insight into underlying relationships in the data. Therefore, this criterion should not be used in isolation but rather in combination with other model parameters, such as R^2 (Bonakdari & Zeynoddin, 2022). In addition, AICc assumes the models being compared are linear, meet the assumptions of linearity and are more suited to data with a Gaussian distribution or data that lacks outliers (Bonakdari & Zeynoddin, 2022). Finally, AICc does not perform hypothesis testing and can only indicate if the model has a good fit, not if particular predictor variables are statistically significant (Akaike, 1974; Bonakdari & Zeynoddin, 2022). Despite these drawbacks, AICc is a valuable tool for model selection when used with other model metrics and for understanding the results in the context of the wider study (Bonakdari & Zeynoddin, 2022).

Likelihood ratio Chi-square tests were conducted using the 'lm test' package in R studio (Zeileis & Hothorn, 2022) to compare each global GLMER with the simplified GLMERs to determine which model best explains the variability in EC_a. Likelihood ratio chi-square tests allow nested models to be compared to identify if the presence or absence of model parameters significantly affects model

fit by comparing a global or full model with a restricted or simplified model (Westfall & Henning, 2013).

A generalised linear mixed effects model was selected based on balanced goodness of fit with complexity and had significant and sensical R^2 and *p-value*s. This generalised linear mixed effects model was assessed for multi-collinearity using Pearson's product-moment correlation, concurrently calculated in R studio as the GLMER summary (Bates et al., 2014). Variable inflation factors were also assessed using the 'vif' function in the 'car' package in R studio (Fox & Weisberg, 2019)

5.2.3 Visualisation of modelled and apparent electrical conductivity using ordinary kriging and inversion software

5.2.3.1 Mapping apparent electrical conductivity using ordinary kriging

Apparent electrical conductivity measured at cumulative depths 50cm and 160cm along with geospatial data (elevation, easting and northing) were transferred to ARC GIS Pro version 3.1.0 (Esri Inc., 2023). The points were kriged using the Spatial Analyst tool (ESRI©) using ordinary kriging and Gaussian semi-variogram model to produce four maps of soil EC_a at 50cm and 160cm depths at Mahurangi Forest and Te Hiku Forest using the inputs listed in **Table 5.4** The input data used for each site differed to compensate for the fact that Mahurangi was a far smaller catchment than Te Hiku with the same number of data points, and Te Hiku was less variable across the study site, so using different inputs highlighted the subtle changes across the catchment.

Table 5.4. *Input data for ordinary kriging for apparent electrical conductivity at sites Mahurangi and Te Hiku for cumulative depths 50cm and 160cm.*

Study site	Mahurangi	Te Hiku
Number of lags	100	10
Lag size	2	300
Nugget	0.2	0.45
Partial sill	0.15	1.93
Measurement error	10%	10%

5.2.3.2 Mapping apparent electrical conductivity using laterally constrained 1D inversion software

The 'grid data' function in EM4Soil's 'Map Module' was used to produce one-dimensional maps of apparent electrical conductivity to 50cm and 160cm cumulative depths using the nearest neighbour technique (EMTOMO LDA, 2018). The input data included apparent electrical conductivity to 50cm and 160cm, geospatial data of each measurement point (eastings, northing and elevation), and pitch and roll of the instrument to adjust for any noise caused by excessive pitch or roll. The 'gridded data' function automatically selects the grid geometry, which uses the easting and northing to create a mean distance between data points and a user-defined "number of lines", increasing the number of rows and columns in the grid. Increasing the user-defined smoothing function produces a more visually aesthetic map at the expense of accuracy, as artefacts are created or removed in the map depending on sample size and sample area.

5.2.3.3 Using quasi-3D inversion software to model electrical conductivity

The same data (geospatial, pitch, roll and apparent electrical conductivity to 50cm and 160cm) used in **Section 5.2.3.2** was used to create quasi-3D inversion maps using the Map module of EM4Soil (EMTOMO LDA, 2018). Four sets of inputs are required: parameterisation, initial model, inversion algorithm and gridding parameters).

Inversion parameters

Five user-defined parameters were required to control the smoothing and fit of the quasi-3D inversion model (**Table 5.5**). The dampening factor (λ) controls model smoothness and was increased from the default for both Mahurangi and Te Hiku maps to create smoother, less blocky maps (**Table 5.5**). Default values of misfit and data error were unchanged, and the number of iterations was increased to 80. There are three inversion algorithms to choose from using different variations of Occam's regularization (EMTOMO LDA, 2018; Khongnawang et al., 2019). Algorithm S2 was selected as the initial model assumes a five-layer earth, and this algorithm produces smoother maps as the algorithm constrains the model response around the reference model (**Table 5.5**) (EMTOMO LDA, 2018; Khongnawang et al., 2019).

***Table 5.5**. Parametisation of quasi-3D inversion model.*

Inversion parameter	Default	Used in this study
Dampening factor	0.07	5
Number of iterations	10	80
Data error	1.00	1.00
Misfit target	0.20	0.20
Algorithm	S3	S2

Initial Model

A heterogeneous, five-layer initial model was considered, with depths to the top of each layer being 0, 30cm, 60cm, 90cm and 120cm. At each depth, the mean electrical conductivity of a 1-part soil to a 5-part water solution was input for each site (**Table 5.6**). It was assumed that below 90cm, the profile was homogenous and used the same input value as at 90cm.

Inversion model

Two models can be used depending on the apparent electrical conductivity data collected: cumulative function (CF) or full solution (FS). The latter is not limited to small induction numbers and is, therefore, more appropriate for highly conductive soils (>100mS/m) (EMTOMO LDA, 2018; Khongnawang et al., 2019). Thus, the former CF model was used for both sites as apparent electrical conductivity values were < 35mS/m (**Table 4.3**).

Gridding model

As in **Section 4.2.3.2**, the grid geometry must be altered to map the final quasi-3D inversion model, which uses the easting and northing to create a mean distance between data points. The user-defined “number of lines" was increased to 50 for the x and y-axis and the smoothing factor to 5 for both the x and y-axis.

5.3 Results

5.3.1 Summary Statistics

5.3.1.1 Soil gravimetric water content and electrical conductivity of a 1-part soil to 5-part water solution

Summary statistics **Table 5.6** and box plots **Figure 5.4** provide details of measured variables of soil samples collected at Mahurangi and Te Hiku at depths 0 – 30cm, 30 - 60cm and 60 – 90cm for soil gravimetric water content (GWC) and electrical conductivity of a one part soil to five parts water solution ($ECe^{1:5}$).

Mean and median GWC and $ECe^{1:5}$ were higher at Mahurangi than at Te Hiku, with low standard errors (0.16 – 1.89) for both sites and variables (**Table 5.6)**. The range at Mahurangi and Te Hiku for both GWC and $ECe^{1:5}$ decreased with soil sample depth, with overall higher ranges for Mahurangi (GWC 34 – 40 and $ECe^{1:5}$ 24 – 29) than for Te Hiku (GWC 33.85 – 16.1 and $ECe^{1:5}$ 3 – 4.9), the exception to this being a higher range for GWC at Te Hiku at depth 60 – 90cm than at depth 30 – 60cm. Overall, there is a clear site difference in GWC and $ECe^{1:5,}$ with little to no overlap of lower, upper and interquartile ranges between sites for both variables (**Figure 5.4).** However, the variability between depths at each site is less obvious with similar standard error of means, particularly for GWC at Mahurangi. Therefore, the significance of these differences will be explored in subsequent sections. Both sites had outliers, which were checked in the original data and notes, and the values themselves made scientific sense in the context of each site, so the values remained in the data (**Figure 5.4 & Figure 5.10**).

5.3.1.2 Particle fraction analysis

Table 5.7 presents the results of the particle fraction analysis with the percentage number of particles per sample broken down by class sizes clay (<0.002mm), silt (0.002 – 0.06mm), fine sand (FSAND) (0.06 – 0.2mm) and medium sand (MSAND) (0.2 – 2mm). Silt-sized particles dominated samples from both Mahurangi and Tehiku forests (mean = 77 to 81 %), followed by clay-sized particles (mean = 10 to 14%) and fine sand-sized particles (mean = 7 to 9%), while medium-sized sand particles made up less than 1% of mean particles present per sample and all with standard error of mean <1.

Table 5.6. Summary statistics of gravimetric water content (GWC), electrical conductivity ($ECe^{1:5}$) Mahurangi and Te Hiku.

Site	Sample depth range (cm)	Mean	S.E.M	LQ	Median	UQ	IQR	Min	Max	Range
GWC (%)										
	0 - 30	45.65	1.89	38.57	45.27	52.06	13.49	25.98	66.32	40.34
Mahurangi	30 - 60	46.95	1.63	37.92	40.87	48.11	10.19	26.41	66.31	39.90
	60 - 90	42.27	1.63	37.30	41.44	44.23	6.94	29.30	63.85	34.54
	0 - 30	8.52	1.38	5.27	6.60	9.98	4.71	3.31	37.16	33.85
Te Hiku	30 - 60	5.74	0.53	4.01	4.73	7.19	3.18	3.27	13.71	10.43
	60 - 90	7.53	0.93	4.71	5.88	8.26	3.55	3.98	20.07	16.09
$ECe^{1:5}$ (mS/m)										
	0 - 30	26.58	1.53	21.52	26.38	32.53	11.01	10.99	40.02	29.03
Mahurangi	30 - 60	21.62	1.25	18.03	20.63	26.02	7.99	10.48	34.97	24.49
	60 - 90	17.98	1.17	14.54	16.68	19.68	5.15	9.58	33.93	24.35
	0 - 30	6.09	0.28	5.15	5.78	7.25	2.10	3.81	8.74	4.93
Te Hiku	30 - 60	3.45	0.20	2.68	3.37	4.00	1.32	1.82	5.89	4.07
	60 - 90	2.66	0.16	2.08	2.51	2.90	0.82	1.31	4.78	3.48

S.E.M = Standard error of mean, UQ = Upper quartile, LQ = Lower quartile, IQR = Interquartile range, Min = Minimum, Max = Maximum

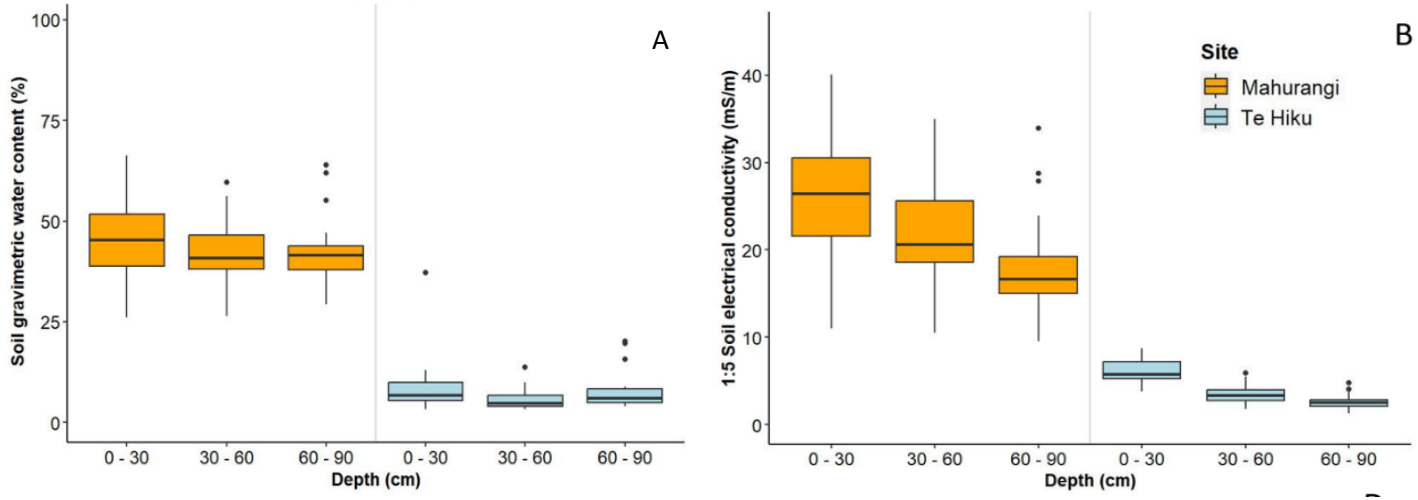

Figure 5.4. Box plots of soil gravimetric water content (left) and electrical conductivity of a 1:5 soil:water solution.

Table 5.7. *Summary statistics of particle fraction analysis showing the percentage number of particles per sample by site, depth range and particle size.*

	Depth range (cm)	Mean	SEM	LQ	Median	UQ	IQR	Min	Max	Range
Clay %										
	0-30	11.46	0.17	10.84	11.34	11.84	1.00	10.07	13.29	3.22
Mahurangi	**30-60**	11.62	0.15	11.13	11.52	12.18	1.05	10.25	13.19	2.94
	60-90	12.19	0.27	11.26	11.70	13.06	1.80	10.73	16.39	5.66
	0-30	14.25	0.40	12.39	14.10	15.99	3.60	11.42	17.48	6.06
Te Hiku	**30-60**	11.71	0.30	10.55	11.49	12.82	2.27	8.85	14.53	5.68
	60-90	10.39	0.28	9.23	10.51	11.24	2.01	7.67	13.14	5.47
Silt %										
	0-30	80.44	0.38	79.25	80.95	81.90	2.65	76.16	83.66	7.50
Mahurangi	**30-60**	79.84	0.36	78.63	79.85	81.33	2.71	76.18	82.73	6.55
	60-90	77.93	0.98	76.72	79.59	80.88	4.16	59.37	82.17	22.80
	0-30	77.79	0.54	75.98	78.28	79.32	3.34	71.78	83.61	11.83
Te Hiku	**30-60**	79.60	0.77	78.52	79.18	81.91	3.40	69.84	85.81	15.97
	60-90	81.83	0.85	77.85	83.04	84.76	6.91	72.94	90.17	17.23
Fine Sand %										
	0-30	7.81	0.21	6.97	7.68	8.65	1.68	6.11	10.17	4.06
Mahurangi	**30-60**	8.25	0.21	7.39	8.37	8.89	1.50	6.57	10.29	3.72
	60-90	9.50	0.67	7.62	8.47	10.22	2.60	6.88	22.77	15.89
	0-30	7.26	0.32	6.40	6.96	8.75	2.35	4.16	9.83	5.67
Te Hiku	**30-60**	7.90	0.52	6.57	7.58	8.83	2.26	3.80	14.92	11.12
	60-90	7.04	0.54	5.03	6.26	9.24	4.22	1.99	12.24	10.25
Medium Sand %										
	0-30	0.29	0.02	0.23	0.28	0.32	0.09	0.16	0.50	0.34
Mahurangi	**30-60**	0.29	0.01	0.24	0.32	0.33	0.10	0.18	0.41	0.23
	60-90	0.38	0.05	0.25	0.31	0.43	0.18	0.20	1.46	1.26
	0-30	0.70	0.04	0.57	0.69	0.80	0.23	0.42	1.13	0.71
Te Hiku	**30-60**	0.79	0.05	0.61	0.75	0.91	0.31	0.41	1.62	1.21
	60-90	0.73	0.07	0.51	0.68	0.94	0.43	0.17	1.68	1.51

S.E.M = Standard error of mean, UQ = Upper quartile, LQ = Lower quartile, IQR = Interquartile range, Min = Minimum, Max = Maximum

5.3.1.3 Weighted means of all measured soil variables

Table 5.8 provides summary statistics of the weighted mean of gravimetric water content (GWC), the electrical conductivity of a 1-part soil to 5-part water soil solution ($ECe^{1:5}$) and the percentage of clay, silt, fine sand, and medium sand particles (CLAY, SILT, FSAND, MSAND). These predictor variables were weighted by two depth ranges, 0 – 60 and 0 – 90 (discussed in **Section 5.2.2.2**).

The summary statistics highlight the differences between the weighted means of Mahurangi and Te Hiku Forest soil properties and the differences between depth ranges within and between each site. Mahurangi consistently reports higher minimum and maximum values for most parameters than Te Hiku (**Table 5.8**). These disparities highlight significant differences in the extremities of the data distribution between the two sites. In comparing the 0 - 60 cm and 0 - 90 cm depth ranges, each site has a consistent trend of higher minimum and maximum values at the greater depth (**Table 5.8**). This indicates that the range of each predictor variable increases with depth. The interquartile ranges at Mahurangi were generally wider for most parameters than Te Hiku, indicating a more diverse distribution of data points. This suggests that Mahurangi's data exhibits greater variability and a broader distribution of values. The interquartile range also shows variations between depth ranges (**Table 5.8**).

The mean and median values show distinct site-wide characteristics. In Mahurangi, the mean values for most parameters are consistently higher than those in Te Hiku across both depth ranges, indicating that, on average, Mahurangi tends to have higher GWC, $ECe^{1:5}$, and different soil texture characteristics than Te Hiku (**Table 5.8**). While both sites generally report low standard error of mean values, Mahurangi often displays slightly higher values than Te Hiku (**Table 5.8**). This suggests that Mahurangi's data may have a marginally higher degree of variability or measurement uncertainty, even though both sites show relatively stable measurements (**Table 5.8**). In contrast, the standard error of mean values remains consistent within each site across different depth ranges. This suggests that the precision of measurements is similar at both depths (**Table 5.8**).

In summary, Mahurangi consistently exhibits higher values for most parameters compared to Te Hiku, implying variations in soil and environmental conditions between the two sites (**Table 5.8**). The differences between depth ranges also suggest depth-dependent variations in soil properties (**Table 5.8**). These insights can be valuable for understanding and managing soil and environmental characteristics in these study areas.

Table 5.8. *Summary statistics of weighted means of gravimetric water content (GWC), the electrical conductivity of a soil water solution (EC1:5), and percentage number of clay, silt, fine sand and medium sand particles per sample at depth ranges 0 - 60 and 0 – 90.*

		Weighted mean for depths 0 - 60						Weighted mean for depths 0 - 90					
		GWC	$ECe^{1:5}$	**CLAY**	**SILT**	**FSAND**	**MSAND**	**GWC**	$ECe^{1:5}$	**CLAY**	**SILT**	**FSAND**	**MSAND**
Mean	**Mahurangi**	64.99	34.91	17.35	120.06	12.15	0.44	71.51	35.26	19.69	131.99	14.44	0.54
	Te Hiku	10.01	6.50	18.83	118.49	11.54	1.14	11.69	6.11	19.48	133.55	12.39	1.25
SEM	**Mahurangi**	1.25	1.04	0.12	0.26	0.15	0.01	1.37	0.94	0.15	0.43	0.28	0.02
	Te Hiku	0.52	0.17	0.25	0.50	0.33	0.04	0.57	0.17	0.22	0.56	0.37	0.04
LQ	**Mahurangi**	58.41	29.96	16.91	118.69	11.35	0.37	63.41	30.49	18.88	130.69	12.61	0.42
	Te Hiku	6.93	5.40	16.75	116.00	9.97	0.88	7.91	4.99	18.01	130.78	10.80	0.98
Median	**Mahurangi**	63.51	36.08	17.23	120.25	11.75	0.45	69.71	35.17	19.55	132.94	13.98	0.50
	Te Hiku	8.67	6.45	18.35	118.17	11.49	1.11	9.42	6.07	19.37	133.74	11.70	1.15
UQ	**Mahurangi**	71.98	40.24	17.92	121.19	13.09	0.49	76.87	41.88	20.38	134.75	15.48	0.60
	Te Hiku	11.37	7.28	21.08	122.22	12.57	1.30	14.14	6.70	21.24	137.33	13.82	1.41
IQR	**Mahurangi**	13.58	10.28	1.01	2.50	1.74	0.12	13.46	11.39	1.50	4.05	2.87	0.19
	Te Hiku	4.44	1.88	4.33	6.22	2.60	0.42	6.23	1.72	3.23	6.54	3.02	0.43
Min	**Mahurangi**	43.19	17.81	15.29	115.55	9.89	0.26	48.33	20.19	17.62	120.28	11.69	0.33
	Te Hiku	5.22	3.73	16.16	109.20	6.29	0.77	6.60	3.36	16.56	121.42	7.55	0.75
Max	**Mahurangi**	90.21	53.41	19.84	124.56	14.69	0.66	102.70	48.79	22.54	137.02	23.01	1.28
	Te Hiku	21.85	9.56	22.61	125.64	18.37	2.06	26.52	9.05	22.42	139.75	20.40	2.49
Range	**Mahurangi**	47.02	35.61	4.55	9.02	4.80	0.40	54.37	28.60	4.93	16.74	11.32	0.95
	Te Hiku	16.62	5.84	6.46	16.44	12.08	1.29	19.92	5.70	5.87	18.33	12.85	1.74

S.E.M = Standard error of mean, UQ = Upper quartile, LQ = Lower quartile, IQR = Interquartile range, Min = Minimum, Max = Maximum

5.3.1.4 Modelled electrical conductivity

The summary statistics and box plots of modelled electrical conductivity (EC^m) for the two study sites (Mahurangi and Te Hiku) across three sample EC^m ranges (0-30mS/m, 30-60mS/m, and 60-90mS/m) are presented in **Table 5.9** and **Figure 5.5**. Significant disparities become evident when examining the modelled electrical conductivity (EC^m) data for Mahurangi and Te Hiku. Across all three depth ranges (0-30 cm, 30-60 cm, and 60-90 cm), Mahurangi consistently displays higher mean EC^m values compared to Te Hiku (**Table 5.9**). This is further underscored by the larger standard errors (SEM) in Mahurangi, indicating more significant variability in the EC^m measurements (**Table 5.9**). Mahurangi exhibits wider interquartile ranges (IQR), reflecting a more diverse distribution of EC^m data points and increased variability in EC^m values (**Table 5.9** and **Figure 5.5**). Furthermore, the maximum EC^m values for Mahurangi consistently surpass those in Te Hiku (**Table 5.9** and **Figure 5.5**). Conversely, Te Hiku has lower mean EC^m and lower SEM values, pointing to more uniform and less variable EC^m measurements (**Table 5.9**). The narrower IQR in Te Hiku signifies a more tightly clustered distribution of EC^m data points and reduced variability with increased EC^m depths, accompanied by consistently lower maximum EC^m values than Mahurangi (**Table 5.9** and **Figure 5.5**). These findings highlight the distinctions in the modelled EC^m values, likely influenced by unique environmental and geological attributes specific to each study site, such as soil texture, soil water content and electrical conductivity. These environmental influences are analysed in **Section 5.3.2**.

Table 5.9. *Summary statistics of modelled electrical conductivity (mS/m) for Mahurangi and Te Hiku Forest.*

Site	Depth range (cm)	Mean	SEM	LQ	Median	UQ	IQR	Min	Max	Range
Mahurangi	0 - 30	9.05	1.37	4.56	7.72	11.12	6.57	2.25	31.25	29.00
	30 - 60	12.21	1.10	8.32	11.17	15.72	7.40	5.04	28.82	23.78
	60 - 90	16.45	1.17	12.45	14.65	19.06	6.61	8.86	31.99	23.13
Te Hiku	0 - 30	0.23	0.08	0.02	0.04	0.32	0.30	0.01	1.64	1.63
	30 - 60	0.52	0.14	0.06	0.12	1.06	0.99	0.04	2.86	2.82
	60 - 90	5.78	0.53	4.44	5.07	6.94	2.49	0.95	11.69	10.74

S.E.M = Standard error of mean, UQ = Upper quartile, LQ = Lower quartile, IQR = interquartile range, Min = Minimum, Max = Maximum

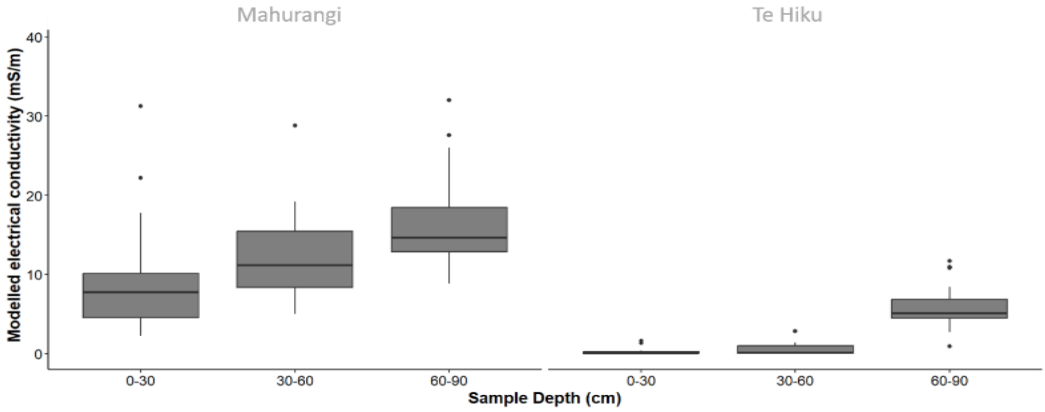

Figure 5.5. *Box plot of modelled electrical conductivity for Mahurangi and Te Hiku at three sample depths 0 – 30cm, 30 – 60cm and 60 – 90cm.*

5.3.2 Using apparent electrical conductivity as a predictor of soil variables

5.3.2.1 Generalised linear mixed effects model selection using Akaike Information Criterion corrected for small sample size for response variable apparent electrical conductivity and weighted means of predictor variables

All global generalised linear mixed effect models selected in **Section 5.3.2.1** had the same random effect "site" with two levels (Mahurangi and Te Hiku). The generalised linear mixed effects models with the same response variables (EC_a^{50} and EC_a^{160}) had random effects that performed similarly across both weighted mean depth ranges.

Table 5.10 presents results from the GLMER using only one predictor variable as a fixed effect and site as a random effect and only summarise predictor variables that had either a weak or strong relationship with EC_a at cumulative depths 50cm (EC_a^{50}) and 160cm (EC_a^{160}) and at the two weighted mean depths of 0 – 60cm and 0 – 90cm. The standard deviation (0.28 – 0.5) and variance (0.08 – 0.28) of the random effect "Site'" are higher for the GLMERs with only one predictor variable (**Table 5.10)** than they are for GLMERs with multiple predictor variables (<0.0001) suggesting "site" has greater within site and also between site variability when only one soil variable is considered as a fixed effect than when multiple soil variables are regarded as fixed effects. The residual variance is slightly higher for GLMERs with only one fixed effect (0.15 – 0.26) compared with GLMERs with multiple fixed effects (0.11 – 0.16), but the residual standard deviation is similar between GLMERs with one fixed effect (0.39 – 0.48) versus GLMER with multiple fixed effects (0.35 – 0.40) indicating GLMER with only one fixed effect have greater variability that isn't explained by both the fixed and random effects, both within site and between sites (**Table 5.10 -** Table 5.13). These results show that the site is an essential source of variability in EC_a within and between sites at 0 – 60cm and 0 – 90cm. However, the source of within and between-site variability decreases with the introduction of more soil variables, which is better at explaining variability in EC_a. Moreover, the importance of multiple soil variables being included in GLMERs as fixed effects is

highlighted by the decrease in residuals, which reduces the unexplained variability of the GLMERs (**Table 5.10**)**.**

Table 5.10. *Summary of generalised linear mixed effects models using one predictor variable.*

Depth (cm)			Random effect		Fixed effect		
EC_a	WM	Predictor variable	Var. / Std. Dev.	Res. Var. / Std. Dev.	Co-eff. log / exp	Std. E.	*p-value*
50	0 - 60	CLAY	0.25 / 0.50	0.21 / 0.46	0.04 / 1.04	0.02	0.06$^{\cdot}$
50	0 - 60	MSAND	0.20 / 0.45	0.22 / 0.47	-0.30 / 1.04	0.16	0.06$^{\cdot}$
50	0 - 90	$ECe^{1:5}$	0.28 / 0.53	0.22 / 0.48	-0.01 / 1.04	0.01	0.36$^{\cdot}$
50	0 - 90	CLAY	0.25 / 0.50	0.26 / 0.46	0.04 / 1.04	0.02	0.06$^{\cdot}$
160	0 - 60	CLAY	0.09 / 0.30	0.16 / 0.40	0.04 / 1.04	0.02	0.05*
160	0 - 60	FSAND	0.08 / 0.28	0.15 / 0.39	0.04 / 1.04	0.01	<0.0001**
160	0 - 60	$GWC:ECe^{1:5}$	0.11 / 0.30	0.16 / 0.40	0.00 / 0.74	0.00	0.09$^{\cdot}$
160	0 - 90	CLAY	0.09 / 0.30	0.16 / 0.40	0.04 / 1.00	0.02	0.05**
160	0 - 90	FSAND	0.08 / 0.28	0.15 / 0.39	0.04 / 1.00	0.01	<0.0001**
160	0 - 90	$GWC:ECe^{1:5}$	0.11 / 0.34	0.16 / 0.40	0.00 / 0.99	0.00	0.09$^{\cdot}$

Significance codes: 0 '***' 0.001 '**' 0.01 '*' 0.05 '.' 0.1 ' ' 1
WM = Weighted mean
Var = Variance
Std = Standard deviation
Res = Residuals
Std. E = Standard Error
Co-eff = Co-efficient

Of the generalised linear mixed effects models with only one soil variable as a fixed effect (Table 5.10), the weighted mean of fine sand and clay at both weighted mean depths held strong, positive relationships with EC_a^{160}, while clay at both weighted mean depths had a weak, positive correlation with EC_a^{50} (**Table 5.10)**. The weighted mean of medium sand and $ECe^{1:5}$ had weak, positive correlations with $EC_a^{50,}$ while the interaction effect of GWC and $ECe^{1:5}$ had a weak, positive correlation with EC_a^{160} (**Table 5.10)**. These results show that apparent electrical conductivity variability at a cumulative depth of 160cm can be better explained by smaller particle sizes (fine sand and clay), regardless of the depth of weighted mean (**Table 5.10)**. However, there is more unexplained variability in EC_a^{50} at both weighted mean depths with only weak relationships with either $ECe^{1:5}$, fine sand, medium sand or clay alone, as with the interaction effect of GWC and $ECe^{1:5}$ (**Table 5.10)**.

Of the generalised linear mixed effects models with multiple fixed effects as predictor variables, all fixed effects strongly correlated with EC_a^{50} and EC_a^{160}, except for one GLMER, which had a weak correlation with the weighted mean of CLAY at a depth range of 0 - 60cm (**Table 5.11** & **Table 5.12**)**.** The weighted mean of percentage clay was present in GLMERs with the EC_a^{50} as a response variable but not with the EC_a^{160} response variable, with a weak positive correlation at a depth range of 0 - 60cm and a strong positive correlation at a depth range of 0 - 90cm (**Table 5.11** & **Table 5.12**)**.** The weighted mean of medium sand had a strong positive correlation with EC_a^{50} and EC_a^{160}, indicating that an increase in medium-sized sand particles increased EC_a. The interaction between $ECe^{1:5}$ and GWC had a strong,

positive relationship with EC_a at both depth ranges and EC_a responses; however, the back-transformed coefficient (1.00) was non-significant (**Table 5.11** & **Table 5.12**). In practical terms, this could mean that while the interaction effect of GWC and $ECe^{1:5}$ may not have a multiplicative effect on the EC_a shown by the back-transformed coefficient, there may still be some other type of association or relationship between EC_a and the interaction between GWC and $ECe^{1:5}$ that is not captured by the multiplicative effect of the GLMER. Gravimetric water content and $ECe^{1:5}$ as main effects had a strong positive effect on EC_a for all four GLMER models (**Table 5.11** & **Table 5.12**). Finally, FSAND did not significantly affect EC_a^{50} for a depth range of 0 - 90 and was therefore excluded. However, the weighted average of FSAND had a strong, positive effect on EC_a in all three GLMER models that included it as a predictor variable (**Table 5.11** & **Table 5.12**).

All four GLMERs had similar variable inflation factors and correlation coefficients (**Table 5.11** & **Table 5.12**). When comparing the correlation coefficients and variable inflation factors for the four GLMERs, the interaction terms GWC and $ECe^{1:5}$ had low VIFs and correlation coefficients with other predictor variables. Gravimetric water content and $ECe^{1:5}$ as individual variables had slightly higher VIFs (> 4) and somewhat higher correlation coefficients when matched against each other. Still, this potential multicollinearity was not of significant concern (**Table 5.11** & **Table 5.12**). The correlation coefficients for CLAY, MSAND, FSAND, and MSAND were slightly raised, and VIFs were marginally higher than recommended. Still, multicollinearity was not a significant concern for these predictor variables (**Table 5.11** & **Table 5.12**).

Table 5.11. *Generalised linear mixed effects models using weighted means of predictor variables for depth range 0 - 60cm for the response variables apparent electrical conductivity to 50cm (left) and 160cm (right).*

Response Variables			**EC_a^{50}**			**Response Variables**			**EC_a^{160}**		
Model	**AICc**	**Log-lik**	**Dev.**	**Df.resid**	**R^2**	**Model**	**AICc**	**Log-lik**	**Dev.**	**Df.resid**	**R^2**
Metrics	513.86	-247.3	494.6	138	0.87	**Metrics**	697.7	-340.3	680.7	139	0.78
Scaled	**Min**	**LQ**	**Med.**	**UQ**	**Max**	**Scaled**	**Min**	**LQ**	**Med.**	**UQ**	**Max**
Residuals	-1.72	-0.8	-0.24	0.69	2.63	**Residuals**	-2.05	-0.75	-0.19	0.38	2.27
			Variance	**Std. dev.**					**Var.**	**Std. dev.**	
Random effects	**Site**	**(Int.)**	0.00	0.00		**Random effects**	**Site**	**(Int.)**	0.00	0.00	
	Residuals		0.16	0.40			**Residuals**	0.11	0.12	0.12	

Fixed effects

	$Slope^{log}$	**$Slope^{exp}$**	**E.S.E**	**t-value**	**p-value**	**Sig.**		**$Slope^{log}$**	**$Slope^{exp}$**	**E.S.E**	**t-value**	**p-value**	**Sig.**
(Int.)	-0.95	0.20	0.39	-2.47	0.01	*	**(Int.)**	0.73	2.08	0.18	4.18	<0.001	***
GWC	0.03	1.04	0.00	9.85	<0.001	***	**GWC**	0.02	1.02	0.00	5.71	<0.001	***
$ECe^{1:5}$	0.06	1.08	0.01	9.30	<0.001	***	**$ECe^{1:5}$**	0.03	1.03	0.01	5.99	<0.001	***
CLAY	0.04	1.08	0.02	1.85	0.06	.	**MSAND**	-1.01	0.37	0.16	-6.17	<0.001	***
MSAND	-1.07	0.60	0.19	-5.69	<0.001	***	**FSAND**	0.12	1.13	0.02	7.19	<0.001	***
FSAND	0.08	1.00	0.02	4.20	<0.001	***	**GWC:$ECe^{1:5}$**	<-0.00	1.00	0.00	-16.86	<0.001	***
GWC:$ECe^{1:5}$	<-0.00	1.00	0.00	-22.91	<0.001	***							

Significance codes: 0 '***' 0.001 '**' 0.01 '*' 0.05 '.' 0.1 ' ' 1

Correlation coefficient							**VIF**	**Correlation coefficient**						**VIF**
	(Int.)	**GWC**	**$ECe^{1:5}$**	**CLAY**	**MSAND**	**FSAND**			**(Int.)**	**GWC**	**$ECe^{1:5}$**	**MSAND**	**FSAND**	
GWC	-0.01						9.09	**GWC**	-0.13					8.62
$ECe^{1:5}$	-0.18	-0.54					7.70	**$ECe^{1:5}$**	-0.30	-0.55				7.41
CLAY	-0.87	-0.05	0.03				1.44	**MSAND**	-0.46	0.49	0.28			5.25
MSAND	0.02	0.49	0.23	-0.27			5.37	**FSAND**	-0.36	-0.43	-0.10	-0.64		1.77
FSAND	-0.01	-0.43	-0.08	-0.18	-0.57		1.90	**GWC:$ECe^{1:5}$**	0.13	-0.20	-0.31	-0.11	0.06	2.40
GWC:$ECe^{1:5}$	0.11	-0.23	-0.35	-0.04	-0.12	0.08	2.94							

AICc	Akaike information criterion	Min	Minimum	Med.	Median	Std. dev.	Standard deviation
log-lik	Log-likelihood	LQ	Lower quartile	UQ	Upper quartile	E.S.E	Estimated standard error
dev	Deviance	Co-eff	Coefficient	Max	Maximum	VIF	Variable inflation factor
df.resid	Residual degrees of freedom						

Table 5.12. *Generalised linear mixed effects models using weighted means of predictor variables for depth range 0 - 90cm for the response variables apparent electrical conductivity to 50cm (left) and 160cm (right).*

Response Variables	**EC_a^{50}**					**EC_a^{160}**					
Model	**AICc**	**Log-lik**	**Dev.**	**Df.resid**	***R^2***	**Model**	**AICc**	**Log-lik**	**Dev.**	**Df.resid**	***R^2***
Metrics	505.37	-244.20	488.30	139.00	0.87	**Metrics**	686.83	-334.90	669.80	139.00	0.80
Scaled	**Min**	**LQ**	**Med.**	**UQ**	**Max**	**Scaled**	**Min**	**LQ**	**Med.**	**UQ**	**Max**
Residuals	-1.72	-0.80	-0.24	0.69	2.63	**Residuals**	-2.17	-0.77	-0.23	0.60	2.29
			Variance	**Std. dev.**					**Var.**	**Std. dev.**	
Random effects	**Site**	**(Int.)**	0.00	0.00		**Random effects**	**Site**	**(Int.)**	0.00	0.00	
	Residuals		0.0.16	0.40			**Residuals**		0.11	0.33	
Fixed effects											
	$Slope^{log}$	**$Slope^{exp}$**	**E.S.E**	***t-value***	***p-value***	**Sig.**		**$Slope^{log}$**	**$Slope^{exp}$**	**E.S.E**	***t-value***	***p-value***	**Sig.**
(Int.)	-1.60	0.20	0.41	-3.92	0.00	***	**(Int.)**	0.87	2.39	0.14	6.09	<0.001	***
GWC	0.04	1.04	0.00	14.56	<0.001	***	**GWC**	0.02	1.02	0.00	7.89	<0.001	***
$ECe^{1:5}$	0.07	1.08	0.01	12.50	<0.001	***	**$ECe^{1:5}$**	0.03	1.03	0.00	5.61	<0.001	***
CLAY	0.08	1.08	0.02	3.26	0.01	**	**MSAND**	-0.83	0.44	0.13	-6.23	<0.001	***
MSAND	-0.50	0.60	0.13	-3.90	<0.001	***	**FSAND**	0.09	1.09	0.01	6.37	<0.001	***
GWC:$ECe^{1:5}$	<-0.00	1.00	0.00	-32.93	<0.001	***	**GWC:$ECe^{1:5}$**	<-0.00	1.00	0.00	-20.98	<0.001	***

Significance codes: 0 '***' 0.001 '**' 0.01 '*' 0.05 '.' 0.1 ' ' 1

Correlation coefficient						**VIF**	**Correlation coefficient**						**VIF**
	(Int.)	**GWC**	**$ECe^{1:5}$**	**CLAY**	**MSAND**			**(Int.)**	**GWC**	**$ECe^{1:5}$**	**MSAND**	**FSAND**	
GWC	0.17					7.49	**GWC**	-0.11					8.09
$ECe^{1:5}$	-0.05	-0.66				7.41	**$ECe^{1:5}$**	-0.25	-0.56				7.39
CLAY	-0.92	-0.28	-0.09			1.54	**MSAND**	-0.44	0.43	0.33			4.80
MSAND	0.23	0.32	0.26	-0.57		3.34	**FSAND**	-0.28	-0.42	-0.21	-0.71		2.28
GWC:$ECe^{1:5}$	0.06	-0.20	-0.28	0.00	-0.04	2.50	**GWC:$ECe^{1:5}$**	0.10	-0.18	-0.25	-0.07	0.06	2.06

AICc	Akaike information criterion	Min	Minimum	Med.	Median	Std. dev.	Standard deviation
log-lik	Log-likelihood	LQ	Lower quartile	UQ	Upper quartile	E.S.E	Estimated standard error
dev	Deviance	Co-eff	Coefficient	Max	Maximum	VIF	Variable inflation factor
df.resid	Residual degrees of freedom						

5.3.2.3 Mapped apparent electrical conductivity using ordinary kriging and 1D laterally constrained inversion

Figure 5.6 and **Figure 5.7** map the spatial variability of EC_a at Mahurangi Forest and Te Hiku Forest. The upper two maps in each figure were mapped using ordinary kriging, and the lower two in each figure were mapped using 1D, laterally constrained inversion software (EMTOMO LDA, 2018). The maps to the left of each figure (A&C) are for EC_a to 50cm (EC_a^{50}), while the maps on the right side of both figures(B&D) are EC_a down to 160cm (EC_a^{160}) (**Figure 5.6** and **Figure 5.7)**.

Mahurangi Forest kriged maps look much smoother and more visually appealing compared to the 1D laterally constrained maps. This is due to the smoothing process taking liberties with extrapolating from measurement points **Figure 5.6**. The EC_a^{50} showed less spatial variability for both mapping techniques than EC_a^{160} across the catchment (**Figure 5.6**). Both mapping techniques and cumulative depths offer similar spatial patterns. For example, the maps are slightly symmetrical (**Figure 5.6**). There is a general decrease in EC_a towards the centre of the catchment, with the greatest decrease on the southwest side of the catchment Figure 5.6. In all instances, the western side of the catchment shows the highest source of EC_a surrounding one isolated plot, which has created a "bull's eye" effect. This is mirrored (though not to the same extent) on the eastern side of the catchment **Figure 5.6**. While in the centre of the catchment, there is a general decreasing trend in EC_a from north to south, the edges of the catchment show a general increase in EC_a going from north to south (**Figure 5.6**).

Te Hiku Forest was mapped on the same colour ramp (**Figure 5.7)** as Mahurangi Forest; however, because of the small range in data, the spatial variability of the catchment was obscured in **Figure 5.7**. Therefore, the range of values was decreased to highlight minute spatial patterns in EC_a at both cumulative depths **Figure 5.7.** Again, EC_a^{50} was more homogenous than EC_a^{160}, and the kriged maps were smooth and more visually appealing than the 1D-laterally constrained maps (**Figure 5.7).** There was a general increasing trend in EC_a moving from northeast to southwest of the catchment in all instances but was more pronounced with EC_a^{160} on the adjusted colour ramp because the catchment is so large (~1800ha) when there are isolated changes in EC_a, as in the north-eastern part of the catchment, the same bullseye effect occurs.

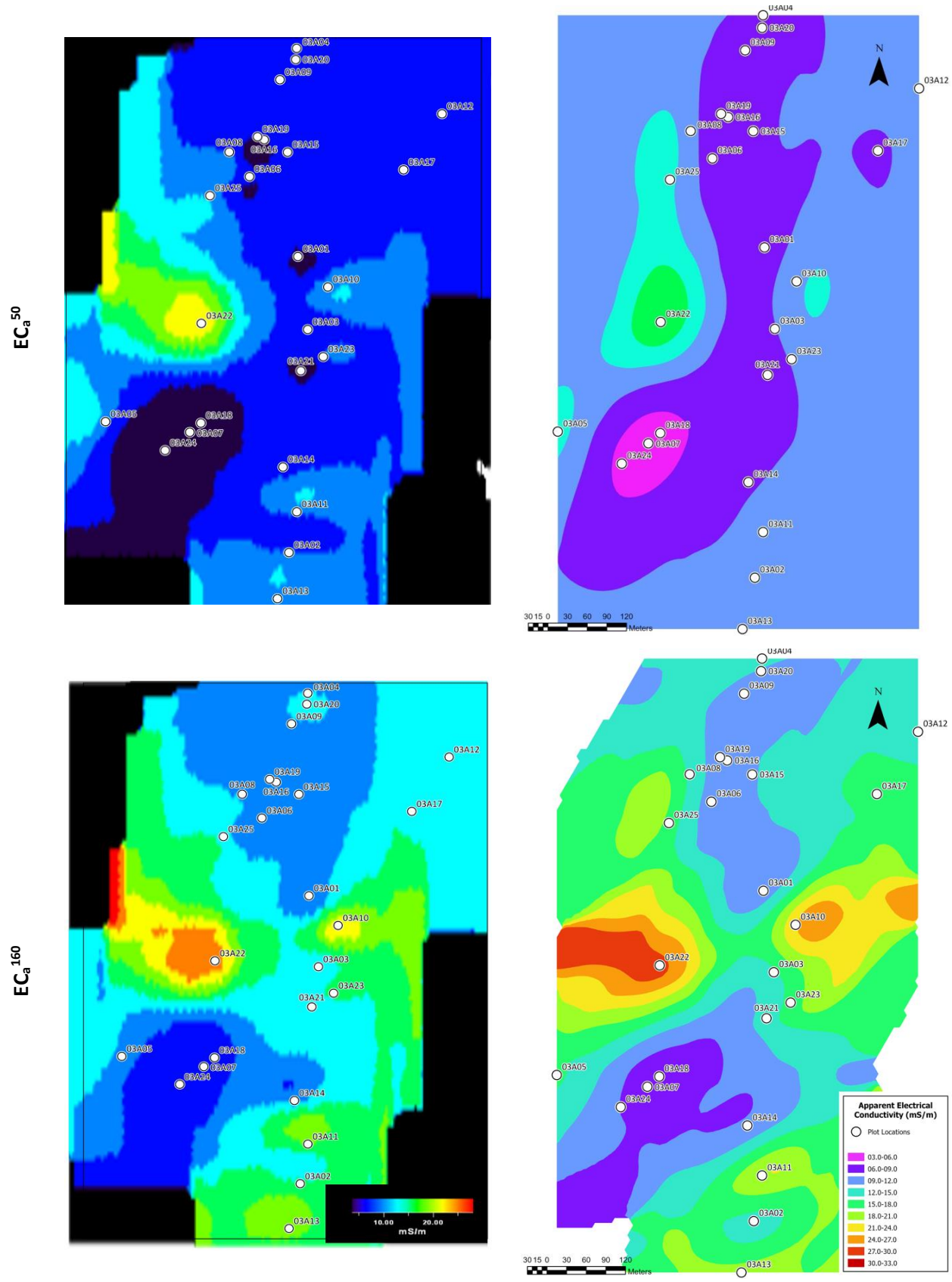

Figure 5.6. *Mahurangi Forest apparent electrical conductivity at 50cm and 160cm cumulative depths (rows) using 1D inversion software (left column), ordinary kriging in ArcGIS Pro (centre and left columns).*

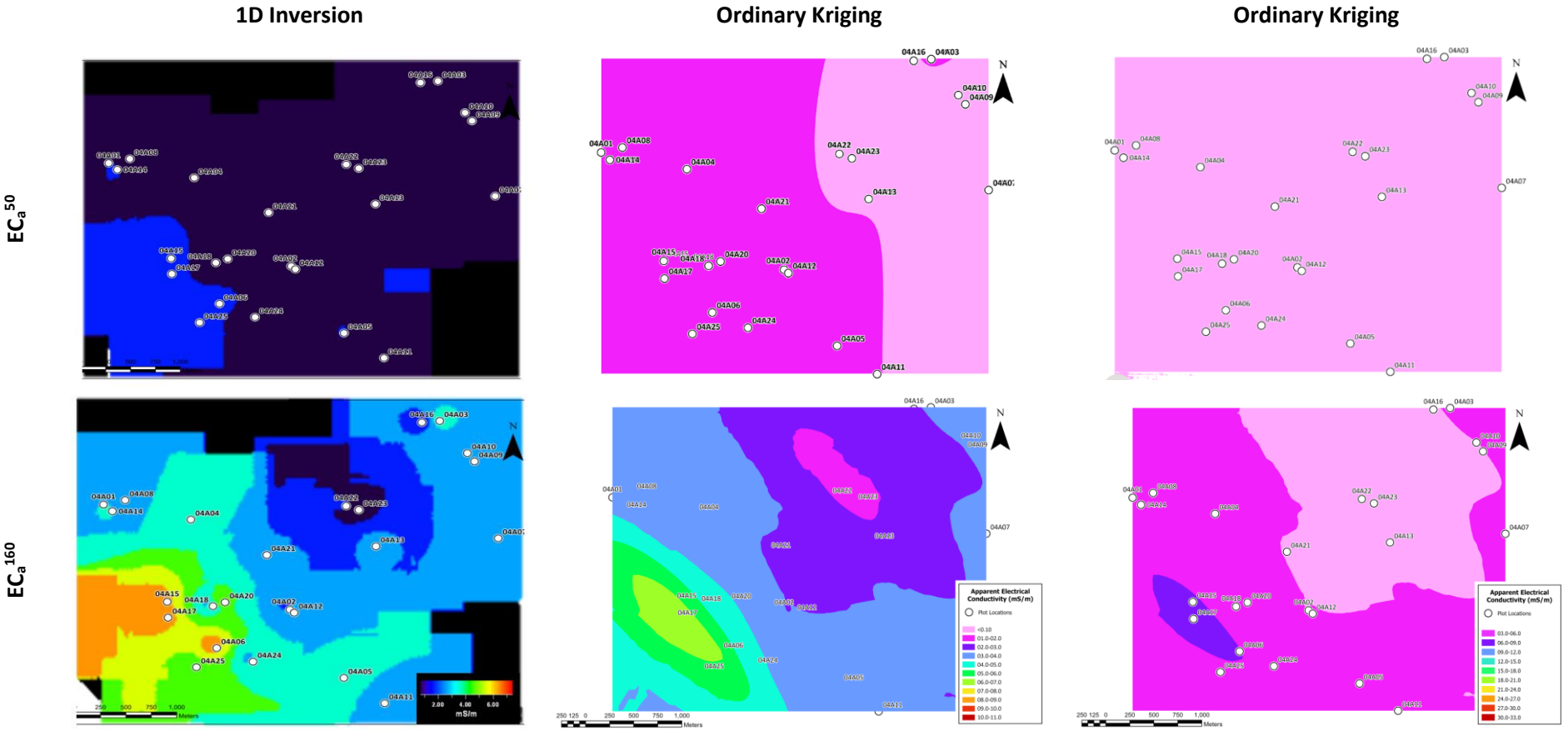

Figure 5.7. *Te Hiku Forest apparent electrical conductivity at 50cm and 160cm cumulative depths (rows) using 1D inversion software (left column), ordinary kriging in ArcGIS Pro (centre and left columns) using a fine scale colour ramp (centre) and the same colour ramp as Mahurangi Forest while to help highlight minute spatial heterogeneiety.*

5.3.3 Using modelled electrical conductivity as a predictor of soil variables

5.3.3.1 Generalised linear mixed effects model selection using Akaike Information Criterion corrected for small sample size for response variable apparent electrical conductivity

Firstly, to assess the relationships between modelled electrical conductivity (EC^m) and predictor variables at sample depths of 0 – 30 cm, 30 – 60 cm, and 60 – 90 cm, GLMERs were fitted, and various predictor combinations were selected for analysis based on predetermined criteria, including the coefficient of determination (R^2), log-likelihood, and AICc (**Table 5.13**). Delta values were also used to identify the GLMERs within 3 AICc points of the lowest AICc score (**Table 5.13**). Predictor variables include GWC, $ECe^{1:5}$ and percentage CLAY, FSAND, and MSAND (**Table 5.13**). **Section 5.2** details why the percentage of silt and coarse sand particles was omitted from further analysis and why percentage volume was not used (**Table 5.13**).

For all sample depths, the GLMERs with only one predictor variable had high AICc with delta scores greater than 5 (the recommended is a delta score ≤ 3) (**Table 5.13**). The delta score for GLMERs with one predictor variable improved with depth range for all variables except for MSAND, which had a higher delta for depth range 30 – 60cm (12.94) compared with depth range 0 – 30cm (12.03). In addition, R^2 were lower and log-likelihood scores were higher for GLMERs with one predictor variable, suggesting these models were less able to explain the variation in EC^m at each sample depth (**Table 5.13**), a similar result found in **Table 5.11** and **Table 5.12**. in **Section 5.3.2**. As mentioned in **Section 5.2.2.2**, AICc does not look at individual significance levels of variables, only how the model fit balances complexity and, thus, the standard deviation, variance and the residuals of the random effects and the *p-value*s of the fixed effects (**Table 5.14**) will be discussed in **Section 5.3.3.1**.

The first set of columns in **Table 5.13** displays the GLMERs used to describe the variability in EC^m at a sample depth of 0 – 30 cm ($GLMER^{0-30}$). Notably, the model comprising predictor variables CLAY + FSAND + MSAND exhibited a high coefficient of determination ($R^2 = 0.83$), implying these predictor variables can explain 83% of the variability in EC^m within this depth range (**Table 5.13**). The GLMER low log-likelihood (-57.61) indicates a relatively good fit to the observed data. Additionally, the comparatively low AICc score (delta = 2.13) suggests that the GLMER achieves a good balance between model fit and complexity compared with GLMERs with other combinations of predictor variables for sample depth range 0 – 30 cm (**Table 5.13**).

Table 5.13. *Generalised linear mixed effects models for modelled electrical conductivity at 0 – 30, 30 – 60 and 60 – 90 depth ranges.*

Sample depth range	**0 – 30cm**					**30 – 60cm**					**60 – 90cm**				
	Int.	R^2	**Log-lik**	**AICc**	**delta**	**Int.**	R^2	**Log-lik**	**AICc**	**delta**	**Int.**	R^2	**Log-lik**	**AICc**	**delta**
$ECe^{1:5}$ + GWC + CLAY + FSAND + MSAND + $ECe^{1:5}$: GWC***	0.58	0.83	-56.54	135.70	8.62	-1.48	0.80	-88.39	199.41	5.77	1.25	0.71	-128.36	279.33	2.97
$ECe^{1:5}$ + GWC + CLAY + FSAND + MSAND	-1.48	0.83	-57.42	134.44	7.36	1.69	0.74	-95.28	210.16	16.52	1.82	0.67	-131.18	281.96	5.60
CLAY + FSAND + MSAND	-1.54	0.83	-57.61	129.21	2.13	1.31	0.73	-95.75	205.51	11.87	1.59	0.62	-134.84	283.68	7.32
$ECe^{1:5}$ + GWC + $ECe^{1:5}$: GWC	-3.48	0.70	-70.93	155.87	28.78	-2.32	0.76	-92.55	199.10	5.46	1.23	0.67	-131.54	277.08	0.72
$ECe^{1:5}$ + GWC	-0.16	0.65	-74.58	160.56	33.48	0.38	0.66	-101.47	214.33	20.69	2.00	0.60	-136.10	283.59	7.23
CLAY	-2.96	0.68	-72.81	154.52	27.44	2.77	0.67	-100.84	210.59	16.95	2.30	0.56	-138.31	285.53	9.17
FSAND	3.15	0.73	-68.38	145.67	18.58	2.63	0.72	-96.39	201.69	8.05	2.21	0.56	-138.23	285.37	9.00
MSAND	2.64	0.76	-65.10	139.12	12.03	1.98	0.70	-98.84	206.58	12.94	2.36	0.56	-137.98	284.88	8.52
$ECe^{1:5}$	0.12	0.65	-74.77	158.45	31.37	0.74	0.66	-101.78	212.48	18.84	2.40	0.57	-137.92	284.76	8.39
GWC	-0.13	0.65	-74.60	158.12	31.04	0.49	0.66	-101.53	211.96	18.33	1.57	0.59	-136.47	281.84	5.48
OTHER SIGNIFICANT MODELS^^^	-1.83	0.82	-57.84	127.08	0.00	-1.07	0.80	-88.45	193.64	0.00	1.37	0.71	-128.38	276.36	0.00
^^^	CLAY + MSAND					$ECe^{1:5}$ + GWC + FSAND + $ECe^{1:5}$: GWC					$ECe^{1:5}$ + GWC + FSAND + MSAND + $ECe^{1:5}$: GWC				

*** = Global model using all predictor variables and the interaction between $Ee^{1:5}$ and GWC
Int. = x-intercept, Log-lik = Log-Likelihood,
AICc = Akaike information criterion

On closer inspection, CLAY and MSAND predictor variables were significant predictors of the variability in EC^m at a depth range of 0 – 30 (*p-value* < 0.0001); however, FSAND showed no significant relationship with EC^m (*p-value* < 0.48). A likelihood ratio test was performed to assess if the presence or absence of FSAND improved model fit in the GLMER, which resulted in a Chi-squared statistic of 0.47 (*p-value* = 0.49). The results show no strong evidence to reject the null hypothesis, indicating no significant difference in model fit between models that include/exclude FSAND at a depth range of 0 – 30. Given that the simpler model excluding FSAND achieves a similar level of fit and reduces model complexity, the GLMER with CLAY and MSAND as predictor variables was selected.

The second set of columns in Table 5.13 shows the GLMERs used to describe the variability in EC^m at a depth range of 30 – 60cm ($GLMER^{30-60}$). The global model, including all predictor variables and the interaction between $ECe^{1:5}$ and GWC, stood out as the best model for explaining the variability in EC^m at this depth (**Table 5.13**). The generalised linear mixed effects model for depth range 30 - 60 was able to explain 80% of the variability in EC^m with a log-likelihood of only 0.06 from the lowest log-likelihood and a comparatively low AICc (delta = 5.77) (**Table 5.13**). These model metrics underscore the GLMER robust fit to the observed data and its ability to explain the variability in EC^m at a depth range of 30 – 60 cm. $GLMER^{30-60}$. Incorporating the interaction terms GWC and $ECe^{1:5}$ again highlighted the importance of this interaction in explaining variability at this depth (**Table 5.13)**. Meanwhile, the global GLMER showed a strong correlation with GWC, ECe1:5, and the predictor interactions and a weak correlation with FSAND. In addition, the combination of predictor variables had high variable inflation factors.

A likelihood ratio test was conducted to establish if the non-significant predictors were required in the GLMER and if the interaction term could be removed to reduce the VIF scores. In both instances, the GLMER containing the interaction term GWC and $ECe^{1:5}$ significantly enhanced model performance (*p-value* of Chi-square statistic < 0.0001). In contrast, adding the non-significant predictor terms did not enhance model fit (*p-value* of Chi-square statistic = 0.9). Therefore, the final selected GLMER for depth range 30 – 60 included FSAND, GWC, $ECe^{1:5}$ and their interaction (**Table 5.13)**.

The last set of columns in **Table 5.13** presents the GLMERs used to describe the variability in EC^m at a sample depth of 60 – 90 cm ($GLMER^{60-90}$) and yielded similar results to the top $GLMER^{30-60}$. Again, the global model with all predictor variables and the interaction between $ECe^{1:5}$ and GWC was the strongest performing GLMER, with the highest R^2 (0.71) and log-likelihood (-128.36) and a low AICc (delta = 2.97). This demonstrates $GLMER^{60-90}$'s strong ability to explain EC^m variability with a good model fit that balances complexity. Despite the strong model performance, the variable inflation factors for the model predictors were high (between 2 and 25). A likelihood ratio test was performed, and the results indicated the interaction between GWC and $ECe^{1:5}$ enhances model fit in $GLMER^{30-60}$.

Based on the GLMER comparison, it is crucial to consider multiple predictor variables and interaction terms to explain the variability in EC^m across different sample depths. The global model, including all predictor variables $ECe^{1:5}$, GWC, CLAY, FSAND, MSAND and the interaction between $ECe^{1:5}$ and GWC, were the best performing at depth ranges 30-60cm and 60-90cm in terms of their AICc scores, log-likelihood and R^2. However, likelihood ratio tests determined the complex models were not necessarily better and omitting non-significant variables created a more stable model. They also had high log-likelihood values and low AICc scores, indicating that both models could balance goodness of fit with model complexity. Therefore, at greater depths, GWC, $ECe^{1:5}$, and their interactions are critical factors in explaining the variability observed in EC^m. However, at a shallower depth range of 0-30 cm, the top-performing model did not include these predictor variables or their interactions, suggesting that these variables have less influence on the variability seen in EC^m.

The model comparison suggests the more complex global GLMER with all predictor variables and interaction between GWC and $ECe^{1:5}$ generally performs better than the simpler GLMER, which omits GWC and $ECe^{1:5}$'s interaction based on several criteria such as R^2, AICc and log-likelihood (**Table 5.13**). However, this GLMER also had concerningly high variable inflation factors between 5.5 and 11.17. The likelihood ratio test (Chi-squared test) indicated that the improvement in model fit provided by the interaction term is not statistically significant at the 0.05 significance level with a relatively high *p-value* of the Chi-square statistic (0.06). This indicates no strong evidence to suggest that adding the interaction of GWC and $ECe^{1:5}$ significantly improves the model fit. Therefore, the preferred model based on a combination of R^2, AICc scores, log-likelihood score and the outcome of the likelihood ratio test is the simpler GLMER with all predictor variables with no interaction.

To further emphasise the importance of including multiple predictor variables in the GLMERs, **Figure 5.8** shows scatter plots of log^{10} transformed, modelled electrical conductivity and all predictor variables at the three depth ranges. The graphs further visualise how the modelled electrical conductivity and measured predictor variables are complex and that it is difficult to model these predictor variables without considering their combined effect. The only relationship that appears to follow a linear pattern is the relationship between medium sand particles and EC^m. According to the GLMER for this variable, the model can explain 76% and 72% of the variability in EC^m at depths 0 – 30 and 30 – 60., respectively. There might be potential outliers for medium sand at 60 – 90 depth ranges, which may have caused the R^2 to be insignificant. However, this is purely speculation based on observation alone, and further investigation would be required.

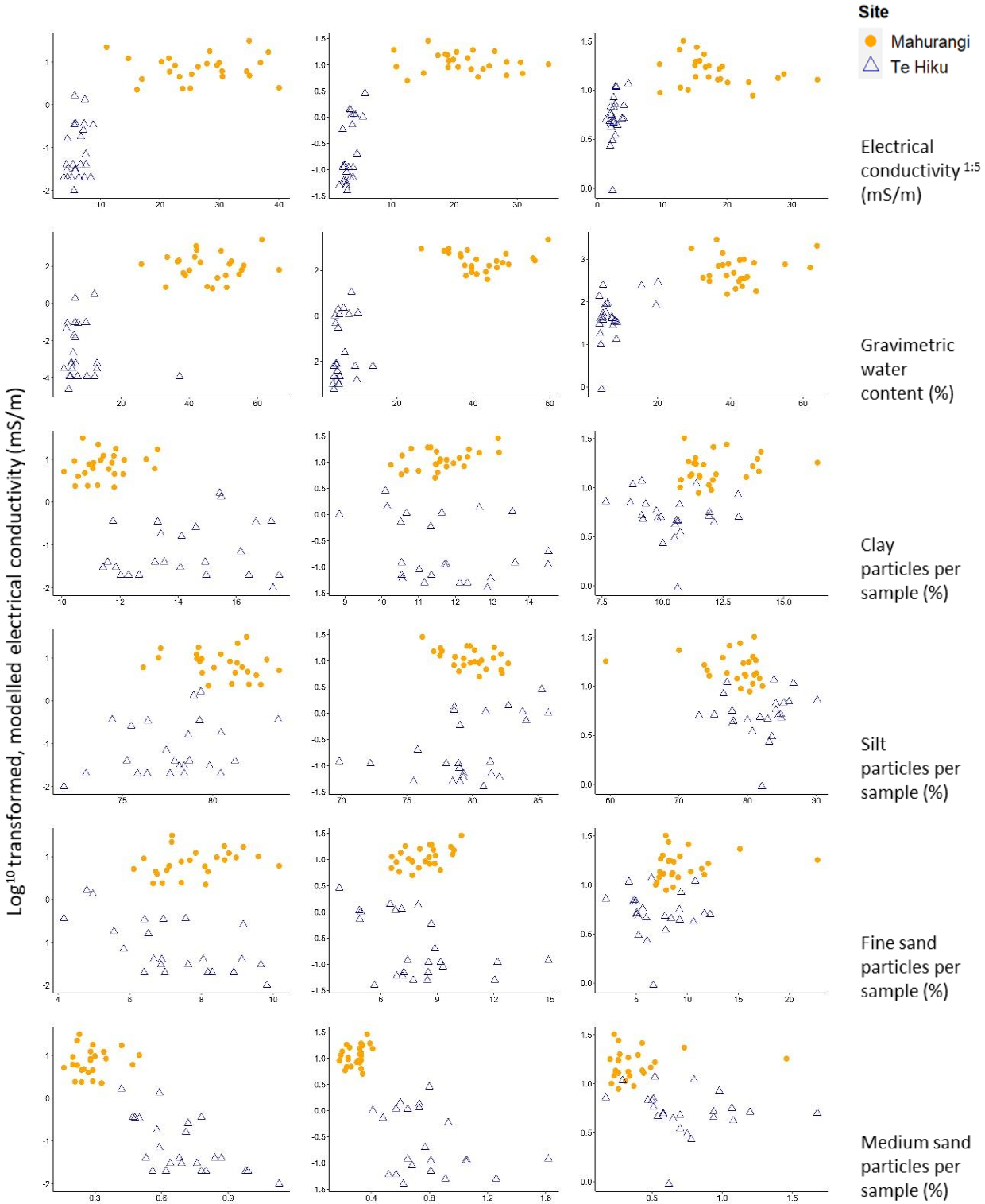

Figure 5.8. *Scatter plots of (log[10] transformed) modelled electrical conductivity (y-axis) and electrical conductivity of a 1-part soil to 5-part water solution, gravimetric water content, clay, silt, fine sand and medium sand particle percentage (x-axis).*

5.3.3.2 Assessing selected generalised linear mixed effects models for response variable modelled electrical conductivity

All global generalised linear mixed effect models had the same random effect "site" with two levels (Mahurangi and Te Hiku). The generalised linear mixed effects models with the same response variables (EC_a^{50} and EC_a^{160}) had random effects that performed similarly across both weighted mean depth ranges.

Table 5.14 summarises the results from the GLMERs using only one predictor variable as a fixed effect and "site" as a random effect. The table shows GLMER results with *p-value*s of significance (*p-value* < 0.05) at sample depths of 0 – 30cm, 30 – 60cm and 60 – 90cm. The standard deviation (0.00 – 7.72) and variance (0.00 – 2.78) of the random effect "site'" are higher for the GLMERs with only one predictor variable (**Table 5.14)** than they are for GLMERs with multiple predictor variables (0 - 1.53 and 0 - 1.24 respectively) **(Table 5.15** and **Table 5.16**) suggesting "site" had a greater within and also between site effect when only one soil variable is considered as a fixed effect than when multiple soil variables are considered as fixed effects. As seen in **Section 5.3.2,** these results highlight the importance of including multiple soil variables in the GLMERs.

Table 5.14*. Summary of generalised linear mixed effects models for response variable modelled electrical conductivity.*

		Random effects		**Fixed effect**		
Depth (cm)	**Predictor variable**	**Var. / Std. Dev.**	**Res. Var. / Std. Dev.**	Co-eff **log / exp**	**Std. E.**	*p-value*
0-30	CLAY	7.72 / 2.78	1.52 / 1.23	0.25 / 1.28	0.12	0.03*
0-30	FSAND	5.45 / 2.33	1.11 / 1.05	-0.3 / 0.67	0.10	0.00***
0-30	MSAND	1.45 / 1.20	1.21 / 1.1	-5.0 / 0.00	1.00	0.00***
30-60	FSAND	2.35 / 1.53	0.73 / 0.85	-0.2 / 0.80	0.06	0.00***
30-60	MSAND	1.29 / 1.13	1.00 / 1.00	-2.0 / 0.13	0.71	0.00**
60-90	GWC	0.00 / 0.00	0.18 / 0.42	0.02 / 1.02	0.00	0.00***

Significance codes: 0 '***' 0.001 '**' 0.01 '*' 0.05 '.' 0.1 ' ' 1

Table 5.14 -Table 5.17 present the generalised linear mixed effects model (GLMER) with the response variable modelled electrical conductivity (EC^m) for sample depth 0 – 30 cm. All GLMERs use the random effect "site" with two levels (Mahurangi Forest and Te Hiku Forest), and all GLMERs use different configurations of predictor variables as selected in the previous section.

Table 5.15. *Generalised linear mixed effect model for modelled electrical conductivity at a depth range of 0 - 30cm*

Model metrics		**Scaled residuals**		**Random effects**			
AICc	127.10	Min	-1.18			Variance	Std. dev.
log-lik	-57.80	LQ	-0.80	Site	(Intercept)	1.53	1.24
dev	115.70	Med.	-0.12	Residual		0.68	0.82
df.resid	44.00	UQ	0.57				
R^2	0.82	Max	3.28				

Fixed effects

	Co-eff^{log}	Co-eff^{exp}	E.S.E	*t-value*	*p-value*	Sig.
(Intercept)	-1.83	0.14	1.57	-1.17	0.24	
CLAY	0.37	1.00	0.09	4.14	0.00	***
MSAND	-5.76	1.45	0.87	-6.62	0.00	***

Significance codes: 0 '***' 0.001 '**' 0.01 '*' 0.05 '.' 0.1 ' ' 1

Correlation coefficient

	(Intercept)	CLAY	**VIF**
CLAY	-0.68		1.03
MSAND	-0.15	-0.17	1.03

AICc	Akaike information criterion	UQ	Upper quartile
log-lik	Log-likelihood	Max	Maximum
dev	Deviance	Std. dev.	Standard deviation
df.resid	Residual degrees of freedom	E.S.E	Estimated standard error
Min	Minimum	VIF	Variable inflation factor
LQ	Lower quartile	Co-eff	Coefficient
Med.	Median		

The GLMER for sample depth range 0 – 30 yielded slightly different results compared to the GLMER for depth ranges 30 – 60 (GLMER$^{30-60}$) and 60 – 90 (GLMER$^{60-90}$) (**Table 5.15**). The random effect "site" had a much higher estimated variance (1.53) and standard deviation (1.24), indicating considerable variability between sites (**Table 5.15**). In contrast, the residual variance and standard deviation suggest unexplained variability within each site after accounting for the site level differences (**Table 5.15)**. The two fixed effects, CLAY and MSAND, had strong correlations with EC^m for a depth range of 0 – 30cm (*p-value* < 0.0001) (**Table 5.15**). The relationship between EC^m and CLAY was positive. In contrast, the relationship between EC^m and MSAND was negative, showing an increase in CLAY I increased EC^m while an increase in MSAND resulted in a decrease in EC^m (**Table 5.15).** The correlation matrix of fixed effects shows that the relationship between predictor variables was not significant, and variable inflation factors (<3) further emphasise the lack of multicollinearity between the predictor variables (**Table 5.15**). Finally, the range of scaled residuals for GLMER$^{0-30}$ (-1.2 to 3.3) suggests some deviation from a normal distribution. However, the median is near zero, meaning the model still has a reasonably good fit and explains 82% of the variability seen in EC^m (**Table 5.15**).

Table 5.16 and **Table 5.17** present the GLMERs best able to explain the variability in EC^m for depths 30 – 60cm (GLMER$^{30-60}$) and 60 – 90cm GLMER$^{60-90}$. The standard deviation and variance of the

random effect "site" for both models were extremely small (<0.0001), indicating minimal variability between sites (**Table 5.16** and **Table 5.17**). In contrast, the standard deviation and variance for the random effect's residuals indicate both GLMERs have unexplained within and between-site variability not explained by the fixed or random effects (**Table 5.16** and **Table 5.17**).

Table 5.16. *Generalised linear mixed effects model for modelled electrical conductivity for sample depth range 30 - 60cm.*

Model metrics		**Scaled residuals**		**Random effects**			
AICc	193.60	Min	-1.11			Variance	Std. dev.
log-lik	-88.45	LQ	-0.78	Site	(Intercept)	0.00	0.00
dev	176.90	Med.	-0.24	Residual		0.67	0.82
df.resid	42.00	UQ	0.57				
R^2	0.80	Max	3.53				

Fixed effects						
	Co-eff^{log}	Co-eff^{exp}	E.S.E	*t-value*	*p-value*	Sig.
(Intercept)	-1.07	0.34	0.52	-2.08	0.04	*
GWC	0.13	1.14	0.02	8.53	0.00	***
$ECe^{1:5}$	0.26	1.30	0.05	5.84	0.00	***
FSAND	-0.18	0.83	0.06	-3.18	0.00	**
GWC:$ECe^{1:5}$	-0.01	0.99	0.00	-6.66	0.00	***

Significance codes: 0 '***' 0.001 '**' 0.01 '*' 0.05 '.' 0.1 ' ' 1

Correlation coefficient					**VIF**
	(Intercept)	GWC	$ECe^{1:5}$	FSAND	
GWC	-0.05				7.11
$ECe^{1:5}$	-0.44	0.02			15.64
FSAND	-0.85	-0.24	0.10		1.08
GWC:$ECe^{1:5}$	0.35	-0.53	-0.83	0.03	21.98

AICc	Akaike information criterion	UQ	Upper quartile
log-lik	Log-likelihood	Max	Maximum
dev	Deviance	Std. dev.	Standard deviation
df.resid	Residual degrees of freedom	E.S.E	Estimated standard error
Min	Minimum	VIF	Variable inflation factor
LQ	Lower quartile	Co-eff	Coefficient
Med.	Median		

Table 5.17. *Generalised linear mixed effects model for modelled electrical conductivity for sample depth range 60 - 90cm.*

Model metrics		Scaled residuals		Random effects			
AICc	276.40	Min	-2.53			Variance	Std. dev.
log-lik	-128.40	LQ	-0.68	Site	(Intercept)	0.00	0.00
dev	256.80	Med.	-0.05	Residual		0.11	0.33
df.resid	41.00	UQ	0.71				
R^2	0.71	Max	2.66				

Fixed effects

	Co-eff^{log}	Co-eff^{exp}	E.S.E	*t-value*	*p-value*	Sig.
(Intercept)	1.37	3.95	0.18	7.73	0.00	***
GWC	0.03	1.03	0.01	5.01	0.00	***
ECe$^{1:5}$	0.05	1.05	0.02	2.81	0.00	**
MSAND	-0.81	0.45	0.33	-2.47	0.01	*
FSAND	0.08	1.09	0.03	2.68	0.01	**
GWC : ECe$^{1:5}$	-0.00	1.00	0.00	-4.58	0.00	***

Significance codes: 0 '***' 0.001 '**' 0.01 '*' 0.05 '.' 0.1 ' ' 1

Correlation coefficient						**VIF**
	(Intercept)	GWC	ECe$^{1:5}$	MSAND	FSAND	
GWC	-0.52					5.84
ECe$^{1:5}$	-0.37	0.17				9.61
MSAND	-0.51	0.55	0.38			4.96
FSAND	0.08	-0.47	-0.38	-0.85		4.05
GWC : ECe$^{1:5}$	0.40	-0.51	-0.78	-0.19	0.16	11.09

AICc	Akaike information criterion	UQ	Upper quartile
log-lik	Log-likelihood	Max	Maximum
dev	Deviance	Std. dev.	Standard deviation
df.resid	Residual degrees of freedom	E.S.E	Estimated standard error
Min	Minimum	VIF	Variable inflation factor
LQ	Lower quartile	Co-eff	Coefficient
Med.	Median		

The fixed effects of GLMER$^{30-60}$ and GLMER$^{60-90}$ differ by the exclusion (GLMER$^{30-60}$) and inclusion (GLMER$^{60-90}$) of MSAND. For both GLMERs, GWC and ECe$^{1:5}$ as a main effect showed a strong, positive correlation with EC^{m,} while their interaction resulted in a strong inverse correlation with EC^{m}. Percentage clay was not considered a significant predictor in both GLMER and was omitted, as was MSAND from GLMER$^{30-60}$ (as discussed above) (**Table 5.17**). FSAND in both GLMER had a strong inverse correlation with EC^{m,} while MSAND had a weak positive correlation with EC^{m} in GLMER$^{30-60}$.

The correlation coefficients for both GLMERs show a strong, negative relationship between ECe$^{1:5}$ and the interaction of GWC and ECe$^{1:5}$ for both sample depths, while MSAND and FSAND also strongly correlate (**Table 5.16** and **Table 5.17**). It should come as no surprise then that these individual variables and the interaction terms had high VIFs ranging from 1.08 – 21.98 (GLMER$^{30-60}$) and 5.84 – 11.09 (GLMER$^{60-90}$), predominantly as a result of the interaction effect of GWC and ECe$^{1:5}$ (**Table 5.16** and **Table 5.17**). The predictor variables are theoretically important, and the multicollinearity caused by these variables should be noted during interpretation. In future studies, a ridge or lasso regression or a principal components analysis could be alternative statistical tests to

assess the necessity of these parameters in predicting EC^m. Finally, $GLMER^{30-60}$ and $GLMER^{60-90}$ had scaled residuals with ranges that showed some deviation from the ideal normal distribution; however, both had medians close to zero, suggesting both models had a reasonably good model fit, which is further emphasised by the high R^2 which show the models explain 80% and 71% of the variability in EC^m for depth ranges 30 – 60cm and 60 – 90cm.

In summary, the fixed effects of the GLMER show soil particle sizes CLAY and MSAND were a more significant predictor variable to describe the variability of EC^m at a depth range of 0 – 30cm, but the interaction of GWC and $ECe^{1:5}$ and sand particle size showed the strongest ability to predict variability in EC^m for depth ranges 30 – 60 and 60 – 90. The random effects show that between-site variability was more pronounced at a depth range of 0 – 30, while within-site variability was greater for depth ranges of 30 – 60 and 60 – 90.

5.3.3.3 Mapped modelled electrical conductivity using quasi-3D inversion software

A similar pattern emerged when mapping modelled electrical conductivity (EC^m), with a resolution far greater than the kriged or 1D laterally constrained maps for Mahurangi forest (**Figure 5.6** and **Figure 5.9)** and Te Hiku forest **(Figure 5.7** and **Figure 5.11),** all created using the quasi-3D inversion software EM4Soil (EMTOMO LDA, 2018). The quasi-3D inversion maps were overlaid onto hillshade maps to better understand the changes in EC^m in the context of the topography of each catchment. It is important to emphasise that the EC_a scale used for Mahurangi Forest maps uses a larger range than those used for Te Hiku Forest maps because it was difficult to see the minute changes occurring at Te Hiku Forest, as was seen in **Figure 5.7**. Because the Te Hiku catchment was larger compared to the number of data points collected, a decision was made to increase gridding and smoothing, but it was important to show what the reduced gridding and smoothing did to the aesthetics of the maps at the cost of accurately interpolating EC^m at this site (**Figure 5.11**)

The maps using EC^m derived from quasi-3D inversion software accentuated the patterns found in the 1D laterally constrained maps and the kriged maps and highlighted some new ones (**Figure 5.9** & **Figure 5.10**). For the Mahurangi catchment, symmetry still exists, with low EC^m moving through the centre of the catchment from northeast to southwest. In the quasi-3D inversion maps, low EC^m is more widespread from northeast to southwest to depths 30cm and 60cm, and the map for depths 90cm closely resembles EC_a^{160} in **Figure 5.7**. The east-west symmetry seen in the middle bounds of

the catchment in the 1D and kriged maps are most pronounced at 60cm and even more so at 90cm, while at 30cm, only the strong EC^m signal appears to the west, again showing the bull's eye effect. There is an overall trend of increasing EC^m with depth, except for the one point west of the catchment with the highest modelled electrical conductivity.

For Te Hiku, the northeast-to-southwest increase in electrical conductivity is seen in the quasi-3D inversion maps at 90cm. The quasi-3D inversion map overlaid on the hillshade shows that at depths 30cm and 60cm, there are either artefacts causing bulls eyes due to small sample size, small decreases in elevation or genuine areas where EC^m decreases; however, this is not immediately clear in the maps provided. The quasi-3D inversion map at 90cm shows an increase in EC^m following the topography of the catchment, with a decrease in elevation resulting in an increase in EC^m.

For the most part, Te Hiku Forest catchment is uniformly non-conductive across the catchment and also down the soil profile to 0 – 60cm. Beyond 60cm, the localised patch of high conductivity to the southwest could be attributed to an increase in GWC, but it could also be attributed to other soil properties. An outlet in the northwest of **Figure 5.12** aligns closely with the raised levels of EC^m. Modelled electrical conductivity appears to radiate outwards from the outlet with decreasing EC^m. Gravimetric water content in this region also appears elevated, particularly at plots 04A15 and 04A06, suggesting GWC could be a dominant factor in the increase in EC^m. **Figure 5.13** uses the same base map overlain by EC^m, but the point size indicates the percentage of medium-sized sand particles this time. The map indicates a general decrease in particle size with an increase in EC^m and shows regions with lower elevations to the north-west and north-east tended to have higher levels of GWC but lower instances of MSAND. **Figure 5.14** is the same hill shade overlaid by the EC^m map at 90cm and shows FSAND, CLAY, and $ECe^{1:5}$ did not show any clear spatial patterns.

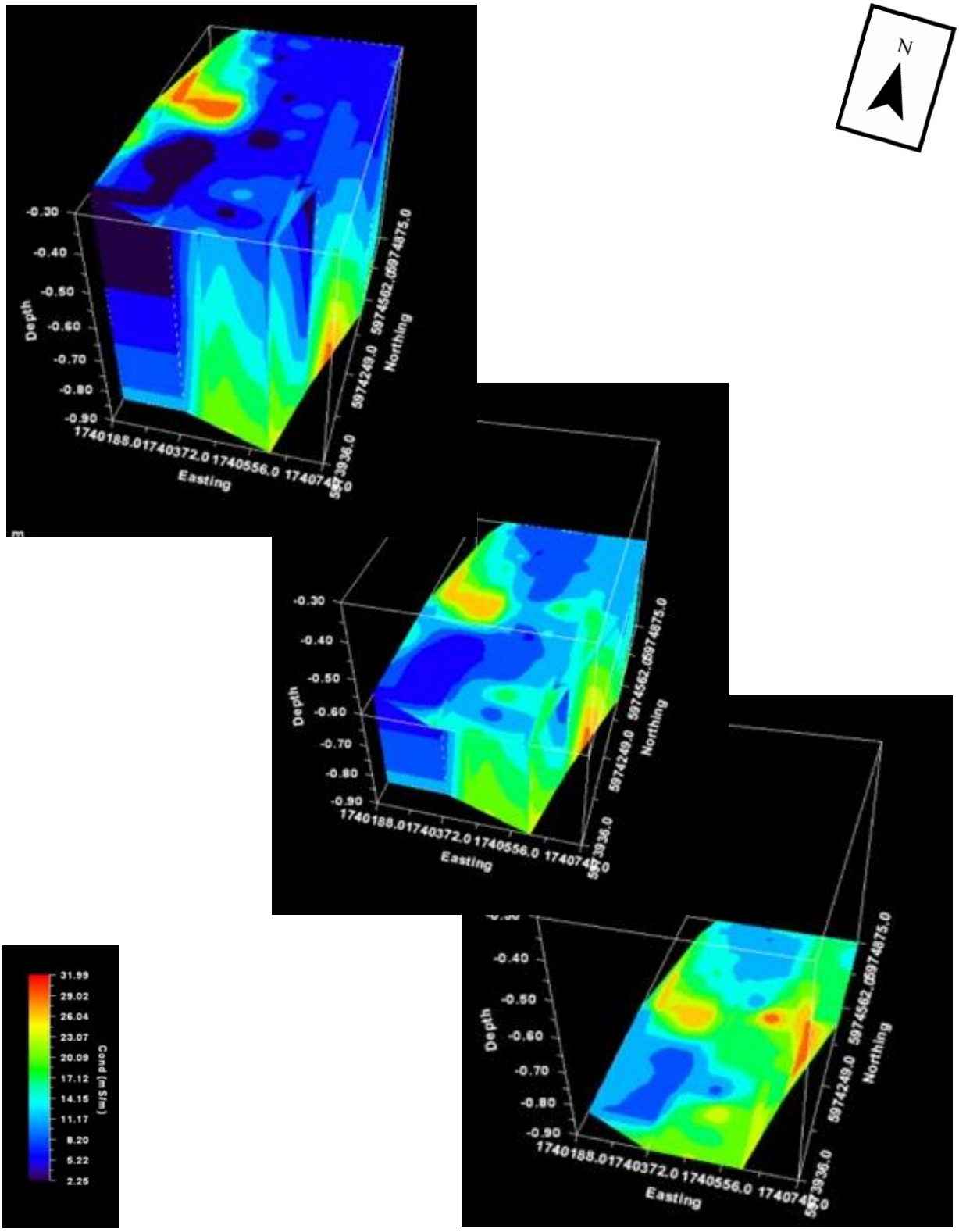

Figure 5.9. *Quasi 3D inversion map of Mahurangi Forest at three depths 30cm (top), 60cm (middle) and 90cm.*

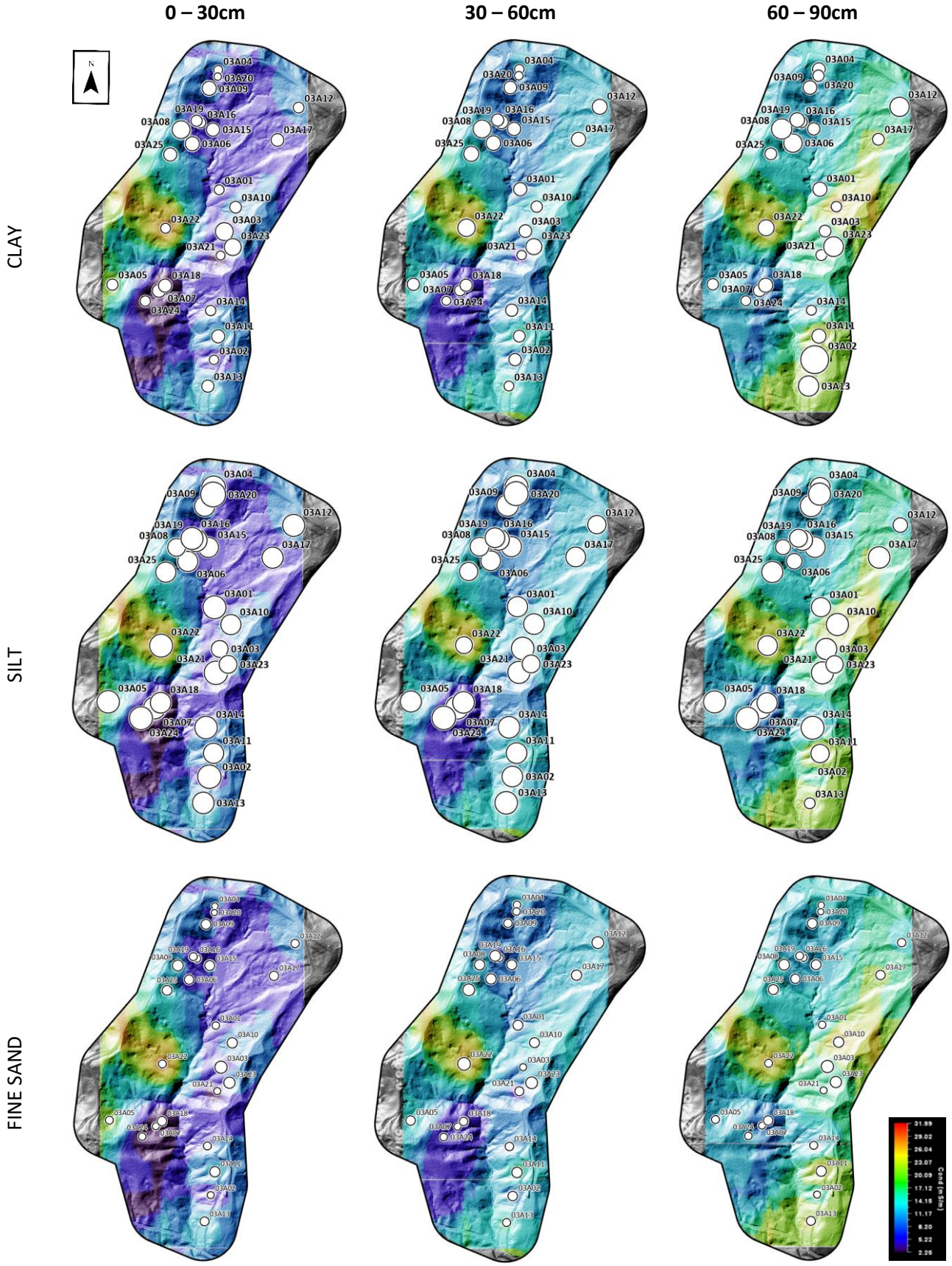
0 – 30cm
30 – 60cm
60 – 90cm
CLAY
SILT
FINE SAND
03A04
03A20
03A09
03A12
03A19
03A16
03A08
03A15
03A17
03A25
03A06
03A01
03A10
03A22
03A03
03A23
03A21
03A05
03A18
03A07
03A24
03A14
03A11
03A02
03A13
31.99
29.02
26.04
23.07
20.09
17.12
14.15
11.17
8.20
5.22
2.25
Sand (in %m)

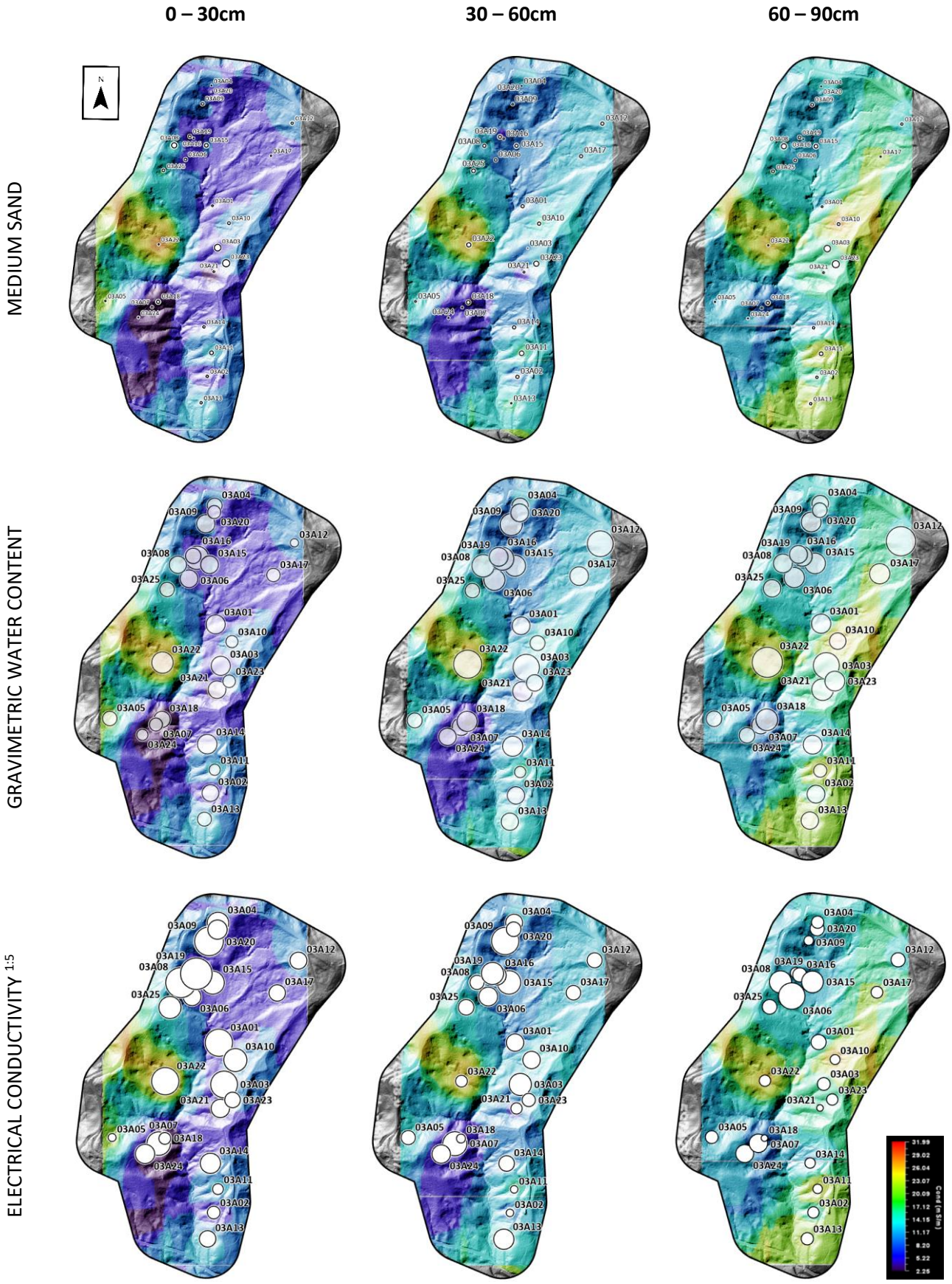

Figure 5.10. *Mahurangi modelled electrical conductivity (mS/m) for sample depths 0 – 30cm, 30 – 60cm and 60 – 90cm, overlaid on hillshades with percentage clay, silt, fine sand, medium sand gravimetric water content and electrical conductivity of a one-part soil to 5-part water solution at each plot where larger circles indicate larger percentages/quantities.*

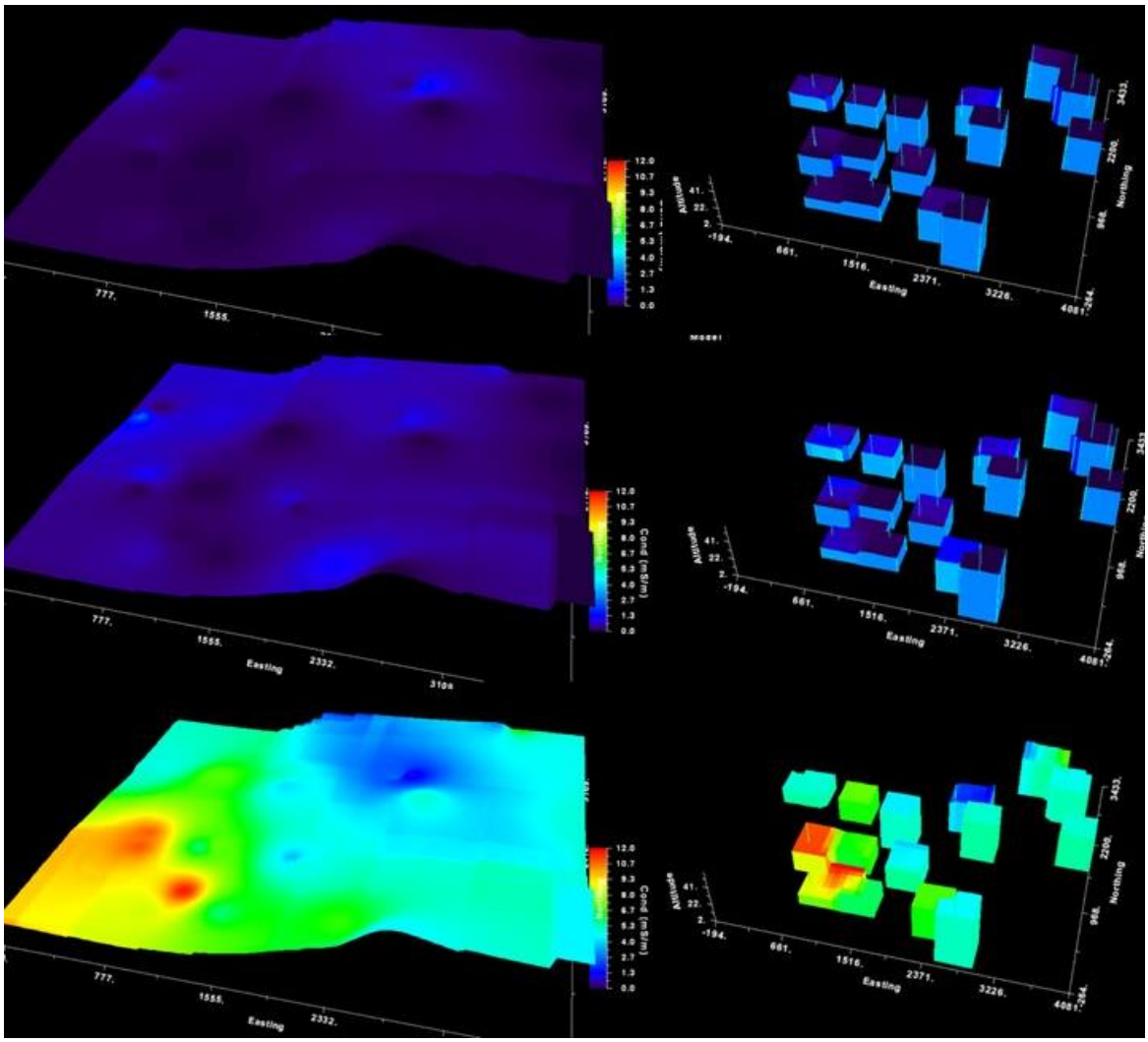

Figure 5.11. *Te Hiku forest modelled electrical conductivity to 30cm (top), 60cm (middle) and 90cm (bottom) with increased gridding and smoothness (left) and reduced gridding and smoothness (right).*

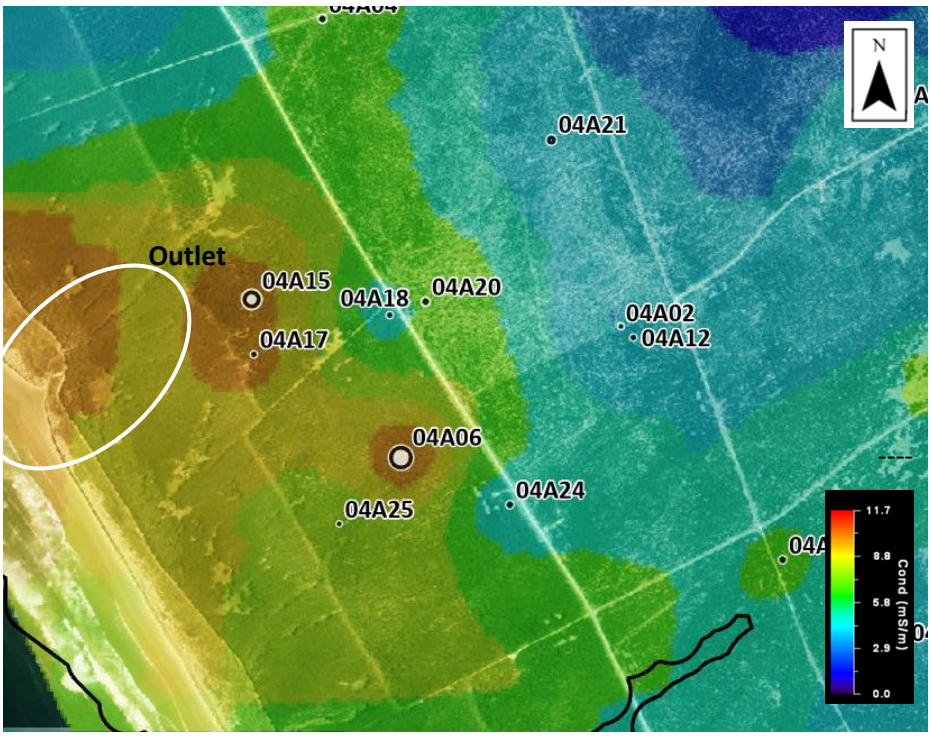

Figure 5.12. *Te Hiku Forest electrical conductivity at 90cm overlaid on an aerial basemap and hillshade and zoomed into the region with higher, modelled electrical conductivity levels. Dots indicate plots and larger point size indicates higher levels of gravimetric water content.*

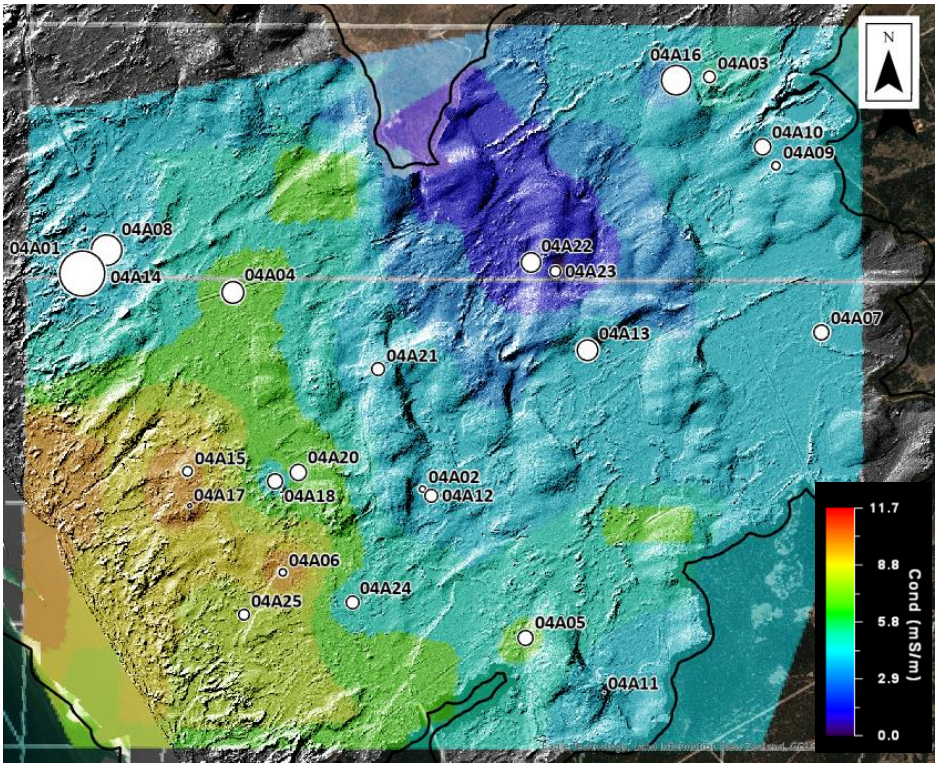

Figure 5.13*. Te Hiku Forest modelled electrical conductivity (colours) and ECe[1:5] (points) at 90cm are overlaid on an aerial base map and hillshade. Plot locations are marked with points. Point size relates to increases in medium sand-sized particles.*

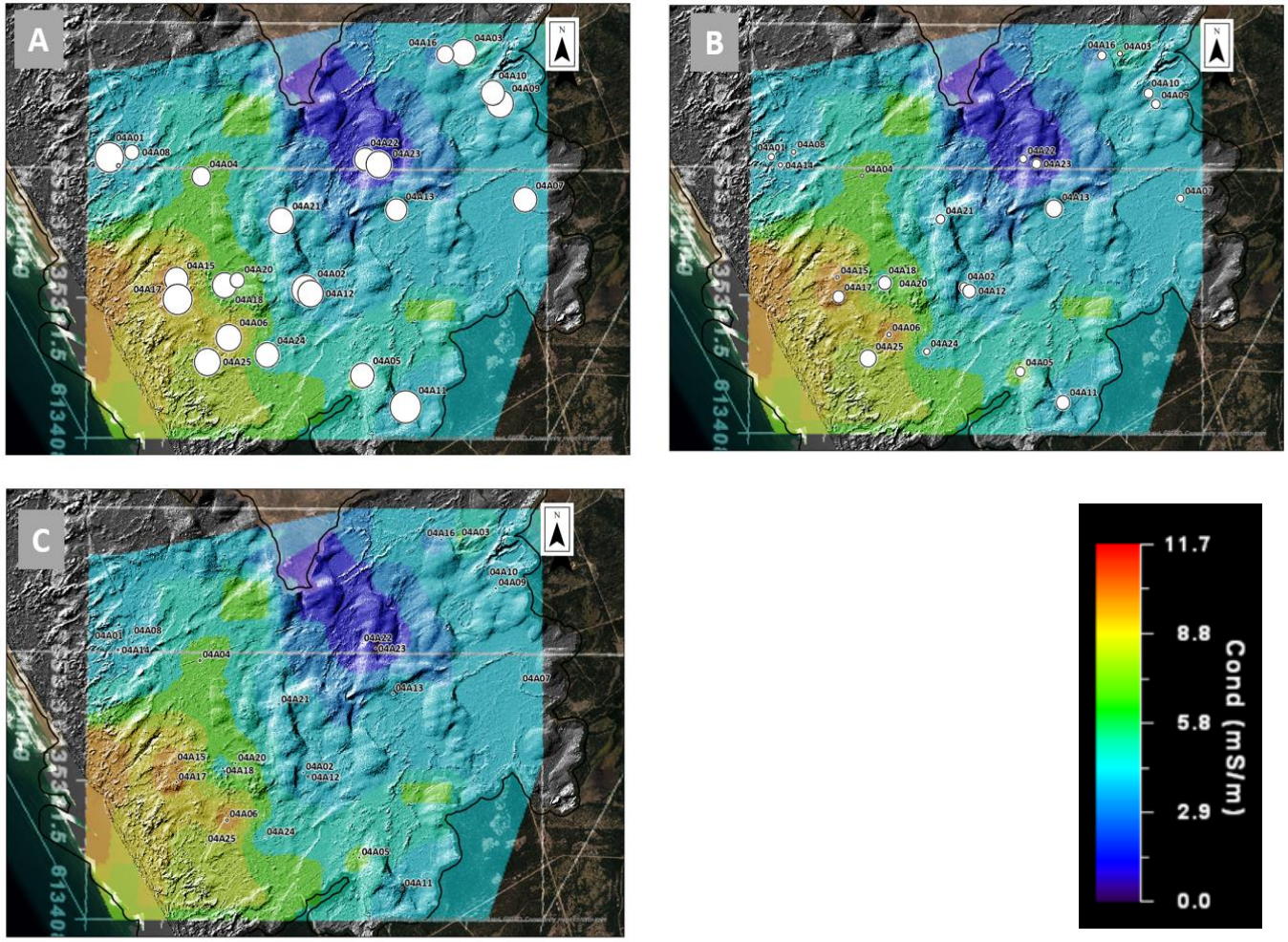

Figure 5.14. *Te Hiku Forest modelled electrical conductivity at 90cm overlain on a hillshade of the catchment. Plot locations are marked with points. Point size indicates the increasing/decreasing amounts of fine sand (A), clay-sized particles (B) and electrical conductivity of a 1 part soil to 5 part water solution (C).*

5.4 Discussion

The discussion is split into three sections. **Section 5.4.1** discusses the complex relationship between apparent and modelled electrical conductivity and soil variables. **Section 5.4.2** looks at the ability of apparent electrical conductivity and modelled electrical conductivity to predict soil variables. **Section 5.4.3** compares the kriged, 1D and 3D conductivity maps in the context of the study sites to derive relationships between soil variables and apparent and modelled electrical conductivity.

5.4.1 Complexity of soil variables

Electrical conductivity is most commonly used to predict the spatial distribution and concentration of soil salinity (Heil & Schmidhalter, 2017). Where electrical conductivity is used in non-saline soils, EC_a is most typically a function of soil water content and electrical charge (Gallart et al., 2019; Heil & Schmidhalter, 2017). Using EC_a and EC^m as predictors of soil variables is challenging as the relationship is not one-to-one, as seen in **Section 5.3**. A combination of GWC, $ECe^{1:5}$ and soil particle size percentage was responsible for the variability in EC_a and EC^m (**Table 5.10** - **Table 5.17**). To further complicate the relationship, the interaction of these variables also affected EC_a and EC^m, and it is this complex interaction between soil physical and chemical properties which makes modelling soil spatial variability using EC_a and EC^m challenging (Brevik et al., 2006; Gallart et al., 2019; Hedley et al., 2004).

For example, there was a positive relationship between EC_a and EC^m and GWC, $ECe^{1:5}$ and FSAND and a negative association with EC_a and EC^m and medium-sized sand particles. However, the interaction effect between GWC and $ECe^{1:5}$ caused a negative relationship with EC_a and EC^m. In addition, generalised linear mixed effects models (GLMERs), which used EC_a and EC^m as response variables, that included multiple variables as fixed effects were able to explain a higher percentage of the variability (80 – 87%) in EC_a and EC^m and had stronger *p-value*s (**Table** 5.17 **5.17**) Therefore, the interaction between soil variables measured in this study is discussed next.

Gravimetric water content remained relatively constant down the soil profile (**Table 5.2)**, which may result from forest soil structure and precipitation events near the period chosen to measure apparent electrical conductivity (EC_a) for this study. Forest soils contain macropores (vertically oriented) and soil pipes (horizontally oriented) (Uchida et al., 2001), which are formed from hydraulic processes, bio and pedoturbation and the decay of tree and plant roots (Amatya et al.,

2016; Bren, 2016; De Jong, 2016; Williams, 2016) and their formation and erosion is influenced by land use, soil type, precipitation and topographic relief (Jones, 2010). While soil macropores influence the infiltration of precipitation, soil pipes influence the flow of moisture at a hillslope or even catchment scale, otherwise referred to as pipe flow (Uchida et al., 2001). Soil pipes "extend the stream network"(Jones, 2010) or act as a "short-circuiting process", allowing water to flow at rates far greater than hydraulic conductivity through the soil matrix alone, with one study reporting rates up to 300 times higher than the flow rates measured in the mineral soil (McGlynn et al., 2002; Mosley, 1979). This allows precipitation to be redistributed through sub-surface storm runoff, reducing the chances of overland flow during rainfall events, resulting in a relatively even distribution of soil moisture across forested catchments (Amatya et al., 2016; Bren, 2016; De Jong, 2016; Uchida et al., 2001; Williams, 2016).

Gravimetric water content, particle size distribution, mineralogy, soil porosity, and pore connectivity are all interrelated with soil electrical conductivity (Bai et al., 2013). Soil moisture enables soil salts and minerals to move within the soil, which can either increase the soil's electrical conductivity or, due to hysteresis, alter the electrical conductivity of soil depending on whether it is in the wetting or drying phase (Hanks, 1992). While soil GWC remained relatively constant down the soil profile, $ECe^{1:5}$ decreased with depth **(Table 5.6**), likely because of soil chemical and physical weathering processes in the soil profile's top Ah and Bs/Bw horizons (McLaren & Cameron, 1996). Electrical conductivity can be a measure of soluble ions such as Ca^{2+}, Mg^{2+}, $Na^{+,}$ k^{+}, Cl^{-}, NO_{3-} and $SO_4^{2-,}$ which leach out and are lost in the soil forming process or re-precipitate in lower horizons (Bai et al., 2013; McLaren & Cameron, 1996). In non-saline soils, electrical conductivity can be used as a measure of the cation exchange capacity of clay minerals because they have a large surface area due to their small particle size (<0.22mm) (Milne et al., 1995). The large surface area allows clay-sized particles to have a cation exchange capacity that changes depending on the original parent material of the clay and how much and the type of weathering, leaching and translocation the clay has endured (McLaren & Cameron, 1996). Soils dominant in clay have high matrix potential and hydrolysis, resulting in poorly drained soils as soil moisture is tightly held in soil pores (McLaren & Cameron, 1996). Soils dominated by larger particles, such as silt and sand, also have larger pore spaces between particles, allowing soils to drain more readily due to the reduced matrix potential.

This section in this thesis emphasises the importance of understanding the interlinkages between soil qualities. The GLMERs utilised to estimate soil properties from EC^{a} and EC^{m} favoured a range of

soil variables in the model, which is likely because this is more reflective of *in situ* soil conditions, as opposed to GLMERs that use only one soil variable as a predictor variable. This complex interaction is highlighted in more detail in subsequent sections.

5.4.2 Weighted mean and apparent electrical conductivity and modelled electrical conductivity

The GLMERs revealed "site" as a random effect that explained some of the variability in EC_a^{50} and EC_a^{160} cumulative depths that wasn't explained by the five fixed effects: GWC, $ECe^{1:5}$, CLAY, FSAND, and MSAND. This was true for between-site variability but more so for within-site variability. When multiple fixed effects were introduced into the GLMERs, within and between site variability reduced as the combination of soil variables as fixed effects were better able to explain the variability in EC_a

According to Hedley et al. (2004), McNeill (1980) and Sudduth et al. (2001), the weighted mean values of the top 75cm of the soil profile should correlate closely with electromagnetic induction perpendicular co-planer coil windings and the weighted mean to 150cm should correlate more closely EMI horizontal co-planer coil windings. In this study, the weighted means were calculated in line with the depths of soil samples 0 – 30cm, 30 – 60cm and 60 – 90cm. It was expected that the perpendicular co-planer-oriented coil windings of the EMI instrument used in this study would correlate with weighted means of soil properties to a depth of 60cm as this sensor's cumulative depth reaches 50cm. It was also expected that the orientation of the horizontal co-planer coil windings would align more closely with the weighted mean of 90cm. In the context of this study, the generalised linear mixed effects models revealed slightly more complex relationships.

The results showed that the weighted mean depth was not necessarily correlated with EC_a^{50} or EC_a^{160} (**Table 5.9** & **Figure 5.5**). Apparent electrical conductivity to a cumulative depth of 160cm was more strongly correlated with individual soil variables CLAY and FSAND (*p-value* < 0.05) and weakly correlated with GWC and $ECe^{1:5}$ (*p-value* < 0.1) at both weighted mean depths with GLMER's that could explain between 73 and 84% of the variability seen in EC_a^{160}. Between 73 and 84% of the variability in EC_a^{50} could be explained by a weak correlation with the weighted mean of CLAY and MSAND to 60cm and the weighted mean of CLAY and $ECe^{1:5}$ to 90cm. These correlations, while significant, do not capture the underlying complexity of the interaction of soil properties, quite like the modelled electrical conductivity was able to do. While this study was not looking for any specific

feature in the soils of the two study sites, it is generally unknown from the analysis of EC_a what depth each soil variable has the most influence or how soil horizonation can be captured across a catchment. For example, because of how conductive clay is, it can dampen the EC^m signal causing the cumulative depth of investigation to decrease or making it more difficult to discern underlying soil properties. For example, Hedley et al. (2004) found EC_a increased in the presence of a clay impedance layer; however, the depth of the layer could not be predicted using EC_a alone, which, in the context of the study, would have been useful given the clay horizon varied in depth when sampled from between 30 and 54cm (Hedley et al., 2004).

Studies that used EMI technology to measure EC_a to capture the variability of soil properties over a study area and that also used inversion software to disseminate the signal at defined depths suggest inverting EC_a allows a better critical assessment of electrical conductivity down a profile and across a catchment compared with using EC_a alone in interpretation. (Huang et al., 2017d; Khongnawang et al., 2022; Murphy et al., 2009; Ogilvy et al., 1991; Triantafilis & Santos, 2013).

Maps visualising EC_a spatial distribution created using ordinary kriging were able to show within-site heterogeneity to the same extent that the 1D laterally constrained maps; however, the maps were unable to show slight changes in conductivity and were more prone to the bull's eye effect in regions where the sample size was small as there were not enough measurement points to extrapolate from based on catchment size (**Figure 5.6 & Figure 5.7**). The 3-dimensional maps created using quasi-inversion software could better interpolate EC_a across the catchment and the profile; however, the bull's eye effect surrounding isolated sample points still exists but to a lesser degree.

In contrast, the modelled electrical conductivity (EC^m) had stronger correlations with measured soil variables at each of the defined depths 30cm, 60cm and 90cm, both as individual variables but even more so with GLMERs consisting of multiple soil variables. The added detail in the quasi-3D inversion maps that were not present in the 1D laterally constrained or the kriged maps further emphasises the point made by users of quasi-3D inversion software that the results both statistically and visually are superior to using apparent electrical conductivity without inversion (Huang et al., 2017d; Khongnawang et al., 2022; Murphy et al., 2009; Ogilvy et al., 1991; Triantafilis & Santos, 2013).

5.4.3 Mapped electrical conductivity using quasi-3D inversion software

The kriged, 1D laterally constrained (**Figure 5.6** and **Figure 5.7**) and quasi-3D inversion maps- (**Figure 5.9)** highlight one important factor. Both catchments display within and between site heterogeneity, echoed in the generalised linear mixed effects models when only one soil variable was used as a fixed effect. In addition, all maps show within-site heterogeneity with clear spatial patterns.

For example, low, modelled electrical conductivity running north/northeast to south/south-west through the centre of the Mahurangi catchment can be seen in the kriged, 1D, spatially constrained maps (**Figure 5.6 and Figure 5.7**). This spatial pattern is also present in the 3D maps (**Figure 5.9**) with more detail as the low EC_a area takes up a greater portion of the map, particularly to the northeast at 30cm. The low conductivity area funnels from 30cm to 90cm and is less widely spread. The presence of this low conductivity zone could be explained by the variable source area theory developed by Hewlett and Hibbert (McDonnell, 2009). The idea relates to the systematic soil saturation in forested catchments during rainfall events whereby slopes near streams become saturated first, and the saturation moves up the slope to adjacent, not yet saturated zones, which are further away (**Figure 5.15**). The inverse occurs when rainfall ceases or the source area decreases during periods with little to no rain (**Figure 5.15**)**.**

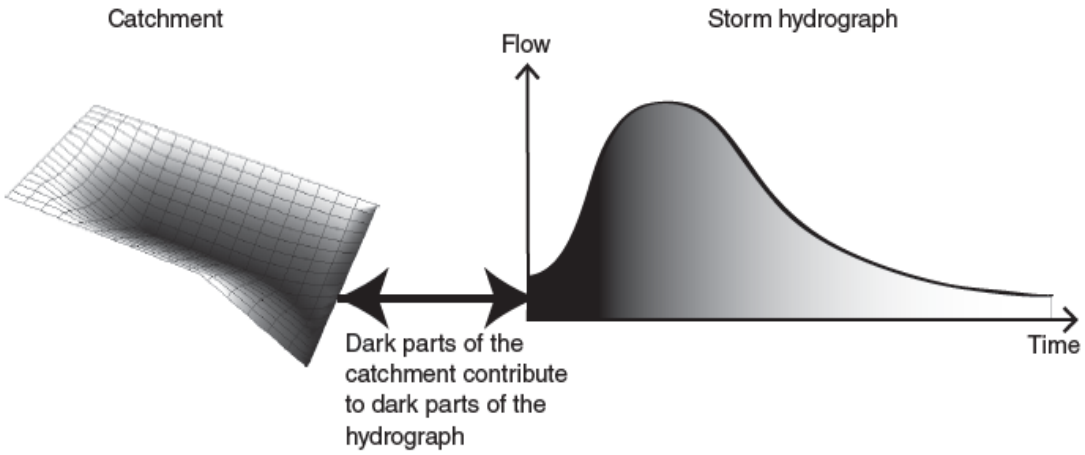

Figure 5.15. *Variable source area as described by Bren (2016) in (Amatya et al., 2016), whereby the darker parts of the catchment have a higher probability of contributing to the darker parts of the hydrograph than the paler colours.*

Running north-northeast to south-southwest through the centre of the Mahurangi catchment is a river channel fed by tributaries running from the surrounding headwaters of the catchment. The river channel is surrounded by steep slopes, which plateau at the edges of the catchment, similar to the catchment in Figure 5.15 The river channel and its surroundings at 90cm are defined by high EC^m, corresponding to an increase in soil moisture content**.** Just as the variable source area theory

states, as one moves up the slopes of the catchment and away from the river channel, moisture content typically decreases, resulting in a decrease in $EC^{m,}$ This theory also holds for the east and west regions exhibiting high $EC^{m,}$ which are in slight depressions in the catchment.

The results from the generalised linear mixed effects models using one variable and multiple variables and their interactions both showed GWC at 90cm had a strong, significant relationship with $EC^{m,}$ and although these models do not separate the significance by site, the standard deviation and variance of the random effects modelling GWC on its own suggest GWC varies both within and between sites.

At Te Hiku Forest, a similar pattern emerges, albeit less extreme. Electrical conductivity in the kriged and 1D laterally constrained map shows a general (but slight) increase in electrical conductivity moving from northeast to southwest (**Figure 5.7**). This spatial pattern follows the contours of the catchment where there is a general northeast-to-southwest dip and the highest electrical conductivity values occurring in a depression at the southwest of the catchment (**Figure 5.7**). The EC^{m} map was overlaid onto a base map in ArcGIS Pro to determine if the observed pattern was purely topographic, which may be related to an increase in EC^{m} in this part of the catchment.

Triantafilis and Monteiro Santos (2013) characterised the spatial distribution of a uniform, course-textured sediment associated with a stream channel while using the relationship of $ECe^{1:5}$ and EC^{m} with regions of heavy clay-textured soils. The catchment in question was generally uniformly non-conductive with patches of heavy conductivity, which were associated with the coarse sand and heavy clay distributions. The mapped results found by Triantafilis and Monteiro Santos (2013) are similar to those found in the Te Hiku forest, where, for the most part, the catchment is uniformly non-conductive across and down the soil profile to 0 – 60cm. Beyond 60cm, the localised patch of high conductivity to the southwest was attributed to medium-sized sand particles and proximity to the catchment's outlet. If gravimetric water content is infact the primary driver of increases in EC^{m} in the region, then the variable source area theory could be attributed to the radial increase in EC^{m} towards the outlet. Two further points of interest, firstly, this pattern only presents itself at 60 - 90cm depth indicating ground water is the potential source of GWC. It would be interesting to measure how quickly soil moisture increases to the overlying soil during precipitation events compared to how stagnant water content remains to establish if variable source area theory

supports this observation. The installation of groundwater wells or monitoring equipment would also be useful to validate this assumption.

Secondly, despite the absence of measurement plots around or close to the outlet (**Figure 5.12**), the quasi-3D inversion still highlighted this region as an area of higher-modelled electrical conductivity. This could be because the quasi-3D software uses a laterally constrained approach to inverting apparent electrical conductivity along with elevation data, or it could be an artefact caused by the smoothing process. Either way, in the context of the study site, the elevated EC^m levels fall in line with the hypothesis that EC^m increases with proximity to the outlet, which follows the rules of variable source area (Amatya et al., 2016; Bren, 2016; De Jong, 2016; McDonnell, 2009; Williams, 2016).

Figure 5.13 showed that at Te Hiku Forest, there was a spatial pattern related to particle size distribution in relation to topographical relief whereby lower-lying regions tended to have less medium-sized sand particles and had lower modelled electrical conductivity at 90cm, while most elevated areas had an inverse trend. This is a known phenomenon in soils whereby finer textured particles can travel further from their source, resulting in courser-grained particles at the tops and plateaus of catchments and finer-sized particles at the bottom of hillslopes (Amatya et al., 2016).

Chapter 6 :
Conclusion

6.1 Introduction

The overall objectives of this thesis were to identify if electromagnetic induction technology (EMI) can be used in a forested environment to capture the spatial heterogeneity of soil properties. If so, this thesis can serve as a 'toolbox' for measurement protocols and analysis for forest owners interested in low-cost, time-effective methods of understanding microsite heterogeneity in their forest soils to guide management practices.

This chapter summarises the factors that affect apparent electrical conductivity in **Chapter 4** and if adjustments were required to compensate for them. Next, this chapter discusses the performance of global generalised linear models used in **Chapter 5** that assess apparent electrical conductivity and modelled electrical conductivity as predictors of soil variables such as gravimetric water content, electrical conductivity of a 1-part soil to 5-part water solution and percentage of clay, fine sand and medium sand. Finally, this chapter looks at how modelled electrical conductivity can be mapped using 1D laterally constrained inversion software and quasi-3D inversion to identify spatial trends of modelled electrical conductivity and how they relate to soil variables. This chapter concludes with recommendations for future research, which may provide relevant information to help land owners and forest managers interested in using electromagnetic induction technology as a management tool to understand spatial heterogeneity in forest soils.

6.2 Instrument voltage, ambient, soil and instrument temperature on and drift in apparent electrical conductivity

6.2.1 Requirement of correction factor to compensate for instrument drift

In the first section of **Chapter 4**, analysis was conducted to determine if factors such as ambient temperature, instrument temperature, soil temperature, and instrument voltage contributed to the drift in apparent electrical conductivity during measurement campaigns. **Table 4.1** presents summary statistics for these variables at Mahurangi Forest and Te Hiku Forest. Notably, ambient temperature exhibited the most significant fluctuations within and between sites, while instrument and soil temperatures remained relatively stable. However, the Pearson correlation analysis (**Table**

4.2) and generalised linear models indicated that these temperature and voltage variables did not correlate statistically with apparent electrical conductivity at both forest sites and cumulative depths.

6.2.2 The effect of forest litter presence and absence

In this subsection of Chapter 4, analysis was conducted to determine if the presence or absence of forest litter impacted apparent electrical conductivity. Summary statistics (**Table 4.3**) and box plots illustrated that Mahurangi generally exhibited higher apparent electrical conductivity than Te Hiku. The presence or absence of forest litter did not significantly alter the median values of apparent electrical conductivity at either depth, but Mahurangi's data showed more variability. An analysis of variance (ANOVA) confirmed that the presence or absence of forest litter did not lead to a statistically significant difference in mean apparent electrical conductivity. However, cumulative depth and forest site were significant factors, indicating that these variables primarily drove differences in apparent electrical conductivity.

6.2.3 The effect of litter gravimetric water content, thickness, and density on apparent electrical conductivity

This subsection of Chapter 4 explored the potential impact of forest litter properties, such as gravimetric water content, thickness and density, on apparent electrical conductivity. A generalised linear model (GLM) assessed the relationships between these litter variables and apparent electrical conductivity (Table 4.6). The GLM results suggested that the litter properties did not significantly explain the variability in apparent electrical conductivity, with weak or non-significant *p-value*s. Furthermore, a likelihood ratio test demonstrated that adding or removing these predictor variables did not significantly affect the model's explanatory power.

6.2.4 Discussion

The results indicated that neither temperature nor voltage fluctuations, the presence or absence of forest litter, nor litter properties like thickness, gravimetric water content, and density explained the variability in apparent electrical conductivity in this study. Therefore, based on these findings, no adjustment factor was required to compensate for instrument drift or litter presence. However, it is essential to note that these results were specific to the conditions observed in the Mahurangi and Te Hiku forests during the measurement campaigns. Therefore, further research in different settings

may yield different outcomes. Based on the results of this study, if full canopy cover is achieved by the forest, resulting in a shield from direct solar radiation and an electromagnetic induction instrument such as the DualEm-1 is used with insulation surrounding the sensors and instrument voltage checked and maintained regularly, then correction factor would be less likely to be required. Even still, if obtaining ambient, soil and instrument temperature and voltage can be done with minimal effort, a quick analysis could be conducted to rule out the requirement of an adjustment factor. Similarly, with litter presence or absence, if instances of unusually thick, moist or dense little are present, then following the methods in this thesis to establish the effect these factors have on apparent electrical conductivity would be wise. However, if little presents itself as 'normal' and time and cost constraints are an issue, forgoing sample collection and data analysis to establish if an adjustment factor is required for litter presence would, if nothing else, provide peace of mind that these variables do not have to be compensated for in further analysis.

6.3 Apparent electrical conductivity and modelled electrical conductivity as a predictor of soil gravimetric water content, 1-part soil to 5-part water solution and percentage of clay, fine sand and medium sand particles

6.3.1 Apparent electrical conductivity as a predictor of soil variables

In this section of **Chapter 5**, the presented results focused on using apparent electrical conductivity (EC_a) as a predictor of soil variables. The primary objective was to identify the most effective predictor variables for explaining EC_a to two cumulative depths of 50cm (EC_a^{50}) and 160cm (EC_a^{160}) using weighted means of soil predictor variables and for explaining EC^m using measured parameters of soil predictor variables to sample depths 0 – 30cm, 30 – 60cm and 60 – 90cm, using generalised linear mixed effects models (GLMERs).

The weighted mean of soil predictor variables, including electrical conductivity of a 1-part soil to 5-part water solution ($ECe^{1:5}$), gravimetric water content (GWC), and percentages of clay, fine sand, and medium sand per sample (CLAY, FSAND, MSAND) were assessed on their ability to explain the variability in EC_a by inputting them into individual GLMERs **(Table 5.7 and Table 5.8)** and also as main effects in one GLMER (**Table 5.6**). Model evaluation parameters showed between 73 and 87% of the variability in EC_a^{50} and EC_a^{160} could be predicted using either individual or a combination of GWC, $ECe^{1:5}$ CLAY, FSAND and MSAND; however, the Akaike Information Criterion corrected for small

sample size (AICc) suggested the more complex GLMERs with multiple predictor variables were better able to balance model complexity with goodness of fit (delta < 3). Models with significant relationships with EC_a and individual soil variables showed strong positive relationships with EC_a^{160} were more common across all weighted mean depths (*p-value* < 0.05) and only weak relationships with EC_a^{50} (*p-value* <0.1). In addition, $ECe^{1:5}$ and GWC as individual predictors could not explain the variability in EC_a at either cumulative depths (*p-value* >0.1). In contrast, when included as main effects into GLMERs, GWC and $ECe^{1:5}$, along with the soil particle sizes, showed strong significant relationships to varying degrees at both cumulative depths and weighted mean depths. Site as a random effect explained more of the variability in EC_a within and between sites when there were fewer predictor variables as fixed effects. An increase in predictor variables resulted in a decrease in the ability of the random effect to explain the variability in EC_a.

Figures 5.8 and **5.9** depicted maps of EC_a variability at Mahurangi and Te Hiku using ordinary kriging and 1D laterally constrained inversion for EC_a^{50} and EC_a^{160}. The maps were coarse and gave a general overview of the spatial variability of EC_a but pale compared to the quasi-3D inversion maps created using modelled electrical conductivity, particularly for Te Hiku Forest.

6.3.2 Modelled electrical conductivity as a predictor of soil variables

In this section of Chapter 5, a thorough examination of various GLMERs was conducted to evaluate their effectiveness in explaining modelled electrical conductivity (EC^m) variability at different soil depths. The GLMERs featured fixed and random effects, with "site" as a consistent random effect, representing Mahurangi and Te Hiku.

As with Section **6.3.1**, when considering GLMERs with only one predictor variable as a fixed effect and "site" as a random effect, these models exhibited higher standard deviations and variances for the random effect "site" compared to models with multiple predictor variables. This indicates a more pronounced within-site and between-site variability when only one soil variable was considered. Furthermore, models with only one fixed effect exhibited slightly higher residual variance and standard deviation, suggesting greater unexplained variability within and between sites. These findings underscore the importance of including or, at the very least, considering multiple soil variables when using EC^m as a predictor of soil spatial heterogeneity, as it significantly reduced unexplained variability.

At specific depth ranges of 0–30cm, a model incorporating CLAY and MSAND as predictor variables demonstrated the highest coefficient of determination (R^2= 0.83). Fine sand was excluded and did not significantly impact model fit. At depths of 30–60cm, the global model, which included all predictor variables and the interaction between gravimetric water content (GWC) and electrical conductivity of a soil-water solution ($ECe^{1:5}$), performed exceptionally well, explaining 80% of EC^m variability. This interaction term was critical for explaining EC^m variability at this depth. Similarly, at 60–90cm depths, the global model with all predictor variables and the GWC-$ECe^{1:5}$ interaction emerged as the top performer, explaining 71% of EC^m variability. However, multicollinearity issues were observed due to high variable inflation factors, primarily driven by the GWC-$ECe^{1:5}$ interaction.

In conclusion, **Section 5.3.3** underscores the importance of comprehensively considering multiple predictor variables and interaction terms to explain EC^m variability across different sample depths. The global models, encompassing GWC, $ECe^{1:5}$, CLAY, FSAND, and MSAND, and their interactions, demonstrated superior performance at 30–60cm depth ranges and 60–90cm. Omitting non-significant variables can lead to more stable models with reduced complexity. While GWC, $ECe^{1:5}$, and their interactions played crucial roles in explaining EC^m variability at greater depths, their influence diminished at shallower depths of 0–30cm. Additionally, the analysis highlighted the presence of multicollinearity, which should be addressed in future studies using alternative statistical techniques.

The 3D inversion of modelled electrical conductivity (EC^m) revealed consistent patterns with previous maps, offering additional insights. In the Mahurangi catchment, a symmetrical low EC^m pattern from northeast to southwest was evident at 30cm and 60cm, resembling ECa160. Depth-dependent variations and increasing EC^m trends were noted, with exceptions at specific locations. Conversely, Te Hiku's EC^m appeared to correlate with catchment topography, displaying variations at 30cm and 60cm. Uniform non-conductivity prevailed across the catchment and down to 60cm, with localised high conductivity beyond 60cm potentially linked to increased GWC. Overlay analysis highlighted EC^m's relationship with soil properties. Notably, finer particles associated with higher EC^m were observed. Spatial patterns linked EC^m to GWC and medium-sized sand particles.

These findings emphasise the importance of multiple predictor variables and interactions in explaining EC^m variability, aligning with our previous GLMER analysis. The observed spatial patterns reflect a complex interplay of factors, including GWC, soil particle size, and topography.

6.3.3 Discussion

This discussion's central theme is the complexity of the relationship between EC_a and EC^m and soil variables. Soil properties like GWC, $ECe^{1:5}$, and soil particle size contribute to the variability seen in EC_a and EC^m. However, their interactions further complicate the relationship, making it challenging for spatial variability modelling with EC_a and EC^m (Brevik et al., 2006; Gallart et al., 2019; Hedley et al., 2004).

Notably, there were positive associations between EC_a/EC^m and GWC, $ECe^{1:5}$, and fine sand particles, while medium-sized sand particles showed a negative relationship. Complex interaction effects between GWC and $ECe^{1:5}$ caused negative relationships with EC_a and EC^m. Generalised linear mixed-effects models (GLMERs) incorporating multiple variables as fixed effects demonstrated their ability to explain higher electrical conductivity variability (80 – 87%) with stronger *p-value*s. This complexity underscores the importance of considering multiple predictor variables and their interactions, as highlighted in the previous GLMER analysis.

The study further investigated the spatial distribution of soil properties by creating maps. Spatial maps, including kriged, 1D laterally constrained, and quasi-3D inversion maps, were crucial in understanding how EC_a and EC^m relate to soil variability across the catchments. Quasi-3D inversion maps, in particular, provided more detailed and nuanced insights into the spatial distribution of modelled EC^m, which were not as apparent in the other types of maps. These maps visually represented how EC^m varied across different depths and locations within the catchments. Overlaying these spatial maps with additional geospatial data, such as raster datasets representing topography and raw soil variable data in points, provided a more comprehensive understanding of the relationship between EC_a, EC^m, and soil properties. These overlays helped validate the patterns observed in the maps and allowed for observations of potential links to topographic features and landscape characteristics.

In summary, the spatial maps and GLMERs are interconnected because GLMERs are statistical tools to analyse and understand the relationships between EC_a, EC^m, and soil variables. They provide valuable insights into the statistical significance of these relationships. On the other hand, spatial maps visualise the spatial distribution of EC_a and EC^m, offering a practical and visual representation of how these variables vary across the study sites. By overlaying these maps with additional geospatial data, researchers can validate and enhance their understanding of the spatial patterns observed in the GLMERs, ultimately leading to a more comprehensive picture of soil variability in the catchments. This integrated statistical analysis and spatial mapping approach contributes to a deeper comprehension of the complex relationship between electrical conductivity and soil properties.

6.4.4 Implications for forest management

Apparent electrical conductivity is frequently used in precision agriculture to define management blocks rather than treating a whole field homogenously. This was particularly successful in studies dealing with saltwater intrusion- where zones were formed based on EC_a and its relationship with $ECe^{1:5}$ to determine the optimal planting and treatment regimes in these zones (Bennett & George, 1995; Davies et al., 2015; Ding et al., 2020; Feikema & Baker, 2011; Hook et al., 2005; Huang et al., 2017b; Huang et al., 2015a; Huang et al., 2015b). Other users of electromagnetic induction technology used the relationship between crop growth and EC_a to define management zones that require specific treatments or to understand better the drivers behind the success of crop production in some areas of a field but not others (Caires et al., 2014; Gallart et al., 2019; Tang et al., 2020).

Precision forestry is not a new concept in New Zealand, with applications ranging from using unmanned vehicle technology for locating and spot-spraying wilding pine with pesticides (Greene et al., 2020) to using the same technology to improve fertiliser practices to reduce waste while targeting the specific trees/blocks of trees that require added nutrients (Smaill & Clinton, 2016). Given the increase in demand for timber products and the use of forest ecosystems for recreation, erosion mitigation, food and carbon sequestration (to name a few), it is important to meet the demand of those that use products derived from forests both now and in the future by increasing both the volume of wood production per area of land as well as using inputs such as fertiliser and pesticides more efficiently and precisely while engaging in sustainable forest management practices and maintaining the environmental services of forests (Clinton, 2018). Since forest soil is an

important driver of forest productivity, understanding the microsite variability of forest soils can help with sustainable forest management practices.

Understanding the heterogeneity of forest soils enables forest owners to make more informed decisions about land use, which is particularly important because of climate change-derived, extreme weather events. For example, knowing what parts of the land are prone to drought or water logging and plant species and genetic variations that are drought tolerant (Ismael et al., 2022) or tolerant towards diseases such as red needle cast (Dungey et al., 2014), understanding the success and failure of root propagation in nurseries (Lad et al., 2019) and the application of fertiliser and other nutrients on forested catchments to support growth (Smaill & Clinton, 2016) and understanding the drivers and mitigation strategies behind soil erosion and land stabilisation (Amatya et al., 2016; Bren, 2016; De Jong, 2016). In all these examples, understanding soil heterogeneity is a way in which management strategies can be put in place to tailor these land use regimes.

This study has found that apparent electrical conductivity, when inverted using 1-dimensional, laterally constrained inversion software and quasi-3D inversion software, can be used to understand microsite changes to soil in forested catchments; however, the relationships are complicated. The implications for forest managers considering using this technology to look at soil variables on their land should consider the following.

Firstly, the results of this thesis found that there was no one-to-one relationship between individual soil variables such as gravimetric water content, electrical conductivity of a 1-part soil to 5-part water solution and soil particle size and modelled electrical conductivity at three different depths. This is not unusual, and most users of EMI technology have similar findings (Hedley et al., 2004; Huang et al., 2017e; Monteiro Santos et al., 2010; Triantafilis & Monteiro Santos, 2013). This is because soil variables have complex interactions with one another *in situ*. When using EMI to understand soil spatial heterogeneity at the catchment scale, these variables should not be considered in isolation.

Taking soil samples to validate EC_a and EC^m will always be required as the EC_a as the influencing factor on EC_a differs. Therefore, results from one catchment should not be used to analyse soil properties or establish management practices in another; however, they could be used as a guide. While soil sampling is still required, the frequency and density are reduced as sample locations can be targeted based on antecedent EMI field campaigns. While soil sampling and lab analysis are time-consuming and expensive, measuring a range of soil variables can help understand soils' complex relationship with EC_a and identify variables that dominate the signal.

While the statistical analysis guided an understanding of which soil variables had strong relationships with EC_a and that no one variable in this study was able to explain variability in EC_a, the 3D quasi-inversion maps showing the spatial distribution of modelled EC^m were more effective at establishing spatial patterns within catchments. Overlaying these maps on raster datasets such as hill shades, digital elevation models, and base maps helped to validate that the patterns occurring in the 3D and 1D maps were artefacts of the smoothing process or if there are visible links to topography or the landscape. Overlaying the raw soil variable data as points of varying sizes was a time-efficient way of determining which variable may have influenced EC_a and EC^m within different regions of each catchment. The latter exercise is purely observational and not statistically robust. For future studies, spatial patterns could be classified, and additional statistical analysis carried out to determine if there is a true relationship.

This study has found that using electromagnetic induction technology is a time and cost-effective approach to measuring soil heterogeneity. The methods established in this study were repeatable, non-destructive, can be conducted at the course and satisfactory resolutions and can act as an ongoing resource that can be added to and refined as well as used in conjunction with geospatial software and technology to gain an understanding between the complex interaction of soil apparent electrical conductivity, soil variables and topographic features.

6.4.5 Implications for future studies

Despite being an essential factor in forest soils, this study did not measure soil organic matter due to time and cost restraints. While studies have found, at best, a weak relationship between EC_a and soil organic matter, these studies were not in planted forests. So, measuring this property would be useful to understand if variability in EC_a is affected by soil organic matter or carbon.

Cation exchange capacity was also not measured, but particle fraction analysis was. While the particle fraction analysis measures the particle distribution, it does not shed light on the particles' chemical makeup. While clay particles are classed as those under < 0.002mm, the parent material they are derived from and the weathering, leaching and translocation in clay soils mean their electrical conductivity differs depending on these circumstances. For example, smectite clays have a higher charge than kaolinite due to their plate-like structure, which comes from their parent material, which is often biotite (Allbrook, 1993; McLaren & Cameron, 1996). Measuring cation exchange capacity could help distinguish if EC_a variability is affected by clay content or if the clay content's water-holding capacity allows gravimetric water content to increase, which also has a strong relationship with EC_a.

This study identified the importance of identifying forests on a catchment scale as heterogeneous units, not one homogenous unit. In future studies, stratifying catchments into management zones to answer a specific question or solve a particular problem, for example, identifying areas of high or low moisture content or specific soil texture to define management zones to ensure planting and fertiliser regimes are effective based on soil characteristics both before planting and during the growth period of a harvestable stand.

While the generalised linear mixed effects model was suitable for this study, using a different statistical analysis method incorporating the interaction effect of all soil variables, dealing with multicollinearity issues and removing unnecessary predictors would be helpful. Ridge or lasso regression or principal components analysis are some statistical tests other authors have used or recommended.

References

Abdu, H., Robinson, D., & Jones, S.B. (2007). Comparing bulk soil electrical conductivity determination using the DUALEM-1S and EM38-DD electromagnetic induction instruments. Soil Science Society of America Journal, 71(1), 189-196.

Acharya, B.S., Stebler, E., & Zou, C.B. (2017). Monitoring litter interception of rainfall using leaf wetness sensor under controlled and field conditions. Hydrological Processes, 31(1), 240-249.

Akaike, H. (1974). A new look at the statistical model identification. IEEE Transactions on Automatic Control, 19(6), 716-723. doi:10.1109/TAC.1974.1100705

Allaire, S.E., Roulier, S., & Cessna, A.J. (2009). Quantifying preferential flow in soils: A review of different techniques. Journal of Hydrology, 378(1), 179-204. doi:https://doi.org/10.1016/j.jhydrol.2009.08.013

Allbrook, R.F. (1993). Shrinkage of some New Zealand soils and its implications for soil physics. Australian journal of soil research, 31(2), 111-118. doi:10.1071/SR9930111

Altdorff, D., von Hebel, C., Borchard, N., van der Kruk, J., Bogena, H.R., Vereecken, H., & Huisman, J.A. (2017). Potential of catchment-wide soil water content prediction using electromagnetic induction in a forest ecosystem. Environmental earth sciences, 76(3), 1. doi:10.1007/s12665-016-6361-3

Alvalá, R.C.S., Gielow, R., da Rocha, H.R., Freitas, H.C., Lopes, J.M., Manzi, A.O., von Randow, C., Dias, M.A.F.S., Cabral, O.M.R., & Waterloo, M.J. (2002). Intradiurnal and seasonal variability of soil temperature, heat flux, soil moisture content, and thermal properties under forest and pasture in Rondônia. Journal of Geophysical Research: Atmospheres, 107(D20), LBA 10-11-LBA 10-20. doi:https://doi.org/10.1029/2001JD000599

Amatya, D.M.E., Williams, T.M.E., Bren, L.E., & de Jong, C.E. (2016). Forest hydrology: processes, management and assessment. Boston, MA: CABI International.

André, F., Jonard, M., & Lambot, S. (2015). Non-Invasive Forest Litter Characterization Using Full-Wave Inversion of Microwave Radar Data. IEEE Transactions on Geoscience and Remote Sensing, 53(2), 828-840. doi:10.1109/TGRS.2014.2328776

Atwell, M., Wuddivira, M., Gobin, J., & Robinson, D. (2013). Edaphic Controls on Sedge Invasion in a Tropical Wetland Assessed with Electromagnetic Induction. Soil Science Society of America Journal, 77(5), 1865-1874. doi:https://doi.org/10.2136/sssaj2013.04.0138

Atwell, M.A., & Wuddivira, M.N. (2019). Electromagnetic-induction and spatial analysis for assessing variability in soil properties as a function of land use in tropical savanna ecosystems. SN Applied Sciences, 1(8), 856. doi:10.1007/s42452-019-0902-9

Aubertin, G.M. (1971). Nature and extent of macropores in forest soils and their influence on subsurface water movement. Research Paper. (NE-192). Upper Darby, PA: U.S. Department of Agriculture, Forest Service, Northeastern Forest Experiment Station.

Bai, W., Kong, L.-W., & Guo, A. (2013). Effects of physical properties on electrical conductivity of compacted lateritic soil. Journal of Rock Mechanics and Geotechnical Engineering, 5, 406–411. doi:10.1016/j.jrmge.2013.07.003

Ballance, P.F. (1976). Stratigraphy and bibliography of the Waitemata Group of Auckland, New Zealand. New Zealand Journal of Geology and Geophysics, 19(6), 897-932. doi:10.1080/00288306.1976.10420746

Balneaves, J., & De La Mare, P. (1989). Root patterns of Pinus radiata on five ripping treatments in a Canterbury forest. New Zealand Journal of Forestry Science, 19(1), 29-40.

Barton, K. (2023). Multi-Model Inference (Version 1.47.5) [User guide for R studio]. CRAN.

Bates, D., Mächler, M., Bolker, B., & Walker, S. (2014). Fitting Linear Mixed-Effects Models Using lme4. Journal of Statistical Software, 67(1), 1 - 48. doi:10.18637/jss.v067.i01

Bathurst, J.J. (2014). Comment on “A paradigm shift in understanding and quantifying the effects of forest harvesting on floods in snow environments” by Kim C. Green and Younes Alila. Water Resources Research, 50(3), 2765-2768. doi:https://doi.org/10.1002/2013WR013586
Bats, M., De Smedt, P., Antrop, M., Bourgeois, J., Court-Picon, M., De Maeyer, P., Finke, P., Meirvenne, M., Verniers, J., Werbrouck, I., & Crombé, P. (2009). Geoarchaeological research of the large palaeolake of the Moervaart (municipalities of Wachtebeke and Moerbeke-Waas, East Flanders, Belgium) From Late Glacial to Early Holocene. Notae Praehistoricae, 29.
Beltrami, H., & Kellman, L. (2003). An examination of short- and long-term air–ground temperature coupling. Global and Planetary Change, 38(3), 291-303. doi:https://doi.org/10.1016/S0921-8181(03)00112-7
Bennett, D.L., & George, R.J. (1995). Using the EM38 to measure the effect of soil salinity on Eucalyptus globulus in South-Western Australia. Agricultural Water Management, 27(1), 69-85. doi:https://doi.org/10.1016/0378-3774(95)91232-V
Blakemore, L.C., Searle, P.L., & Daly, B.K. (1981). Methods for chemical analysis of soils. Retrieved from Lower Hutt, N.Z.: https://doi.org/10.7931/DL1-SBSR-10A
Blume, T., Zehe, E., & Bronstert, A. (2009). Use of soil moisture dynamics and patterns at different spatio-temporal scales for the investigation of subsurface flow processes. Hydrol. Earth Syst. Sci., 13(7), 1215-1233. doi:10.5194/hess-13-1215-2009
Bonakdari, H., & Zeynoddin, M. (2022). Goodness-of-fit & precision criteria. In H. Bonakdari & M. Zeynoddin (Eds.), Stochastic Modeling (pp. 187-264): Elsevier.
Bottega, E., Safanelli, J., Zeraatpisheh, M., Amado, T., Queiroz, D., & Oliveira, Z. (2022). Site-Specific Management Zones Delineation Based on Apparent Soil Electrical Conductivity in Two Contrasting Fields of Southern Brazil. Agronomy, 12, 1390. doi:10.3390/agronomy12061390
Brandon, K. (2014). Forests and Natural Disasters. Retrieved from http://www.jstor.org/stable/resrep29725.9
Bréchet, L., Oatham, M., Wuddivira, M., & Robinson, D.A. (2012). Determining Spatial Variation in Soil Properties in Teak and Native Tropical Forest Plots Using Electromagnetic Induction. Vadose zone journal, 11(4), vzj2011.0102. doi:https://doi.org/10.2136/vzj2011.0102
Bren, L. (2016). An Introduction to Forest Hydrology. In D. M. Amataya, T. M. Williams, L. Bren, & C. De Jong (Eds.), Forest Hydrology: Processes, Management and Assessment: CABI International.
Brevik, E.C., Fenton, T.E., & Lazari, A. (2006). Soil Electrical Conductivity as a Function of Soil Water Content and Implications for Soil Mapping. Precision Agriculture, 7(6), 393-404. doi:10.1007/s11119-006-9021-x
Buckland, H.M., Saxby, J., Roche, M., Meredith, P., Rust, A.C., Cashman, K.V., & Engwell, S.L. (2021). Measuring the size of non-spherical particles and the implications for grain size analysis in volcanology. Journal of volcanology and geothermal research, 415, 107257. doi:10.1016/j.jvolgeores.2021.107257
Caires, S.A.D., Wuddivira, M.N., & Bekele, I. (2014). Assessing the temporal stability of spatial patterns of soil apparent electrical conductivity using geophysical methods. In International Agrophysics (Vol. 28, pp. 423).
Callegary, J., Ferré, T., & Groom, R. (2007). Vertical Spatial Sensitivity and Exploration Depth of Low-Induction-Number Electromagnetic-Induction Instruments. Vadose zone journal, 6, 158-167. doi:10.2136/vzj2006.0120
Chappell, P.R. (2013a). The Climate and Weather of Auckland. Retrieved from Auckland:
Chappell, P.R. (2013b). The Climate and Weather of Northland (59). Retrieved from
Clinton, P., & Owens, J. (2023). Structure and function of forested soils☆. In Reference Module in Earth Systems and Environmental Sciences: Elsevier.
Clinton, P.W. (2018). Future expectations of forest soils: increasing productivity within environmental limits using new knowledge. New Zealand Journal of Agricultural Research, 61(3), 389-401. doi:10.1080/00288233.2018.1446992

Colazo, J.C., & Buschiazzo, D. (2015). The impact of agriculture on soil texture due to wind erosion. Land Degradation & Development, 26(1), 62-70.
Conrad, O., Bechtel, B., Bock, M., Dietrich, H., Fischer, E., Gerlitz, L., Wehberg, J., Wichmann, V., & Böhner, J. (2015). System for Automated Geoscientific Analyses (SAGA) v. 2.1.4. Geosci. Model Dev., 8(7), 1991-2007. doi:10.5194/gmd-8-1991-2015
Dabas, M., Anest, A., Thiesson, J., & Tabbagh, A. (2016). Slingram EMI Devices for Characterizing Resistive Features Using Apparent Conductivity Measurements: check of the DualEM-421S Instrument and Field Tests. Archaeological prospection, 23(3), 165-180. doi:https://doi.org/10.1002/arp.1535
Dal Bo, I., Klotzsche, A., Bol, R., Moradi, G., Weihermüller, L., Vereecken, H., & van der Kruk, J. (2021). GPR and EMI Characterization of the Hyperarid Study Site of Yungay, Chile: Implications of Applying Geophysical Methods on Mars. Earth and Space Science, 8(12), e2021EA001790. doi:https://doi.org/10.1029/2021EA001790
Davies, G., Huang, J., Monteiro Santos, F.A., & Triantafilis, J. (2015). Modelling Coastal Salinity in Quasi 2D and 3D Using a DUALEM-421 and Inversion Software. Groundwater, 53(3), 424-431. doi:https://doi.org/10.1111/gwat.12231
De Jong, C. (2016). European Perspectives on Forest Hydrology. In D. M. Amataya, T. M. Williams, L. Bren, & C. De Jong (Eds.), Forest Hydrology: Processes, Management and Assessment (pp. 69-87). CABI International.
De Smedt, P., Van Meirvenne, M., Meerschman, E., Saey, T., Bats, M., Court-Picon, M., De Reu, J., Zwertvaegher, A., Antrop, M., Bourgeois, J., De Maeyer, P., Finke, P.A., Verniers, J., & Crombé, P. (2011). Reconstructing paleochannel morphology with a mobile multi-coil electromagnetic induction sensor. Geomorphology, 130(3), 136-141. doi:https://doi.org/10.1016/j.geomorph.2011.03.009
Delefortrie, S., De Smedt, P., Saey, T., Van De Vijver, E., & Van Meirvenne, M. (2014). An efficient calibration procedure for correction of drift in EMI survey data. Journal of Applied Geophysics, 110, 115-125. doi:10.1016/j.jappgeo.2014.09.004
Delignette-Muller, M.L., & Dutang, C. (2015). fitdistrplus: An R Package for Fitting Distributions. Journal of Statistical Software, 64(4), 1 - 34. doi:10.18637/jss.v064.i04
Ding, J., Yang, S., Shi, Q., Wei, Y., & Wang, F. (2020). Using Apparent Electrical Conductivity as Indicator for Investigating Potential Spatial Variation of Soil Salinity across Seven Oases along Tarim River in Southern Xinjiang, China. Remote Sensing, 12(16), 2601. Retrieved from https://www.mdpi.com/2072-4292/12/16/2601
DualEm. (2014). DualEm-1 User's Manual. Retrieved from Canada:
DualEm. (n.d). Analysis of Conductive Layering by Electromagnetic (EM) Vertical Sounding. Retrieved from https://dualem.com/documents/vertical-sounding/
DualEm. (n.d.). EM Induction. Retrieved from https://dualem.com/documents/em-induction/#:~:text=(DUALEM%20instruments%20are%20sensitive%20only,9%2DkHz%20DUALEM%20frequency.)
Dungey, H.S., Williams, N.M., Low, C.B., & Stovold, G.T. (2014). First evidence of genetic-based tolerance to red needle cast caused by Phytophthora pluvialis in radiata pine. New Zealand Journal of Forestry Science, 44(1), 31. doi:10.1186/s40490-014-0028-1
El-Naggar, A., Hedley, C., Roudier, P., Horne, D., & Clothier, B. (2021a). Imaging the electrical conductivity of the soil profile and its relationships to soil water patterns and drainage characteristics. Precision Agriculture, 22(4), 1045-1066.
El-Naggar, A., Hedley, C.B., Dj, H., Roudier, P., & Clothier, B. (2017). Using electrical conductivity imaging to estimate soil water content. Paper presented at the FLRC Workshop, Massey University, Palmerston North, New Zealand.
El-Naggar, A., Hedley, C.B., Roudier, P., Horne, D., & Clothier, B. (2021b). Imaging the electrical conductivity of the soil profile and its relationships to soil water patterns and drainage characteristics. Precision Agriculture, 22, 1-22. doi:10.1007/s11119-020-09763-x

Ellis, J.C., & Hayes, J.D. (1997). Field guide for sample plots in New Zealand forests: New Zealand Forest Research Institute.
EMTOMO LDA. (2018). EM4Soil A program for 1-D laterally constrained inversion of EM data. Italy.
Esri Inc. (2023). ArcGIS Pro (Version 3.1.0). United States of America.
Ewell, C.M. (2006). Methods and modelling equations to quantify the litter layer of coniferous forests in California national forests. (Master of Science). Humboldt State University,
Farooque, A., Zare, M., Zaman, Q., Abbas, F., Bos, M., Esau, T., Acharya, B., & Schumann, A. (2019). Evaluation of DualEM-II sensor for soil moisture content estimation in the potato fields of Atlantic Canada. Plant, Soil and Environment, 65(6), 290-297.
Farooque, A.A., Khan, F.S., Zaman, Q.U., Easu, T.J., & Schumann, A.W. (2020). Estimation of water table depth using DUALEM-2 system. Computers and Electronics in Agriculture, 169, 105227. doi:https://doi.org/10.1016/j.compag.2020.105227
Fatma, K., Yacine, D., Haydar, B., Ahmed, Y., Mohammed, D., Karim, H., & Abdelatif, B. (2020). Use of electrical resistivity tomography (ERT) and electromagnetic induction (EMI) methods to Characterize Karst Hazards in North-Eastern of Algeria. Arabian journal of geosciences, 13(22). doi:10.1007/s12517-020-06206-9
Feikema, P.M., & Baker, T.G. (2011). Effect of soil salinity on growth of irrigated plantation Eucalyptus in south-eastern Australia. Agricultural Water Management, 98(7), 1180-1188. doi:https://doi.org/10.1016/j.agwat.2011.03.005
Fox, J., & Weisberg, S. (2011). An R Companion to Applied Regression: SAGE Publications.
Fox, J., & Weisberg, S. (2019). An R Companion to Applied Regression (3 ed.). Thousand Oaks, CA: Sage.
Fryrear, D.W. (1985). Soil cover and wind erosion. Transactions of the ASAE, 28(3), 781-0784.
Gallart, M., Love, J., Meason, D.F., Coker, G., Clinton, P.W., Xue, J., Jameson, P.E., Klápště, J., & Turnbull, M.H. (2019). Field-scale variability in site conditions explain phenotypic plasticity in response to nitrogen source in Pinus radiata D. Don. Plant and Soil, 443(1), 353-368. doi:10.1007/s11104-019-04237-0
Greene, T.C., Sprague, R., De Schutter, A., Raal, P., Schurink, C., Briden, K., & Earl, R. (2020). Use of Aerial Remote Sensing to Detect Pre-Coning Wilding Conifers in a Dry Grassland Environment (D. o. Conservation Ed.). Wellington, New Zealand: New Zealand Department of Conservation.
Groenendijk, F.M., Condron, L.M., & Rijkse, W.C. (2002). Effects of afforestation on organic carbon, nitrogen and sulfur concentrations in New Zealand hill country soils. Geoderma, 108(1), 91-100. doi:https://doi.org/10.1016/S0016-7061(02)00125-8
Hanks, R.J. (1992). Applied soil physics: soil water and temperature applications (Second edition. ed.). New York: Springer Science + Business Media, LLC.
Hanson, B.R., & Kaita, K. (1997). Response of Electromagnetic Conductivity Meter to Soil Salinity and Soil-Water Content. Journal of Irrigation and Drainage Engineering, 123(2), 141-143. doi:doi:10.1061/(ASCE)0733-9437(1997)123:2(141)
Haverd, V., & Cuntz, M. (2010). Soil–Litter–Iso: A one-dimensional model for coupled transport of heat, water and stable isotopes in soil with a litter layer and root extraction. Journal of Hydrology, 388(3), 438-455. doi:https://doi.org/10.1016/j.jhydrol.2010.05.029
Hayward, B.W., & Smale, D. (1992). Heavy minerals and the provenance history of Waitemata Basin sediments (early Miocene, Northland, New Zealand). New Zealand Journal of Geology & Geophysics, 35(2), 223-242. doi:10.1080/00288306.1992.9514516
He, J., Wang, Q., Li, H., Tullberg, J.N., McHugh, A.D., Bai, Y., Zhang, X., McLaughlin, N., & Gao, H. (2009). Soil physical properties and infiltration after long-term no-tillage and ploughing on the Chinese Loess Plateau. New Zealand Journal of Crop and Horticultural Science, 37(3), 157-166. doi:10.1080/01140670909510261

Hedley, C.B., Yule, I.J., Eastwood, C.R., Shepherd, T.G., & Arnold, G. (2004). Rapid identification of soil textural and management zones using electromagnetic induction sensing of soils. Australian journal of soil research, 42(4), 389-400. doi:10.1071/SR03149

Heil, K., & Schmidhalter, U. (2017). The Application of EM38: Determination of Soil Parameters, Selection of Soil Sampling Points and Use in Agriculture and Archaeology. Sensors (Basel, Switzerland), 17(11), 2540. doi:10.3390/s17112540

Henderson, R., & McMahon, T. (2001). Experimental Design and Initial Results from the Mahurangi River Variability Experiment: MARVEX. In V. Lakshmi, J. Albertson, & J. Schaake (Eds.), Land Surface Hydrology, Meteorology, and Climate: Observations and Modeling (1 ed., pp. 201-213): Wiley.

Hewitt, A.E., Balks, M.R., & Lowe, D.J. (2021). The Soils of Aotearoa New Zealand. Cham: Springer International Publishing AG.

Hook, W., Ferré, T., & Livingston, N. (2005). The Effects of Salinity on the Accuracy and Uncertainty of Water Content Measurement. Soil Science Society of America Journal - SSSAJ, 69. doi:10.2136/sssaj2005.0931a

Hossain, M.B., Lamb, D.W., Lockwood, P.V., & Frazier, P. (2010). EM38 for volumetric soil water content estimation in the root-zone of deep vertosol soils. Computers and Electronics in Agriculture, 74(1), 100-109. doi:https://doi.org/10.1016/j.compag.2010.07.003

Huang, H., Won, I.J., & San Filipo, B. (2003). Detecting buried nonmetal objects using soil magnetic susceptibility measurements (Vol. 5089): SPIE.

Huang, J., Kilminster, T., Barrett-Lennard, E.G., & Triantafilis, J. (2017a). Characterization of field-scale dryland salinity with depth by quasi-3d inversion of DUALEM-1 data. Soil Use and Management, 33(2), 205-215. doi:https://doi.org/10.1111/sum.12345

Huang, J., Koganti, T., Santos, F.A.M., & Triantafilis, J. (2017b). Mapping soil salinity and a fresh-water intrusion in three-dimensions using a quasi-3d joint-inversion of DUALEM-421S and EM34 data. Science of The Total Environment, 577, 395-404. doi:https://doi.org/10.1016/j.scitotenv.2016.10.224

Huang, J., Minasny, B., Whelan, B.M., McBratney, A.B., & Triantafilis, J. (2017c). Temperature-dependent hysteresis effects on EM induction instruments: An example of single-frequency multi-coil array instruments. Computers and Electronics in Agriculture, 132, 76-85. doi:https://doi.org/10.1016/j.compag.2016.11.013

Huang, J., Mokhtari, A.R., Cohen, D.R., Monteiro Santos, F.A., & Triantafilis, J. (2015a). Modelling soil salinity across a gilgai landscape by inversion of EM38 and EM31 data. European Journal of Soil Science, 66(5), 951-960. doi:https://doi.org/10.1111/ejss.12278

Huang, J., Pedrera-Parrilla, A., Vanderlinden, K., Taguas, E.V., Gómez, J.A., & Triantafilis, J. (2017d). Potential to map depth-specific soil organic matter content across an olive grove using quasi-2d and quasi-3d inversion of DUALEM-21 data. CATENA, 152, 207-217. doi:https://doi.org/10.1016/j.catena.2017.01.017

Huang, J., Scudiero, E., Clary, W., Corwin, D.L., & Triantafilis, J. (2017e). Time-lapse monitoring of soil water content using electromagnetic conductivity imaging. Soil Use and Management, 33(2), 191-204. doi:https://doi.org/10.1111/sum.12261

Huang, J., Taghizadeh-Mehrjardi, R., Minasny, B., & Triantafilis, J. (2015b). Modeling Soil Salinity along a Hillslope in Iran by Inversion of EM38 Data. Soil Science Society of America Journal, 79(4), 1142-1153. doi:https://doi.org/10.2136/sssaj2014.11.0447

Huggins, D.R., & Uberuaga, D.P. (2010). Field Heterogeneity of Soil Organic Carbon and Relationships to Soil Properties and Terrain Attributes. Retrieved from Puyallup, WA:

Intergovernmental Panel on Climate Change. (2000). Land use, land-use change and forestry: a special report of the Intergovernmental Panel on Climate Change. United Kingdom: Cambridge University Press.

Ismael, A., Xue, J., Meason, D.F., Klápště, J., Gallart, M., Li, Y., Bellè, P., Gomez-Gallego, M., Bradford, K.-T., & Telfer, E. (2022). Genetic variation in drought-tolerance traits and their relationships to growth in Pinus radiata D. Don under water stress. Frontiers in Plant Science, 12, 766803.
Jenny, H.A. (1941). Factors of soil formation. A system of quantitative pedology. New York: Dover Publications, Inc.
Jones, J.A.A. (2010). Soil piping and catchment response. Hydrological Processes, 24(12), 1548-1566. doi:https://doi.org/10.1002/hyp.7634
Joschko, M., Gebbers, R., Barkusky, D., Rogasik, J., Höhn, W., Hierold, W., Fox, C.A., & Timmer, J. (2009). Location-dependency of earthworm response to reduced tillage on sandy soil. Soil and Tillage Research, 102(1), 55-66. doi:https://doi.org/10.1016/j.still.2008.07.023
Joschko, M., Gebbers, R., Barkusky, D., & Timmer, J. (2010). The apparent electrical conductivity as a surrogate variable for predicting earthworm abundances in tilled soils. Journal of Plant Nutrition and Soil Science, 173(4), 584-590. doi:https://doi.org/10.1002/jpln.200800071
Kang, S., Cockett, R., Heagy, L.J., & Oldenburg, D.W. (2015). Moving between dimensions in electromagnetic inversions. In SEG Technical Program Expanded Abstracts 2015 (pp. 5000-5004): Society of Exploration Geophysicists.
Khongnawang, T., Zare, E., Srihabun, P., Khunthong, I., & Triantafilis, J. (2022). Digital soil mapping of soil salinity using EM38 and quasi-3d modelling software (EM4Soil). Soil Use and Management, 38(1), 277-291. doi:10.1111/sum.12778
Khongnawang, T., Zare, E., Zhao, D., Srihabun, P., & Triantafilis, J. (2019). Three-Dimensional Mapping of Clay and Cation Exchange Capacity of Sandy and Infertile Soil Using EM38 and Inversion Software. Sensors (Basel), 19(18). doi:10.3390/s19183936
Kinal, J., Stoneman, G.L., & Williams, M.R. (2006). Calibrating and using an EM31 electromagnetic induction meter to estimate and map soil salinity in the Jarrah and Karri forests of South-Western Australia. Forest Ecology and Management, 233(1), 78-84. doi:https://doi.org/10.1016/j.foreco.2006.06.003
Krishna, M.P., & Mohan, M. (2017). Litter decomposition in forest ecosystems: a review. Energy, Ecology and Environment, 2(4), 236-249. doi:10.1007/s40974-017-0064-9
Lad, P., Meason, D.F., Wade, A., & Evanson, T. (2019). Electromagnetic survey of Te Ngae Nursery soil physical properties. Retrieved from Rotorua, New Zealand:
Landcare Research Ltd. S-Map Online; Glossary. Retrieved from https://smap.landcareresearch.co.nz/support/glossary/
Landcare Research Ltd. (2000). Fundamental Soil Layer - New Zealand Classification. FSL New Zealand Soil Classification v1.0. Retrieved from https://lris.scinfo.org.nz/layer/48079-fsl-new-zealand-soil-classification-v10/metadata/
Lardo, E., Coll, P., Xiloyannis, C., Le Cadre, E., Palese, A., Villenave, C., & Celano, G. (2012). Electromagnetic induction (EMI) measurements as a proxy of earthworm presence in Southern French vineyards. Applied Soil Ecology, 61, 76. doi:10.1016/j.apsoil.2012.06.003
Lê, S., Josse J., & F., H. (2010). FactoMineR: A Package for Multivariate Analysis. Journal of Statistical Software, 25(1), 1-18. doi: doi:10.18637/jss.v025.i01
Lee, Y., & Nelder, J.A. (2001). Hierarchical Generalised Linear Models: A Synthesis of Generalised Linear Models, Random-Effect Models and Structured Dispersions. Biometrika, 88(4), 987-1006. Retrieved from http://www.jstor.org/stable/2673697
Lemmon, T., & Wetherbee, L. (2005). TRIMBLE® INTEGRATED SURVEYING™ TECHNIQUES. White Paper, 1-7.
Li, X., Niu, J., & Xie, B. (2014). The effect of leaf litter cover on surface runoff and Soil Erosion in Northern China. PloS one, 9(9), e107789. doi:10.1371/journal.pone.0107789
Liu, X., Feng, Y., Liu, P., Zhang, Q., Njoroge, B., Zhou, Q., Gan, X., Zhang, W., & Li, Y. (2022). Soil moisture dominated the temporal dynamics of litter moisture content in subtropical forests: a 7-year observation in south China. Journal of Hydrology: Regional Studies, 41, 101102. doi:https://doi.org/10.1016/j.ejrh.2022.101102

Lyles, L. (1975). Possible effects of wind erosion on soil productivity. Journal of soil and water conservation, 30(6), 279-283.
Lynn, I., Manderson, A., Page, M., Harmsworth, G., Eyles, G., Douglas, G., Mackay, A., & Newsome, P. (2009). Land use capability survey handbook (3rd ed.): AgResearch Ltd, Hamilton; Landcare Research New Zealand Ltd, Lincoln; Institute of Geological and Nuclear Sciences Ltd, Lower Hutt.
Manaaki Whenua - Landcare Research. (2019). S-map - New Zealand's national digital soil map. Retrieved from https://smap.landcareresearch.co.nz/
Manaaki Whenua - Landcare Research. (2023). The New Zealand SoilsMapViewer. Retrieved from https://soils-maps.landcareresearch.co.nz/?layername=fsl_nzsc&idcolumn=&idvalue=&mapfile=fsl&srs=EPSG:2193&mode=normal#maps
Manaaki Whenua - Landcare Research. (n.d). Soil Testing. Retrieved from https://www.landcareresearch.co.nz/partner-with-us/laboratories-and-diagnostics/environmental-chemistry-laboratory/soil-testing/#s110
Manderson, A., Palmer, A., Mackay, A., Wilde, H., & Rijkse, W. (2007). Introductory guide to farm soil mapping. AgResearch, Palmerston North.
Marden, M., Rowan, D., & Lambie, S. (2016). Root development and whole-tree allometry of juvenile trees of five seed lots of Pinus radiata D.Don: implications for forest establishment on erosion-prone terrain, East Coast region, North Island, New Zealand. New Zealand Journal of Forestry Science, 46(1), 24. doi:10.1186/s40490-016-0082-y
Mari, L. (2020). An Introduction to Soil Resistivity. Retrieved from https://eepower.com/technical-articles/an-introduction-to-soil-resistivity/#
Martindale, M., Hicks, D., Singleton, P. (2018). Soil information inventory: Mahurangi and related soils. Retrieved from Auckland, New Zealand:
Martinez, G., Huang, J., Vanderlinden, K., Giráldez, J.V., & Triantafilis, J. (2018). Potential to predict depth-specific soil–water content beneath an olive tree using electromagnetic conductivity imaging. Soil Use and Management, 34(2), 236-248. doi:https://doi.org/10.1111/sum.12411
Martinez, G., Vanderlinden, K., Ordóñez, R., & Muriel, J.L. (2009). Can Apparent Electrical Conductivity Improve the Spatial Characterization of Soil Organic Carbon? Vadose zone journal, 8(3), 586-593. doi:https://doi.org/10.2136/vzj2008.0123
Mat Su, A.S., & Adamchuk, V.I. (2023). Temporal and operation-induced instability of apparent soil electrical conductivity measurements. Frontiers in Soil Science, 3. doi:10.3389/fsoil.2023.1137731
McBratney, A., Minasny, B., & Whelan, B. (2005). Obtaining 'Useful' High-resolution Soil Data from Proximally-Sensed Electrical Conductivity/Resistivity (PSEC/R) Surveys. Paper presented at the 5th European Conference on Precision Agriculture, Uppsala, Sweden.
McDonnell, J.J. (2009). Hewlett, J.D. and Hibbert, A.R. 1967: Factors affecting the response of small watersheds to precipitation in humid areas. In Sopper, W.E. and Lull, H.W., editors, Forest hydrology, New York: Pergamon Press, 275—90. Progress in Physical Geography: Earth and Environment, 33(2), 288-293. doi:10.1177/0309133309338118
McGlynn, B.L., McDonnell, J.J., & Brammer, D.D. (2002). review of the evolving perceptual model of hillslope flowpaths at the Maimai catchments, New Zealand. Journal of hydrology (Amsterdam), 257(1/4), 1-26. doi:10.1016/S0022-1694(01)00559-5
McIsaac, G. (2010). Time Domain Reflectometry Measurement of Water Content and Electrical Conductivity Using a Polyolefin Coated TDR Probe. (Master of Environmental Studies in Geography). University of Waterloo, Waterloo, Ontario, Canada. Retrieved from http://hdl.handle.net/10012/5213
McLaren, R.G., & Cameron, K.C. (1996). Soil science: Sustainable production and environmental protection (2nd. ed. ed.). Auckland: Oxford University Press.

McNeill, J.D. (1980). Electromagnetic Terrain Conductivity Measurement at Low Induction Numbers. Retrieved from Ontario, Canada:
Meason, D.F. (2023). Forest Flows. Retrieved from https://www.forestflows.nz/
Mester, A., Zimmermann, E., Van der Kruk, J., Vereecken, H., & Van Waasen, S. (2014). Development and drift-analysis of a modular electromagnetic induction system for shallow ground conductivity measurements. Measurement science & technology, 25(5), 55801. doi:10.1088/0957-0233/25/5/055801
Meter Group. (n.d.). Soil Moisture Sensors - How they work. Why some are not research-grade. Retrieved from https://www.metergroup.com/en/meter-environment/measurement-insights/tdr-fdr-capacitance-compared
Microtrac, M. (2020). CAMSIZER X2-Particle Size & Shape Analyzer-Microtrac [WWW Document]. Retrieved from
Milne, J.D.G., Clayden, B., Singleton, P.L., & Wilson, A.D. (1995). Soil description handbook revised edition. Christchurch, New Zealand: Manaaki Whenua Press.
Monteiro Santos, F.A., Triantafilis, J., Bruzgulis, K.E., & Roe, J.A.E. (2010). Inversion of multiconfiguration electromagnetic (DUAEMm-421) profiling data using a one-dimensional laterally constrained algorithm. Vadose zone journal, 9(1), 117-125. doi:10.2136/vzj2009.0088
Mosley, M.P. (1979). Streamflow generation in a forested watershed, New Zealand. Water Resources Research, 15(4), 795-806. doi:10.1029/WR015i004p00795
Murphy, P.N.C., Ogilvie, J., & Arp, P. (2009). Topographic modelling of soil moisture conditions: a comparison and verification of two models. European Journal of Soil Science, 60(1), 94-109. doi:10.1111/j.1365-2389.2008.01094.x
Neary, D.G., Ice, G.G., & Jackson, C.R. (2009). Linkages between forest soils and water quality and quantity. Forest Ecology and Management, 258(10), 2269-2281. doi:https://doi.org/10.1016/j.foreco.2009.05.027
Neeraj, K., & Chandra, M. (2021). Basics of Clay Minerals and Their Characteristic Properties. In N. Gustavo Morari Do (Ed.), Clay and Clay Minerals (pp. Ch. 2). Rijeka: IntechOpen.
O'Brien, R.M. (2007). A caution regarding rules of thumb for variance inflation factors. Quality & quantity, 41(5), 673-690. doi:10.1007/s11135-006-9018-6
Ogée, J., & Brunet, Y. (2002). A forest floor model for heat and moisture including a litter layer. Journal of Hydrology, 255(1), 212-233. doi:https://doi.org/10.1016/S0022-1694(01)00515-7
Ogilvy, R.D., Cuadra, A., Jackson, P.D., & Cuellar, V. (1991). Delineation of a resistive drainage channel by EM conductivity survey. Geoexploration, 28(2), 139-152. doi:https://doi.org/10.1016/0016-7142(91)90045-E
Palacky, G. (1988). Resistivity characteristics of geologic targets. Electromagnetic methods in applied geophysics, 1, 52-129.
Park, H.-T., Hattori, S., & Tanaka, T. (1998). Development of a numerical model for evaluating the effect of litter layer on evaporation. Journal of Forest Research, 3, 25-33.
Phillips, C., Bloomberg, M., Marden, M., & Lambie, S. (2023). Tree root research in New Zealand: a retrospective 'review ' with emphasis on soil reinforcement for soil conservation and wind firmness. New Zealand Journal of Forestry Science, 53.
R Development Core Team. (2018). R: A language and environment for statistical computing. R Foundation for Statistical Computing. Vienna, Austria. Retrieved from https://www.r-project.org/
Rigby, B. (1985). A history of Aupouri State Forest. (Wai 46 M25, Ngati Awa - Eastern Bay of Plenty inquiry). Wellington, New Zealand: Waitangi Tribunal Retrieved from https://forms.justice.govt.nz/search/Documents/WT/wt_DOC_93920998/Wai%2046%2C%20M025.pdf
Rigby, B. (1998). The Crown, Maori and Mahurangi 1840-1881: A Historical Report Commissioned by the Waitangi Tribunal. Retrieved from Wellington, New Zealand:

Robinson, D.A., Lebron, I., Lesch, S.M., & Shouse, P. (2004). Minimizing drift in electrical conductivity measurements in high temperature environments using the EM-38. Soil Science Society of America Journal, 68(2), 339-345. doi:10.2136/sssaj2004.3390

Roe, J., Triantafilis, J., & Santos, F. (2010). Detecting a landfill leachate plume using a DUALEM-421 and a laterally constrained inversion model. Paper presented at the 2010 19th World Congress of Soil Science, Soil Solutions for a Changing World.

Ryland, R.C., Thompson, A., Sutter, L.A., & Markewitz, D. (2020). Mapping depth to the argillic horizon on historically farmed soil currently under forests. Geoderma, 369, 114291. doi:https://doi.org/10.1016/j.geoderma.2020.114291

Saey, T., Simpson, D., Vermeersch, H., Cockx, L., & Van Meirvenne, M. (2009). Comparing the EM38DD and DUALEM-21S sensors for depth-to-clay mapping. Soil Science Society of America Journal, 73(1), 7-12.

Salekin, S., Bloomberg, M., Morgenroth, J., Meason, D.F., & Mason, E.G. (2021a). Within-site drivers for soil nutrient variability in plantation forests: A case study from dry sub-humid New Zealand. CATENA, 200, 105149. doi:https://doi.org/10.1016/j.catena.2021.105149

Salekin, S., Mason, E.G., Morgenroth, J., Bloomberg, M., & Meason, D.F. (2019). Modelling the effect of microsite influences on the growth and survival of juvenile Eucalyptus globoidea (Blakely) and Eucalyptus bosistoana (F. Muell) in New Zealand. Forests, 10(10), 857.

Salekin, S., Mason, E.G., Morgenroth, J., Bloomberg, M., & Meason, D.F. (2021b). Hybrid height growth and survival model for juvenile Eucalyptus globoidea (Blakely) and E. bosistoana (F. Muell) in New Zealand. Forest Ecology and Management, 490, 119074. doi:https://doi.org/10.1016/j.foreco.2021.119074

Salomão, R.P., Pires, D.d.A., Baccaro, F.B., Schietti, J., Vaz-de-Mello, F.Z., Lima, A.P., & Magnusson, W.E. (2022). Water table level and soil texture are important drivers of dung beetle diversity in Amazonian lowland forests. Applied soil ecology : a section of Agriculture, ecosystems & environment, 170, 104260. doi:10.1016/j.apsoil.2021.104260

Santos, F.A.M., Triantafilis, J., Bruzgulis, K.E., & Roe, J.A.E. (2010). Inversion of Multiconfiguration Electromagnetic (DUALEM-421) Profiling Data Using a One-Dimensional Laterally Constrained Algorithm. Vadose zone journal, 9(1), 117-125. doi:https://doi.org/10.2136/vzj2009.0088

Sato, Y., Kumagai, T.o., Kume, A., Otsuki, K., & Ogawa, S. (2004). Experimental analysis of moisture dynamics of litter layers-the effects of rainfall conditions and leaf shapes. Hydrological Processes, 18(16), 3007-3018. doi:10.1002/hyp.5746

Schabenberger, O., & Pierce, F.J. (2001). Contemporary statistical models for the plant and soil sciences. United States: CRC Press.

Schofield, J.C. (1970). Coastal sands of Northland and Auckland. New Zealand Journal of Geology and Geophysics, 13(3), 767-824. doi:10.1080/00288306.1970.10431354

Serrano, J., Shahidian, S., & da Silva, J.M. (2013, 2013//). Comparing the DUALEM and VÉRIS sensors for mapping soil properties. Paper presented at the Precision Agriculture '13, Wageningen.

Serrano, J., Shahidian, S., & Silva, J.M.d. (2014). Spatial and Temporal Patterns of Apparent Electrical Conductivity: DUALEM vs. Veris Sensors for Monitoring Soil Properties. Sensors, 14(6), 10024-10041. Retrieved from https://www.mdpi.com/1424-8220/14/6/10024

Silva, S., Santos, R., Queiroz, D., Lima, J., Pajehú, L., & Medauar, C. (2021). Apparent soil electrical conductivity in the delineation of management zones for cocoa cultivation. Information Processing in Agriculture, 9. doi:10.1016/j.inpa.2021.04.004

Simpson, D., Van Meirvenne, M., Saey, T., Vermeersch, H., Bourgeois, J., Lehouck, A., Cockx, L., & Vitharana, U.W.A. (2009). Evaluating the multiple coil configurations of the EM38DD and DUALEM-21S sensors to detect archaeological anomalies. Archaeological prospection, 16(2), 91-102. doi:10.1002/arp.349

Smaill, S.J., & Clinton, P.W. (2016). Overview of the issues affecting fertiliser use in New Zealand's radiata pine forests. New Zealand Journal of Forestry, 61(2), 11-15.

Sonmez, S., Buyuktas, D., Okturen, F., & Citak, S. (2008). Assessment of different soil to water ratios (1: 1, 1: 2.5, 1: 5) in soil salinity studies. Geoderma, 144(1-2), 361-369.
Sparling, G., Lilburne, L., & Vojvodic-Vukovic, M. (2008). Provisional Targets for Soil Quality Indicators in New Zealand. Retrieved from Lincoln, Canterbury, New Zealand:
Sparling, G., & Schipper, L. (2004). Soil quality monitoring in New Zealand: trends and issues arising from a broad-scale survey. Agriculture, Ecosystems & Environment, 104(3), 545-552. doi:https://doi.org/10.1016/j.agee.2003.11.014
Stockmann, U., Huang, J., Minasny, B., & Triantafilis, J. (2017). Utilizing a DUALEM-421 and inversion modelling to map baseline soil salinity along toposequences in the Hunter Valley Wine district. Soil Use and Management, 33(3), 413-424. doi:https://doi.org/10.1111/sum.12352
Sudduth, K.A., Drummond, S.T., & Kitchen, N.R. (2001). Accuracy issues in electromagnetic induction sensing of soil electrical conductivity for precision agriculture. Computers and Electronics in Agriculture, 31(3), 239-264. doi:10.1016/S0168-1699(00)00185-X
Tang, S., Farooque, A.A., Bos, M., & Abbas, F. (2020). Modelling DUALEM-2 measured soil conductivity as a function of measuring depth to correlate with soil moisture content and potato tuber yield. Precision Agriculture, 21(3), 484-502. doi:10.1007/s11119-019-09678-2
Terra, J.A., Shaw, J.N., Reeves, D.W., Raper, R.L., van Santen, E., & Mask, P.L. (2004). SOIL CARBON RELATIONSHIPS WITH TERRAIN ATTRIBUTES, ELECTRICAL CONDUCTIVITY, AND A SOIL SURVEY IN A COASTAL PLAIN LANDSCAPE. Soil Science, 169(12), 819-831. Retrieved from https://journals.lww.com/soilsci/Fulltext/2004/12000/SOIL_CARBON_RELATIONSHIPS_WITH_TERRAIN_ATTRIBUTES,.1.aspx
Thiesson, J., Tabbagh, A., Simon, F.X., & Dabas, M. (2017). 3D linear inversion of magnetic susceptibility data acquired by frequency domain EMI. Journal of Applied Geophysics, 136, 165-177. doi:https://doi.org/10.1016/j.jappgeo.2016.10.038
Thode, P. (1983). Northland's forest history and present resources. New Zealand Journal of Forestry, 28(2), 203-224.
Thorup-Kristensen, K., Halberg, N., Nicolaisen, M., Olesen, J.E., Crews, T.E., Hinsinger, P., Kirkegaard, J., Pierret, A., & Dresbøll, D.B. (2020). Digging Deeper for Agricultural Resources, the Value of Deep Rooting. Trends in Plant Science, 25(4), 406-417. doi:https://doi.org/10.1016/j.tplants.2019.12.007
Triantafilis, J., & Lesch, S.M. (2005). Mapping clay content variation using electromagnetic induction techniques. Computers and Electronics in Agriculture, 46(1), 203-237. doi:https://doi.org/10.1016/j.compag.2004.11.006
Triantafilis, J., & Monteiro Santos, F.A. (2013). Electromagnetic conductivity imaging (EMCI) of soil using a DUALEM-421 and inversion modelling software (EM4Soil). Geoderma, 211-212, 28-38. doi:https://doi.org/10.1016/j.geoderma.2013.06.001
Triantafilis, J., Roe, J.A.E., & Monteiro Santos, F.A. (2011). Detecting a leachate plume in an aeolian sand landscape using a DUALEM-421 induction probe to measure electrical conductivity followed by inversion modelling. Soil Use and Management, 27(3), 357-366. doi:https://doi.org/10.1111/j.1475-2743.2011.00352.x
Triantafilis, J., & Santos, F.A.M. (2011). Hydrostratigraphic analysis of the Darling River valley (Australia) using electromagnetic induction data and a spatially constrained algorithm for quasi-three-dimensional electrical conductivity imaging. Hydrogeology Journal, 19(5), 1053-1063. doi:10.1007/s10040-011-0739-9
Triantafilis, J., & Santos, F.M. (2013). Electromagnetic conductivity imaging (EMCI) of soil using a DUALEM-421 and inversion modelling software (EM4Soil). Geoderma, 211, 28-38.
Trojan, M.D., & Linden, D.R. (1998). Macroporosity and Hydraulic Properties of Earthworm-Affected Soils as Influenced by Tillage and Residue Management. Soil Science Society of America Journal, 62(6), 1687-1692. doi:https://doi.org/10.2136/sssaj1998.03615995006200060029x

Uchida, T., Kosugi, K.i., & Mizuyama, T. (2001). Effects of pipeflow on hydrological process and its relation to landslide: a review of pipeflow studies in forested headwater catchments. Hydrological Processes, 15(11), 2151-2174. doi:10.1002/hyp.281

Urdanoz, V., & Aragüés, R. (2012). Comparison of Geonics EM38 and Dualem 1S electromagnetic induction sensors for the measurement of salinity and other soil properties. Soil Use and Management, 28(1), 108-112. doi:https://doi.org/10.1111/j.1475-2743.2011.00386.x

Valckx, J., Cockx, L., Wauters, J., Van Meirvenne, M., Govers, G., Hermy, M., & Muys, B. (2009). Within-field spatial distribution of earthworm populations related to species interactions and soil apparent electrical conductivity. Applied Soil Ecology, 41(3), 315-328. doi:https://doi.org/10.1016/j.apsoil.2008.12.005

Vereecken, H., Huisman, J.A., Hendricks Franssen, H.J., Brüggemann, N., Bogena, H.R., Kollet, S., Javaux, M., van der Kruk, J., & Vanderborght, J. (2015). Soil hydrology: Recent methodological advances, challenges, and perspectives. Water Resources Research, 51(4), 2616-2633. doi:https://doi.org/10.1002/2014WR016852

Veris Technologies Inc. (2010). Veris Technologies Operating Instructions 2000XA, 3100, 3150 Soil EC Mapping System. Retrieved from Salina, KS USA:

Von Wilpert, K. (2022). Forest Soils—What's Their Peculiarity? Soil Systems, 6(1), 5. Retrieved from https://www.mdpi.com/2571-8789/6/1/5

Wait, J.R. (1962). A Note on the Electromagnetic Response of a Stratified Earth. Geophysics, 27, 382. doi:10.1190/1.1439028

Watson, A., & O'loughlin, C. (1990). Structural root morphology and biomass of three age classes of Pinus radiata. New Zealand Journal of Forestry Science, 20(1), 97-110.

Webb, T.H., & Lilburne, L. (2011). Criteria for defining the soil family and soil sibling: the fourth and fifth categories of the New Zealand soil classification. Landcare Research Science Series(3).

Westfall, P.H., & Henning, K.S.S. (2013). Understanding advanced statistical methods. Boca Raton: CRC Press, Taylor & Francis roup.

Weymer, B.A., Everett, M.E., Houser, C., Wernette, P., & Barrineau, P. (2016). Differentiating tidal and groundwater dynamics from barrier island framework geology: Testing the utility of portable multifrequency electromagnetic induction profilers. Geophysics, 81(5), E347-E361. doi:10.1190/geo2015-0286.1

Wiekenkamp, I., Huisman, J.A., Bogena, H.R., Graf, A., Lin, H.S., Drüe, C., & Vereecken, H. (2016). Changes in measured spatiotemporal patterns of hydrological response after partial deforestation in a headwater catchment. Journal of Hydrology, 542, 648-661. doi:https://doi.org/10.1016/j.jhydrol.2016.09.037

Williams, T. (2016). Forest runoff processes. In D. M. Amataya, T. M. Williams, L. Bren, & C. De Jong (Eds.), Forest Hydrology: Processes, Management and Assessment (pp. 17–31). Oxfordshire, UK: CABI International.

Wilson, S., Shokri, A. (2015). Aupouri Aquifer Review. Retrieved from Christchurch, New Zealand:

Zare, E., Beucher, A., Huang, J., Boman, A., Mattbäck, S., Greve, M.H., & Triantafilis, J. (2018). Three-dimensional imaging of active acid sulfate soil using a DUALEM-21S and EM inversion software. Journal of Environmental Management, 212, 99-107. doi:https://doi.org/10.1016/j.jenvman.2018.02.008

Zeileis, A., & Hothorn, T. (2022). Diagnostic Checking in Regression Relationships. R News, 2(3), 7-10. Retrieved from https://cran.r-project.org/package=lmtest

Zemni, N., Bouksila, F., Persson, M., Slama, F., Berndtsson, R., & Bouhlila, R. (2019). Laboratory Calibration and Field Validation of Soil Water Content and Salinity Measurements Using the 5TE Sensor. Sensors (Basel), 19(23). doi:10.3390/s19235272